THE UNIVERSITY OF MICHIGAN

COLLEGE OF LITERATURE, SCIENCE, AND THE ARTS
Department of Astronomy

Final Report

ORBITING CORONAGRAPH

Richard G. Teske
Orren C. Mohler

ORA Project 07270

under contract with:

May 1966

TABLE OF CONTENTS

TABLE OF CONTENTS (Concluded)

## LIST OF ILLUSTRATIONS

LIST OF ILLUSTRATIONS (Concluded)

# I.  OBSERVATIONAL OBJECTIVES OF AN ORBITING CORONAGRAPH

Observation of the solar corona from a ground station is limited by scattered light in the terrestrial atmosphere and in the telescope.  While it is possible to observe the inner E corona, it is not possible to observe directly the K corona.  Of the two sources of the scattered light, the dominant one will be the coronagraph objective lens, given a suitable mountain observing site and an unusually good observing day.  Thus, total elimination of atmospheric scattering of light will not by itself make possible direct observation of the K corona.

The advantage to be enjoyed by an orbiting coronagraph lies in the increased angular resolution which it affords through elimination of the problem of "astronomical seeing," and in the increased opportunity for observation which is permitted by its independence of weather.

The name coronagraph is applied to an instrument which is capable of observing the solar chromosphere and such structures as spicules, prominences, surges, flares at the limb, etc., in addition to the lower E corona.  One of the present objectives of solar astronomy is to examine these features with a high angular resolution, and as free from scattered light as possible, in an attempt to define their physical structure with greater precision than heretofore.

Studies which might be carried out with a coronagraph operating at visual wavelengths are the following.

## A.  Corona

(i)   Study of the chromospheric/coronal interface at high resolution. Rarely have eclipse or coronagraphic observations provided details of structures at this level of the solar atmosphere with high resolution.  Some work (e.g., the 1930 eclipse plates by Marriott) suggests  strongly that such observations be carried out.  Desiderata are spectra and direct photographs.

(ii)  Refinement of model of lower corona.  Observational desiderata are coronal spectra at all position angles around limb and at available distances from limb.

(iii) Refinement of model of coronal condensation.  Observational desiderata are coronal spectra.

1

(iv) Determine physical nature and extent of coronal changes which accompany changes in solar activity and which accompany active events such as flares and eruptive prominences. Observational desiderta are coronal spectra and direct photographs of corona in emission lines.

(v) Test theories of polarization of coronal emission. Observational desiderta are polarization measures in emission lines.

Observation of the corona in the ultraviolet emissions of highly-ionized atoms, using grazing incidence techniques, affords the unique advantage of viewing the corona against the sun's disk. There is no doubt important information to be gained from such observations. However, there is in the visual portion of the coronal spectrum sufficient physical information to permit further strides in the study of coronal structure, given observations of sufficient quality and continuity. Further it will be difficult to achieve, with grazing incidence observations, the angular resolution which is possible with a well-designed telescope operating at visual wavelengths.

B. Chromosphere and Limb

(i) Obtain data on dimensions and life-times of spicules, prominence threads, flare filaments, Ellerman bombs, etc., with high angular resolution. Desiderata are direct monocrhromatic photographs, obtained at intervals suitable for the studies being pursued.

(ii) Refine models of structures such as spicules, prominences. Desiderata are stigmatic spectroscopic observations with high angular resolution and high dispersion.

(iii) Observe magnetic fields in structures at solar limb. Spectroscopic observations of high dispersion required.

(iv) Study polarization of emission at solar limb. Polarization measures in emission lines are desired.

(v) Observe active events at the solar limb and the interrelations of chromospheric and coronal phenomena associated with these events. Desiderata are time-series of monochromatic direct photographs ar rapid cadence.

## C. Disk

(i)   Contrast of granulation at the limb.

(ii)  Sunspot structure at the limb.

(iii) Distribution of specific intensity in the continuum across
the limb.

Achievement of a significant increase in angular resolution demands a
large instrument and great expenditure of effort and funds. In our opinion
the instrument to be designed should be one of as broad a usefulness as pos-
sible in justification of these expenditures.

## D.   Recommendation

The proposed instrument should incorporate a spectrograph of speed and
dispersion suitable for studying the coronal emission lines. Provision should
be made for spectroscopic observation of brighter features above the limb and
of the chomosphere itself. The telescope should have a station or stations
for direct monochromatic photography of the corona in its emission lines and
for direct monochromatic photography of the chromospheric spicules, of promi-
nences, etc. At these stations the filters should be interchangeable to per-
mit observations in different wavelengths and to permit polarizing optics to
be employed. The instrumental contribution to polarization must be minimal
if polarization studies are to be carried out successfully.

In its application to some physical studies of the corona, the tele-
scope's spatial resolution is not a critical design factor. However, a reso-
lution of at least a few tenths arc-seconds is highly desirable for study of
limb phenomena, the chromosphere, the interface between chromosphere and
corona and coronal structures which are associated with spicules, prominences,
etc. Every effort should be made to obtain diffraction-limited resolution at
all foci of the instrument.

If the telescope can be designed for observation of the solar disk, the
scope of its programs will be vastly enchanced. If external occultation can
be provided, a great extension of its contribution to study of the corona will
result.

## II.  DESIGN OF TELESCOPES TO MEET OBSERVATIONAL OBJECTIVES

### A.  Optical Designs

Two preliminary optical designs have been examined.  These were sketched out by us at The University of Michigan and submitted to the Bendix Systems Division of the Bendix Corporation for verification.  This subcontractor's report of his optical evaluation forms Appendix  B  of this report.  A detailed and complete ray-tracing analysis has not been undertaken.

Both designs incorporate an f/18, 10-inch diameter objective lens, a large spectrograph of the Czerny-Turner type, a small, fast spectrograph containing a Schmidt camera, and two stations for direct photography—one at an f/42 focus, one at an F/3.6 focus.  Each of these components—the two spectrographs and two direct-photography stations—is desired to satisfy the observational needs discussed in Section I.  Their physical arrangement, suggested here, is dictated by our beliefs that the cameras should be located close together to simplify access for changing of film reels, and that to locate them near the center-of-mass will have some advantages in the dynamics of the telescope.

The design which folds the light path at nearly normal incidence incorporates a Mangin corrector, and the subcontractor refers to it variously as the "Unfolded System" or the "Straight-Through System."  In this part of the report we will call it the Schupmann System.  The design which folds the beam with 90° reflections is referred to by the subcontractor as the "Folded System," and by us in this part of the report as the Compact System.

### 1.  THE SCHUPMANN SYSTEM

A schematic diagram of the optical system is shown in Figure 1, and a listing of the optical elements and data pertaining to them forms Table I.
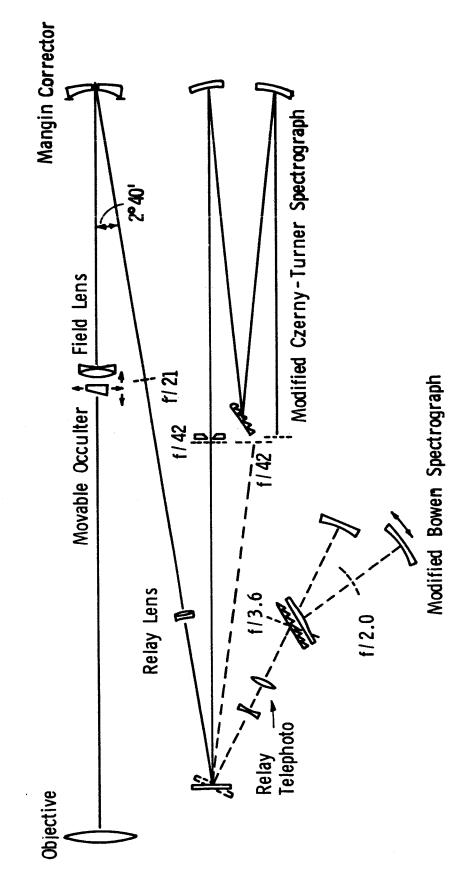
Figure 1. Optical scheme of Schupmann system.

Objective

Mangin Corrector

Movable Occulter

Field Lens

Relay Lens

2°40'

f/21

f/42

Modified Czerny-Turner Spectrograph

f/42

Relay
Telephoto

f/3.6

f/2.0

Modified Bowen Spectrograph

TABLE I

SCHUPMANN OPTICAL SYSTEM

| Element | f, cm | Diam, cm | Separation, cm |
|---|---|---|---|
| Objective lens | 457 | 25.4 | 430-460 |
| Occulting disk | - | 4.4 | |
| Field lens | 172 | 9.0 | 33-3 |
| Stop | - | 13.0 | 274 |
| Mangin mirror | 140 | 14.0 | - |
| Relay lens | 136 | 11.0 | 492 |
| Folding flat | - | 9.0 | 102 |
| Telephoto | -218 | 7.0 | 87 |
| | + 18.7 | 7.0 | 54 |
| Folding flat<br>f/42 focus | - | - | 294 |

a.  Objective Lens

     Since scattered light and the multiplicity of extra, spurious solar im-
ages due to internal reflections must be stringently minimized, a single-
element lens is superior to any other type.  We have assumed here that the
lens is BSC-2 glass.  Newkirk and Bohlin[1] have investigated the scattering and
fluorescing properties of various materials for coronagraph lenses; BSC-2 ap-
pears to be of useful quality in these respects.


TRANSMISSION PROPERTIES OF BSC-2[2]

(10 mm thickness)

| $\lambda$(Å) | T (%) |
|---|---|
| 2,960 | cut-off |
| 3,600 | 76.0 |
| 3,800 | 95.0 |
| 4,000 | 99.5 |
| . | . |
| . | . |
| 10,000 | 94.5 |
| 20,000 | 85.0 |

[1]Newkirk, G., Jr., and David Bohlin, Applied Optics, 2, 131, 1963.
[2]Smithsonian Physical Tables; Ninth Ed., 1951, p. 512.

Preliminary calculations suggest a lens with the following geometry:

$$r_1 = 258.4 \text{ cm}$$

$$r_2 = -2782 \text{ cm}$$

$$q_D = +0.83 \text{ for minimim coma in the yellow.}[3]$$

Spherical aberration of a spherically-surfaced lens results in a focal difference of 3.6 mm between marginal and paraxial rays. The amount of aspheric figuring needed to remove this abberation amounts to a few wavelengths departure from the spherical figure. For an object $\phi$ degrees from the optical axis, the longitudinal displacement of the focal point from the paraxial focal point is given in the following table:

| $\phi$ | $\Delta f$ (astigmatism) | |
|---|---|---|
| 2° arc | 0.6 | cm |
| 10' arc | 0.1 | mm |
| 5' arc | 0.05 | mm |

It is thus desirable to maintain the place on the sky which is being observed as close to the optical axis as possible. As will again be mentioned, the optimum field of view of the Schupmann system is also very small (~5' arc), and therefore an on-axis system is mandatory. Hence the coronagraph's internal occulting disk must be movable and servo-controlled to follow the sun's disk.

10-INCH DIAMETER BSC-2 LENS, $f_D$ = 15 FEET

| | $\lambda$, Å | Theoretical Angular Resolution, arc-sec | $n'$ | $f$, cm | Radius of Solar Image, cm |
|---|---|---|---|---|---|
| | 3000 | 0.30 | – | – | – |
| | 3300 | – | 1.540: | 436 | 2.03 |
| G' | 4307 | – | 1.52708 | 448.5 | 2.09 |
| F | 4861 | – | 1.52264 | 452.3 | 2.10 |
| | 5000 | 0.50 | – | – | – |
| D | 5890 | – | 1.51700 | 457.2 | 2.13 |
| C | 6563 | 0.66 | 1.51642 | 457.8 | 2.13 |
| | 8000 | 0.79 | – | – | – |
| | 10000 | – | 1.510: | 462 | 2.15 |
| | 12000 | 1.19 | – | – | · |

---

[3]The optimum shape factor is a matter for more careful consideration. We here choose the value in the yellow for illustrative purposes.

The chromatic aberration is large, requiring a considerable longitudinal motion of the internal occulting disk. The Mangin correcting mirror will however remove almost all the longitudinal and lateral chromatic aberrations.

Internal reflections in the objective lens result in formation of a real solar image, diameter 6 mm, at a distance of 64 cm behind the objective.

b. Internal Occulting Disk

The internal occulter must be freely movable laterally to permit bringing solar features under observation to the optical axis of the telescope.

Design and selection of a mechanism for carrying the internal occulter is a critical factor in the telescope design. In Appendix B the subcontractor discusses his conception of a possible design for a servo-controlled device. In this design the disk automatically seeks to position itself laterally and is driven by the observer-astronaut to the correct longitudinal position corresponding to the wavelength region of interest.

An override, or partial override, of the servo-system will be necessary. The occulting disk, somewhat larger than the solar image, will obscure regions very close to the limb. To observe these, it must be decentered from the solar disk a bit. If the telescope is to be used to observe the photosphere, the internal occulter must be removed from the light path.

The occulter is to carry or consist of a mirror to direct unused photospheric radiation out of the telescope.

c. Field Lens

The field lens must exactly image the first nodal point of the objective onto the vertex of the Mangin mirror surface.[4] This lens must be achromatic, since in principle it is the only source of chromatic aberration in the image formed by the Mangin.

c. Mangin Mirror

Employment of a Mangin mirror in a coronagraph is dicussed by Rush and Schnable,[5] as well as by Baker.[4] Its primary attraction as a principle in coronagraph design is that it permits practically perfect achromatization of the optical system. Requirements in its employment are: (1) use at equal

---

[4]Baker, J. G., Astronomical Journal, 59, 74, 1954.
[5]Rush, J. H. and G. K. Schnable, Applied Optics, 3, 1347, 1964.

object and image conjugates to eliminate coma; (2) use as close to the optical axis as possible to avoid large astigmatism; (3) an aspheric figure; and (4) restriction of the working field of view to minimize field curvature and the off-axis astigmatism of (2).

It must be admitted that while we are interested in using the advantages of this system, we do not consider ourselves experts in the design principles of a Schupmann system. A more careful assessment of its optical intricacies is needed before a final design can be attained. Rush and Schnable[5] indicate that their coronagraph attains diffraction-limited resolution.

The Mangin is to have an unaluminzed central spot which will transmit light from the spurious solar image formed by internal reflections in the objective lens.

e. Relay Lens

The subcontractor, following Bush and Schnable,[5] suggests that the relay lens be figured aspheric to avoid the necessity for aspherizing the Mangin. This field lens must also be achromatic.

Its function in the design is to provide a final image of such size as to match the resolution of the telescope objective to the resolution of photographic emulsions, for which we have assumed a 20 -30µ resolution element.

f. Folding Mirror

Particular engineering attention should probably be paid to the mounting of the beam-folding flat. It is to be rotatable so as to direct light to three stations: (1) the Czerny-Turner spectrograph; (2) the fast Schmidt-type spectrograph; and (3) the f/42 direct-photography position.

In its position at the sunward end of the telescope, its mounting may be particularly vulnerable to the effects of solar heating, either by direct conduction or by the secondary effects of radiation by the telescope's protective cover. The mounting must permit the accurate positioning of the mirror in any of the three directions. This accuracy is specified by the following considerations: By requiring that the accuracy of "aiming" at the f/42 direct-photography station be $\pm$ 20 arc-seconds on the sky, or $\pm$ 900 microns on the focal plane at a distance of 294 cm from the folding flat, the angular accuracy of positioning of the flat is

$$\frac{\pm\ 900\ \text{microns}}{294\ \text{cm}} \times 10^{-4}\ \text{cm/micron} \simeq \pm\ 3 \times 10^{-4}\ \text{or} \simeq \pm\ 1\ \text{arc-minute}.$$

9

Similarly, to align the telescope axis with the optical axis of the large spectrograph, permitting a $\pm$ 5% deviation in illumination of the collimater requires an angular accuracy of positioning of the flat of about

$$\frac{\pm\ 0.05 \times 8.5}{596\ \text{cm}} \sim \pm\ 7.1 \times 10^{-4} \quad \text{or} \quad \sim \pm\ 2\ \text{arc-minutes.}$$

During an exposure, the orientation of the flat must be maintained to within a value given by half the resolution of the telescope

$$\pm\ 0.15\ \text{arc-second} \times 45\ \text{microns/arc-second} \times \frac{1}{294\ \text{cm}} \times 10^{-4}\ \text{cm/micron}$$

$$=\ \pm\ 2.3 \times 10^{-6} \quad \text{or} \quad \pm\ 1/2\ \text{arc-second}$$

g.  The Telephoto Relay Lenses

An inverted telephoto system is employed to provide an $f/3.6$ focus to feed the fast spectrograph of the focus for direct coronal photography. The negative element of this pair of lenses collimates the light beam, and within the collimated portion of the beam may be inserted broad-band or narrow-band filters.

2.  THE COMPACT SYSTEM

A schematic diagram of the optical system is shown in Figure 2, and a listing of the optical elements and data pertaining to them forms Table II. Less effort has been expended on analysis of this system than on the Schupmann system.

TABLE II

COMPACT TELESCOPE OPTICAL SYSTEM

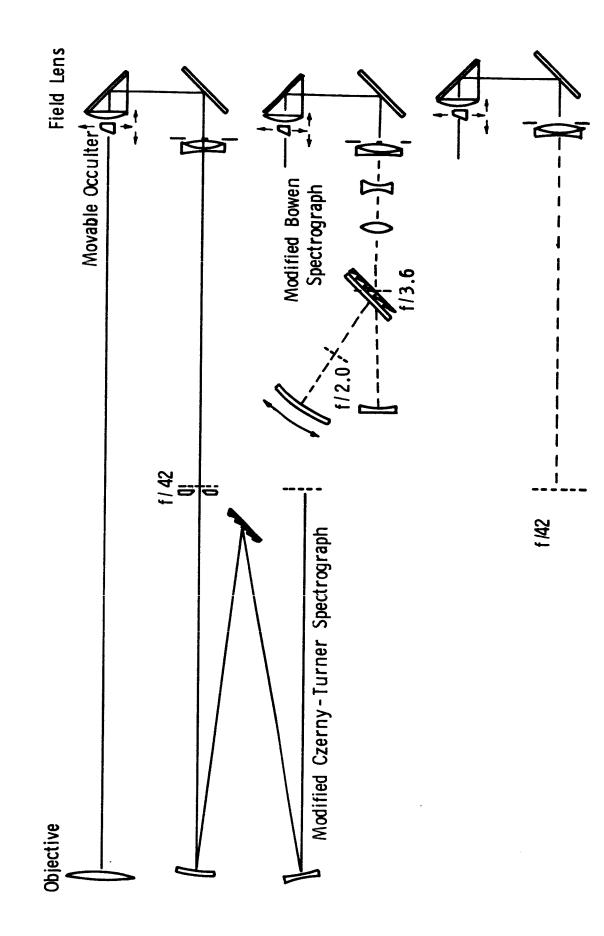| Element | f, cm | Diam, cm | Separation, cm |
|---|---|---|---|
| Objective lens | 457 | 25.4 | 430-460 |
| Occulting disk | - | 4.4 | 33-3 |
| Field lens | 54 | 9.0 | |
| 45° flat | - | 14.0 | 61 |
| Stop | - | 3.3 | - |
| Second objective | 45 | 4.0 | 5 |
| Telephoto | -122 | 4.0 | 120 |
| | + 11.2 | 4.0 | |
| Second objective f/42 focus | - | - | 127 |

Figure 2. Optical scheme of Compact system.

11

(i) Objective lens. This element is conceived as identical to the objective in the Schupmann system.

(ii) Internal occulating disk. Conceived as identical to that in Schupmann system.

(iii) Field lens and 45° prism. The field lens must be overcorrected chromatically to provide an achromatic image. It is mounted integrally with a 45° prism to minimize light losses, the prism deviating the light path through 90° towards a mirror which provides a second 90° deviation.

(iv) 45° flat mirror. The prism and this mirror fold the light path through 180°.

(v) Second objective lens. An achromat, this lens has an opaque spot on its forward vertex to intercept light from the small solar image which is produced by internal reflections in the main objective lens.

Since it was found difficult to illuminate both foci and both spectrographs with a singly-folded light path, we have suggested that these foci be placed at different azimuths around the telescope optical axis. To feed light to each, the field lens-prism, the 45° flat and the second objective lens may be structurally integrated into a housing which rotates about the telescope's optical axis—that is, about the axis through the center of the field lens.

Calculations show that angular orientation of the optical paths at the three azimuths needed must be within 1 arc-minute of true.

(vi) The telephoto relay lenses. This pair of lenses matches the focal ratio of the light beam to the focal ratio (f/3.6) of the collimator of the fast spectrograph. They also provide the f/3.6 beam for direct coronal photography.

It should be noted that in Appendix B, containing a drawing of this system, the telephoto combination is incorrectly located. The data in Table II of this report are preferred.


3. THE LARGE SPECTROGRAPH

A schematic drawing is shown as Figure 3. Dimensional data are given there.

Coma is minimized by the over-and-under Czerny-Turner arrangement suggested here, a system which is achromatic through its use of all-reflecting optics. Spherical aberration and astigmatism are present, however, the latter

12
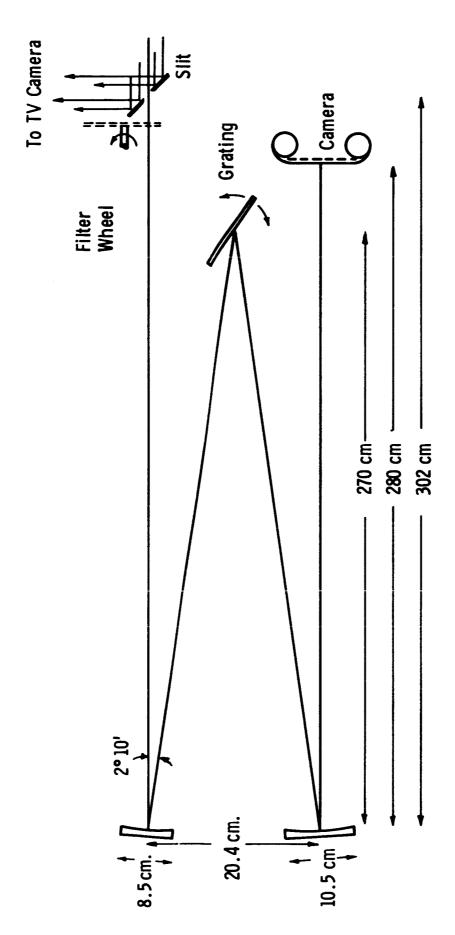
Figure 3. Optical scheme of modified Czerny-Turner spectrograph.

being improved by keeping the collimator and camera mirrors as close together as possible. Aberrations of this system have not been fully explored by us, but we feel it is a spectrograph worth careful consideration.

For example, the spherical aberration of the camera mirror: if a photographic plate is placed at the axial focus, 280 cm from the mirror, marginal rays parallel to the optic axis (5.25 cm from the axis) are focussed

$$\frac{h^2}{8f} = \frac{(5.25)^2}{8 \times 280} \text{ cm} = 0.123 \text{ mm}$$

in front of the plate. These rays intersect the photographic plate $\frac{h^3}{8f^2} = 2.3$ microns from the optical axis, well within the resolving power of the emulsion.

Assuming the grating has 600 grooves per millimeter, the following table describes the dispersive characteristics of the spectrograph.

CZERNY-TURNER SPECTROGRAPH

| $\lambda$ | Order | Dispersion, A/mm | Milliangstroms per Photographic Resolution Element $(30\mu)$ |
|---|---|---|---|
| 4,000 | 2 | 2.9 | 87 mA |
|  | 3 | 1.8 | 54 |
|  | 4 | 1.3 | 39 |
| 6,000 | 2 | 2.7 | 81 |
|  | 3 | 1.6 | 48 |
|  | 4 | 1.0 | 30 |
| 8,000 | 1 | 5.7 | 171 |
|  | 2 | 2.5 | 75 |
|  | 3 | 1.3 | 39 |
| 10,000 | 1 | 5.5 | 165 |
|  | 2 | 2.1 | 63 |

The half-widths of chromospheric lines are thus resolvable in the second and higher grating orders, and of photospheric lines in the third and higher grating orders. While a Doppler displacement at 6000 Å which corresponds to

0.1 km/sec is only 2 mA (roughly 2 microns or 1/15 resolution element), Doppler shifts of this magnitude should be observable, since the whole line shifts.

Auxiliary devices for use with the spectrograph will be essential.

(i)  A means of guiding the spectrograph slit upon the solar region of interest by means of a TV monitor is suggested by the subcontractor. The TV monitor, which provides the astronaut-observer with an image of the reflecting slit jaws, should be illuminated through a narrow-band filter set upon Hα, or perhaps Ca II K.

(ii)  Filters should be provided at the spectrograph entrance slit to eliminate overlapping grating orders. An indexable wheel containing several filters might be employed for this purpose. The wheel may be placed behind the spectrograph entrance slit.

At the spectrum focal plane the length of spectrum observed is limited by dispersion, by vignetting and by film format. The usable spectrum height is about 1.3 cm, corresponding to the presumed diffraction-limited field of view of 5 arc-minutes. The length of unvignetted spectrum depends upon the diameter of the camera mirror. A 10.5 cm mirror subtends 0.0389 radian at the grating, so that the entire length of the spectrum, including the vignetted portion, is about 100 Å in the IV order at λ6000. A collimator diameter of 8.5 cm and camera mirror diameter of 10.5 cm permits an unvignetted spectrum length of 2 cm = 20 Å in the IV order at λ6000.

The height of the spectrum is approximately 1.3 cm, its (vignetted) maximum length about 10 cm. Hence it may be possible to photograph the spectrum on 16 mm film which is transported parallel to the dispersion or on 100 mm film which is transported perpendicular to the dispersion.

This spectrograph is intended to be used for high-dispersion studies of the solar chromosphere and near-limb phenomena. Its speed will be discussed in Section B.1.


4.  THE SMALL SPECTROGRAPH

A drawing of the optical system is in Figure 4, which also contains dimensional data. (In this figure, the radii of curvature of the mirrors are not to scale.)

In securing observations of the coronal emission lines close to the limb, and in work where measures of line profiles are not important, a fast spectrograph is desirable. Such a spectrograph is incorporated in our design. The focal ratio of the collimator, f/3.4, is matched by using an inverted tele-
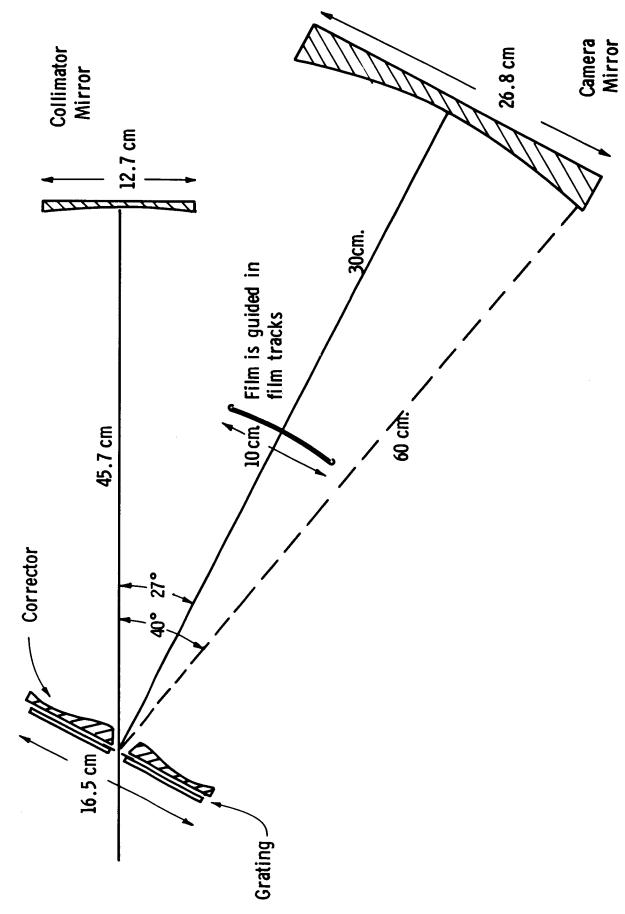
Figure 4. Optical scheme of modified Bowen spectrograph.

Collimator Mirror

12.7 cm

Camera Mirror

26.8 cm

30cm.

45.7 cm

Film is guided in film tracks

10cm

60 cm.

27°

40°

Corrector

16.5 cm

Grating

photo system in the telescope beam. The spectrograph camera focal ratio is f/2.1 in the first order.

Our conceptual spectrograph employs principles of design in use elsewhere.[6,7] A Schmidt corrector plate is placed nearly in contact with the grating and parallel to its surface. Light is admitted to the collimator mirror through a hole in grating and corrector plate, directed back to the grating and dispersed. The spectrum is formed by the 27-cm diameter camera mirror which is placed on the grating normal. Since the corrector plate is twice traversed by a light ray, its figure must be modified from the conventional figure.[7] We have in mind a camera which mounts film to be transported past the focal surface in the same manner as is done for the Baker Super-Schmidt satellite-tracking telescopes.

The intention of this design is to provide a very compact instrument which could be fit within the sunward end of the telescope body. There are, however, three severe design difficulties which will require careful attention in detailed studies of the optical system.

(i) The telephoto system must be strongly corrected for spherical aberration as well as for chromatic aberration.

(ii) A spherical collimator mirror will produce, in the present configuration, large spherical aberration (the lateral extent of the circle of confusion is 150 microns). Hence a nonspherical figure must be computed.

These problems may be lessened by increasing the focal ratio of the beam delivered by the inverted telephoto, but which would require a relocation of the spectrograph. Its present physical location has been suggested by our desire to locate all cameras close to the center of the telescope boty and, in the case of the Schupmann system, to minimize the angle of reflection from the beam-folding flat.

(iii) The spectrograph camera is to be used in two orientations: at angles of 27° and 40° with the optical axis (telephoto-collimator axis). (See below.) The correct curvature for a twice-through corrector plate is $\dfrac{\cos\theta}{1+\cos\theta}$ times the curvature for a once-through corrector,[7] where $\theta$ is the angle 27° or 40°. The value of the correction favor is 0.471 ($\theta = 27°$) and 0.434 ($\theta = 40°$). If the average correction factor is employed, the $\theta = 34°.4$, and a decrease in definition from the optimum will be experienced at the extreme ends of the spectra

---

[6]Bowen, I. S. Ap. J., 116, 1, 1952.
[7]Bowen, I. S. Telescopes, eds. Kuiper and Middlehurst (Chicago: University of Chicago Press), 1960, Chapter 4.

observed.  The circle of confusion at worst will be $\sim$ 45
microns, corresponding to $\sim$ 12 arc-seconds on the sky.

With the above difficulties in mind, we review the characteristics of
the conceptual spectrograph (Figure 4).

The collimator axis is maintained in coincidence with the telephoto-slit
axis.  To photograph the entire spectrum from the objective lens cut-off to
the near infrared (2900 Å - 12500 Å) the camera must be moved to two posi-
tions.  The camera axis is maintained parallel to the grating normal, and the
assembly (camera plus grating plus corrector plate), rotated about an axis in
the face of the grating which is parallel to the grating rulings.  The two re-
quired positions are $\alpha$ = 27°, $\alpha$ = 40°, where $\underline{\alpha}$ = angle between camera axis
and collimator axis.  Thus $\underline{\alpha}$ = $\underline{i}$ angle of incidence of collimated beam on
grating.

We have adopted a camera field of view of 12°, a camera focal length of
30 cm and have assumed a 600 groove/mm grating.  Hence the angle of disper-
sion of included radiation is $-6° \leq \theta \leq +6°$.


### DISPERSIVE CHARACTERISTICS OF FAST SPECTROGRAPH

| $\theta$ | Grating Order | $\lambda$, Å | Dispersion, A/mm | Angstroms per Photographic Resolution Element, Å |
|---|---|---|---|---|
| $\alpha$ = 27° | | | | |
| -6° | 1 | 5850 | 55 | 1.6 |
| -6 | 2 | 2925 | 27.5 | 0.8 |
| 0 | 1 | 7590 | 56 | 1.6 |
| 0 | 2 | 3795 | 28 | 0.8 |
| +6 | 1 | 9320 | 55 | 1.6 |
| +6 | 2 | 4660 | 27.5 | 0.8 |
| $\alpha$ = 40° | | | | |
| -6 | 1 | 9000 | 55 | 1.6 |
| -6 | 2 | 4500 | 27.5 | 0.8 |
| 0 | 1 | 10720 | 56 | 1.6 |
| 0 | 2 | 5360 | 28 | 0.8 |
| +6 | 1 | 12500 | 55 | 1.6 |
| +6 | 2 | 6250 | 27.5 | 0.8 |

In Appendix B, engineering drawings show the film camera for this spectrograph to be located 21° off the mirror axis. Objectionably large aberrations will be encountered in such an arrangement. It is desirable to place the film at an on-axis focal surface, as in Figure 4.

Focal ratios are f/2.1 for $\alpha = 27°$, and f/1.8 for $\alpha = 40°$. Bowen[8] provides data and equations which indicate that to cover the entire range 2900 Å - 12500 Å a fused quartz correcting plate is perhaps required, and that the camera focal ratio for our application should not be less than f/1.4. This limit is set by consideration of the chromatic aberration introduced by the correcting plate, and is met by our camera.

An f/2 Schmidt camera with a 12° field of view produces images for which the maximum radius of the circle of confusion is 8.5 microns, below the assumed resolution of photographic emulsions.

The system discussed here is geometrically practical. The maximum length of spectrum to be obtained is 6.5 cm. Thus a 70-mm film may be employed, the film being transported perpendicularly to the direction of dispersion (the height of the spectrum is about 0.65 mm) between exposures. At the focal plane of the camera there is about 7.3 cm clearance between the camera optical axis and the edge of the collimator beam. Since 1/2(7.0 cm) = 3.5 cm is needed on each side of the camera axis for the film, there is adequate room for film tracks to be mounted as well, without interfering with the collimator beam.

Separation of orders in the sepctrograph may be achieved by using glass filters as, for example, a Schott OG-1 to isolate the first order and a Schott BG-18 to isolate the second order. Selectable insertion of these into the beam will be discussed below.


5. DIRECT PHOTOGRAPHY

Two cameras for direct photography are included in the design. They are located at: (i) an f/42 focus for photography of the chromospheric structure and of prominences and other supra-limb features of sufficient surface brightness, and (ii) an f/3.6 focus for photography of the corona. Generally, direct photography is to be accomplished through narrow-band filters centered on the important emission lines such as Hα, Hβ, Ca II K for the chromosphere and at λ 5303, λ 5694 for the corona, to provide phenomenological data and data on spatial structures of features. White-light or wide-band photography of the disk and of the K corona will be possible at these foci if the internal thermal characteristics of the telescope warrant and/or if external occulation can be accomplished.

---

[8] Ibid.

a.  The f/42 Focus

Here the image scale is 1 arc-second = 45 microns, permitting photographic resolution of features down to 0.5 arc-second.  The diffraction-limited field of view can be about 5 arc-minutes diameter.  This field is included on an area 13.5 mm in diameter, and calls for application of a 16-mm film camera.  A filter wheel, which will mount those narrow-band filters desired plus polarizing filters, should be placed in front of the cmaera, the wheel to be controlled by the astronaut-observer.  The solar beam is directed to the filter wheel and camera by positioning the beam-folding flat.

b.  The f/3.6 Focus

At this focus the image scale is 1 arc-second = 4 microns, permitting photographic resolution of features down to 6 arc-seconds.  Such resolution is not necessarily unsatisfactory for those coronal features which have a smoother spatial structure than chromospheric features.  The 5 arc-minute image spans a diameter here of 1.2 millimeters, suggesting application of an 8-mm film camera.  Again a filter wheel mounting filters and polarizing optics should be in front of or part of the camera.

The subcontractor has supported an arrangement in which both this camera and the fast spectrograph grating are mounted on an arm which swings one or the other into the light path from the inverted telephoto system, while the collimator and camera mirrors of the spectrograph are separately mounted.  If this suggestion proves practical, then filters for direct coronal photography and for isolating orders in the spectrograph should be mounted separately from the camera or spectrograph.  A useful place for a filter wheel would be between the elements of the inverted telephoto system, in the collimated beam from the negative lens.

B.  Performance

1.  EXPOSURE TIMES

Results are collected as Table III.  Calculations are reproduced as Appendix A.

a.  Direct Photography of Corona in the Emission Lines

Data given by Wlerick et al.[9] yield an intensity of the coronal green line

---

[9]Wlerick, G., J.-P. Dumont, and J.-C. Perche, The Solar Corona, ed. J. Evans, Academic Press, 1963, p. 177.

## TABLE III

### EXPOSURE TIMES FOR INSTRUMENTS

| Observation | Exposure Time, second | Displacement $\Delta\Theta$, arc-second | Field Periphery, micron | Yaw and Pitch, micron |
|---|---|---|---|---|
| f/42 direct focus spicule in Hα | 0.2 | 0."7 | 0.02 | 32. |
| Hα line in large spectrograph, III order (spicule) | 35. (50μ slit.) | 126". | 4.1 | 5700. |
| Coronal photo at ρ = 1.2, green line radiation | | | | |
| f/3.6 focus | 0.7 | 2."5 | 0.007 | 10.0 |
| f/42 focus | 8.2 | 29" | 0.9 | 1300. |
| Coronal spectrum, green line at ρ = 1.2 f/2 spectrograph | 0.2 | 0."7 | 0.002 | 2.8 |
| Photo of K-corona at ρ = 4, Δλ = 500 Å | | | | |
| f/3.6 focus | 2.2 | 7."9 | 0.023 | 32. |
| f/42 | 280. | 1010" | 33. | 45.5 mm |

( 5305) of 62 ergs $cm^{-2}$ $sec^{-1}$ steradian$^{-1}$, measured at the earth, at $\rho =$ $R/R_{\odot} = 1.2$. Assuming telescope losses of 50%, filter transmission of 30% and a photographic exposure of 0.1 meter-candle second (fine-grain, high-contrast emulsion) the exposure time for a direct photograph of the corona in the green line and at $\rho = 1.2$ is 0.7 second at the f/3.6 focus and 8.2 seconds at the f/42 focus. Van de Hulst[10] gives for the average ratio of intensities (yellow line)/(green line) = 0.3/20, so that a direct photograph of the corona at $\rho = 1.2$ in the yellow line will in principle require an exposure time of about 50 seconds at the f/316 focus. Whether this can actually be accomplished will depend upon the filter employed in isolating the line, and especially upon the scattered light in the telescope. It is highly probable that the corona will be unobservable, to this instrument, in such weak lines.

b. Photography of Coronal Spectrum

Assuming a spectrograph slit width of 50 microns, which projects to a width of 28 microns at the spectrum focal surface, and referring to the table of dispersions for this camera, we see that the spectrum lines will be essentially images of the spectrograph slit. Therefore spectrum exposure times for optimum density will be similar to exposure times for direct photography, decreased for absence of a dense filter (we adopt a glass filter transmission of 100%), and decreased again for focal ratio. Assuming telescope losses of 50%, and a grating efficiency of 30%, the f/2 focal ratio will permit an exposure time for the green line of 0.2 second. To reach the faintest available lines will in principle require exposures of only a few seconds. It is of interest to determine the faintness of lines which can actually be observed by this instrument against the background of scattered light present in the coronagraph. Assume for purposes of this discussion that optical perfection and relative freedom from UV fluorescence of the objective keep scattered light in the instrument to $5 \times 10^{-6}$ the average disk brightness. Then the green line is observable to 4 arc-minutes from the limb and the red line to 2 arc-minutes from the limb. Other coronal lines are generally much fainter than these. The table below presents an estimate of lines available to the spectrograph, assuming a scattered light of $5 \times 10^{-6}$ $B_{\odot}$. Therefore the coronal spectrograph, which is desirable for the information it can provide regarding relative intensities of some spectrum lines, will attain a wider usefulness if external occultation is available to decrease the instrumental scattered light.

---

[10]Van de Hulst, H. C., The Sun, ed. G. P. Kuiper, University of Chicago Press, 1953, p. 268.

| Line | Can Be Observed To (arc-minutes from limb) |
|------|--------------------------------------------|
| 10747 Fe XIII | 4!5 |
| 10798 Fe XIII | 4!5 |
| 5303 Fe XIV | 4' |
| 3388 Fe XIII | 3!5 |
| 7892 Fe XI | 2' |
| 6374 Fe X | 2' |
| 5694 Ca XV | ~ 1' (active regions) |
| Others | ≤ 1' |

c.  Direct Photography of Chromosphere in Emission Lines

Data given by Dunn (see Appendix B) permit calculation of exposure times needed to register spicules in Hα.  At the f/42 focal plane, the spicule Hα radiation over a band-pass of 3.4 Å produces an illuminance of 0.045 meter-candle $cm^{-2}$, if we take into account 5% telescope losses and a filter transmission of 30%.  Assuming an exposure of 0.1 meter-candle-second, the required exposure time is 0.2 second.

d.  Photography of Chromospheric Spectrum

The high dispersion at the spectrum focal plane reduces the illuminance to very low levels.  According to the calculations of Appendix A, the exposure time to obtain a good image of Hα in a spicule is about 71 seconds, for a slit width of 25 microns.  For optimum performance of the spectrograph in chromospheric studies, the slit may be widened to 50 microns or more, thus reducing exposure times to below 30 seconds.

2.  RESOLUTION

Optical design of all components except the small, fast spectrograph should be directed towards diffraction-limited resolution.  The theoretical angular resolution of our designs is about 0.5 arc-second at λ 5000.

3.  SPECTRAL RANGE

The accessible spectral region is λλ 3000 - > 12,000 Å.  Capability to utilize the range λλ 3000 - 12,500 Å has been designed into all components discussed here.  A requirement for the infrared is for photographic emulsions which are sensitive there.

## 4. POLARIZATION

Of especial astronomical interest is the polarization of light from the solar limb, chromosphere, and corona. The only way to measure polarization with high precision is to eliminate all optical surfaces. Since this is impractical, we are interested in the amount of spurious polarization introduced by our instruments. A full assessment of telescopic polarization at this stage is neither practical nor necessary, and so we have confined our attention to nonnormal reflections in the instruments, since these will be the major source of spurious polarization.

### a. The Schupmann System

To minimize polarization introduced by nonnormal reflections, the system was designed for small angles of incidence. The maximum angle of incidence is about $8°$ arc, occurring at the beam-folding flat.

We have adopted, for purposes of exposition, an incidence angle of $10°$ arc and have calculated the instrumental polarization for one reflection and for two reflections at this angle. We assumed that reflections occurred at aluminum metal.

It was assumed that linearly-polarized light is incident upon a mirror at $10°$ arc. The Stokes paramrters I, Q, U, and V for the reflected light were calculated assuming that the plane of the electric vibration makes an angle $\alpha$ with the plane of incidence ($90° \leq \alpha \leq 0°$). This was done for three wavelengths $\lambda$ 4000, $\lambda$ 7000, $\lambda$ 9500. The degree of linear polarization

$$\rho = \frac{(Q^2 + U^2)^{1/2}}{I}$$

and the degree of ellipticity

$$\rho_V = \frac{V}{I}$$

were computed for the reflected radiation. Figure 5 presents the results for a single reflection. (For perfectly linear polarization, $\rho = 1$, $\rho_V = 0$.) The maximum degree of ellipticity is about 1.5% in the blue for $\alpha = 45°$.

We then computed the resulting polarization for two reflections at angles of incidence of $10°$. The results, also given in Figure 5, are in terms
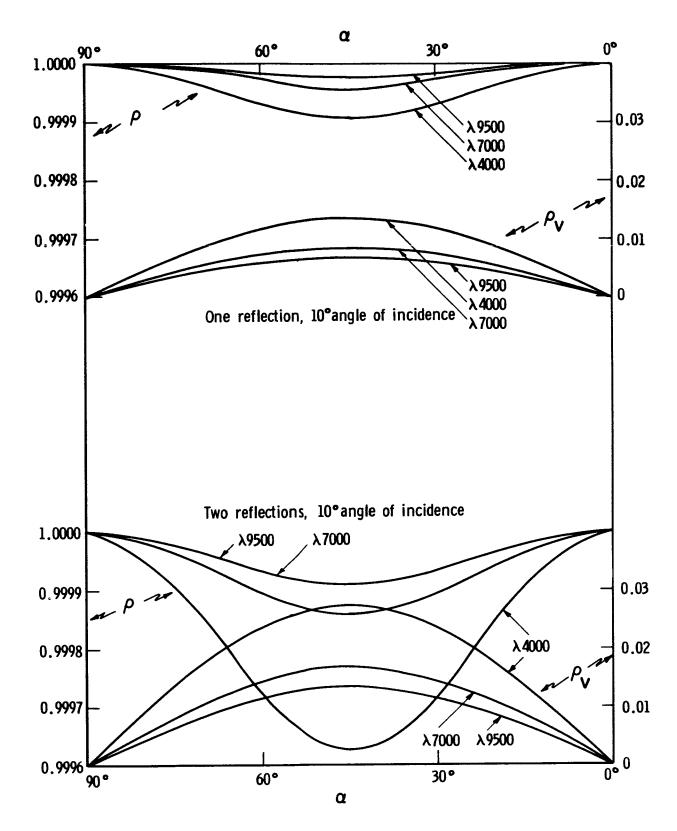
24

Figure 5. Polarization of light after reflection, 10° angles of incidence: degree of linear polarization and degree of ellipticity.

of $\rho$ and $\rho_V$ defined above. In this case, the maximum degree of ellipticity is less than 3% (2.73% at $\lambda$ 4000 for $\alpha = 45°$), and the degree of linear polarization remains above 99.95%.

In the Schupmann telescope design presented here, the spurious instrumental polarization will be less than that computed, and we tentatively conclude that the degree of ellipticity introduced by the reflections at the Mangin mirror and at the beam-folding flat will be of small importance.


b.  The Compact System

Two reflections at angles of incidence of 45° arc are required in this telescope. We assumed that both reflections occurred at a vacuum-to-aluminum metal surface. We have not checked to see whether this assumption will adequately approximate the actual polarization introduced by the prismatic internal reflection plus mirror. However the results for even one 90° reflection are enough inferior to the results for the Schupmann telescope to suggest that the Compact system will introduce a serious amount of polarization.

As before, the Stokes parameters for reflected light were computed, assuming linearly-polarized light to be incident on the first mirror. The plane of the electric vibration makes an angle $\underline{\alpha}$ with the plane of incidence.

Figure 6 presents values of $\rho$ and Figure 7 presents $\rho_V$, as defined above, for one reflection. The degree of ellipticity is about 30%, and the degree of linear polarization about 95%, for blue light and for $\alpha = 45°$.

Results for two reflections are also shown in Figures 6 and 7. In blue light, for $\alpha = 45°$, the maximum degree of ellipticity approaches 60% and the degree of linear polarization approaches 80%.

From these theoretical data, we conclude that significant polarization observations could probably not be made with our Compact telescope.


5.  REMARKS

For a telescope orbit plane arbitrarily inclined to the earth-sun direction, there will generally be a (changing) component of telescope velocity towards or away from the sun. It may be necessary to take this into account in using narrow-band filters for direct chromospheric photography, depending upon the narrowness of the band-pass and the desired criticality of wavelength tuning. In general, band-passes of the order of a tenth to a few tenths of an angstrom are desirable.

In operating the large spectrograph, the observer-astronaut will select the wavelength regions of interest by rotating the grating to the necessary
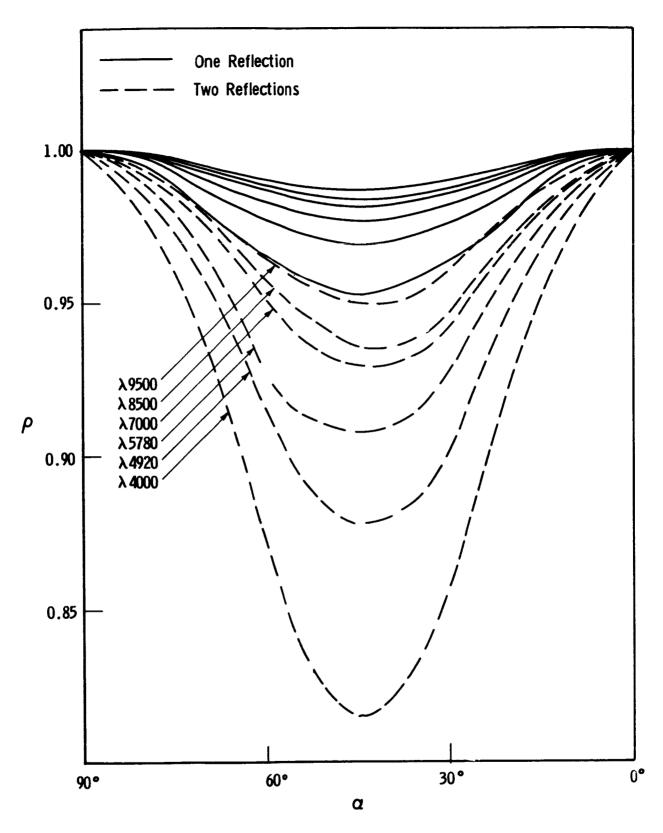
Figure 6.  Polarization of light after reflection, 45° angles
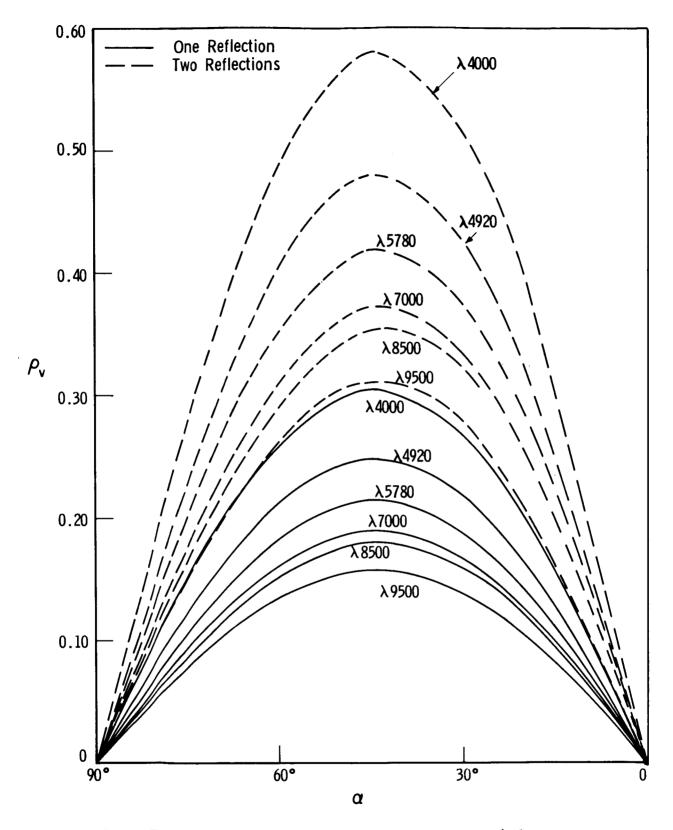of incidence: degree of linear polarization.

Figure 7. Polarization of light after reflection, 45° angles
of incidence: degree of ellipticity.

28

angular orientation. To do this he will need either (1) a command system into which the selected angular setting is fed, or (2) a monitor read-out which informs him of grating angular setting, or both.

Similarly, selection of the different filters for direct photography and for separating orders in the spectrographs will require either a command system or monitor read-out, or both.

It may be desirable to incorporate into the cameras a meter which provides the observer-astronaut with information about the amount of unexposed film remaining in them.

Shutters on the cameras should have varying and selectable speeds which can be chosen by the observer. A continuing series of exposures, as well as single and intermittent exposures, will be desired for some observations. Thus the cameras should be "programmable."

## C.  Comparison of Telescope Designs

### 1. PERFORMANCE

The Schupmann system is superior to the Compact system in terms of its relative freedom from spurious instrumental polarization. The relative merits of other optical aspects should be the subject of detailed optical studies.

### 2. STRUCTURE AND GUIDANCE

A comparative study was not undertaken in detail. However, we can guess that:

   (i)   The lighter weight (see Section III) of the Compact system
         is an advantage during launch.

   (ii)  The shorter Compact system may offer some advantage in the
         launch configuration. However, the Schupmann does fit in
         the LEM adapter.

   (iii) The principal moment of inertia of the Compact system is
         less than for the Schupmann telescope (see Appendix B),
         which may have some significance in expenditure of fuel
         for guidance.

29

(iv) The Compact system's rotatable turret, as conceived here, may be difficult to align and to keep in adjustment. Further, rotation of the turret is a great source of torque and the resulting angular momentum must be somehow removed from the telescope. The Schupmann telescope's rotatable mirror, while also a source of torque, will produce much less angular momentum.

Of the two instruments, the more valuable from the standpoint of the astronomical experiments to be performed is the Schupmann telescope.

## III. ENGINEERING THE TELESCOPES


Appendix B of this report is the engineering report by the subcontractor.

He has devised structures for both telescopes.  These are truss-column, and are to be covered with a two-layer heat shield to maintain an equilibrium thermal environment.  The telescope is to be open to vacuum.

Estimated dimensions and weights are:

(i)  Schupmann System:  762 cm x 80 cm x 60 cm; 440 lb.

(ii)  Compact System:  498 cm x 80 cm x 70 cm; 390 lb.

Methods of gimballing the telescope are discussed by the subcontractor, assuming it to be attached to the spacecraft body.

## IV. CONTROL AND GUIDANCE OF TELESCOPES

Appendix B contains the subcontractor's report on control and guidance.

He has assumed the telescope to be mounted in a manned Apollo vehicle in earth orbit. This assumption provides a point of departure from which control and guidance methods and requirements may be developed. Two Apollo mountings are assessed: (a) one in which the telescope is fixed to the vehicle and the entire vehicle is pointed and guided; and (b) one in which the telescope is mounted to the vehicle on gimbals—the vehicle is pointed as coarse control while the telescope is driven against it for fine pointing and tracking.

A third aprroach—use of the telescope as a separately-orbiting but tethered vehicle—is also explored by the subcontractor.

### A. Distrubance Torques

An analysis of the sources of disturbance torques leads to the usual conclusion that man motion is of several orders of magnitude more importance than other sources. Table 5, Appendix B, summarizes the calculations.

### B. Pointing and Guidance

To utilize fully the resolving power of the telescope, it must be guided with an accuracy of better than 0.3 arc-second. The subcontractor's report states that there is no sensor available to supply error signals for guidance of this accuracy and therefore one must be developed.

In assessing guidance requirements it was assumed that the angular drift rate of Apollo vehicle is 3.6°/hr in all three axes. Table III on page 21 of this report lists exposure times for various operational modes of the telescopes. In that table is listed the angular spacecraft drift about any axis during an exposure (column 3). If we assume a field of view of 5 arc-minutes, then the periphery of the field of view at a focal surface will be rotated through the linear distance given in column 4. The linear distance at a focus through which the image is translated, during an exposure, due to drift in pitch and yaw is listed in column 5.

It is clear that no roll guidance is needed, since the displacement of

the field periphery is well below the emulsion resolution at all foci, and only a fraction of the slit widths of both spectrographs. However, fine guidance in pitch and yaw is needed.

Different methods of pointing and guidance are explored by the subcontractor in Appendix B, where both sensors and guidance techniques are evaluated, for the different ways in which the telescope may be mounted (body-fixed, gimballed, tethered).

It is concluded by the subcontractor that:

(i) The body-fixed mounting will be satisfactory if disturbance torques due to main motion are kept below 0.1 ft-lb for a duration of 0.7 second. An improvement in the Apollo guidance system is required for this, however.

(ii) The gimballed mounting is of practical advantage, though there remains sugnificant technical problems in the area of actuation techniques.

(iii) The tethered concept is wholly within the state-of-art knowledge (except for fine-pointing sensors, as mentioned above).

Although a strict roll guidance is not indicated for the duration of a single exposure, it will be desirable to maintain a given roll orientation with precision, as for example during a time-series of exposures of spicules. The solar vector may be defined by a fine-angle sun-sensor. Roll orientation about this vector requires use of a star-tracking sensor. The precision of roll orientation desired is about 1 arc-minute, corresponding to a 2-micron displacement of the periphery of the field of view at the f/42 focus.

Because the telescope is in an orbit about the earth, the sun's eastward motion among the stars, as seen from it, will not be uniform. For this reason, the solar vector should be defined by the sun itself. The use, for example, of three star trackers for orientation would be cumbersome, requiring on-board computers. Also for this reason the single star-tracker which supplies roll orientation should be directed nearly normally to the orbit plane.

# V.  THE ROLE OF MAN

The design, intended mode of operation and means of acquiring data are based upon a close relationship of man and instrument.

## A.  Telescope Maintenance

Any maintenance or service could be supplied by the observer-astronauts. Attention towards a possible need for realignment of the telescope and spectrograph optics while in orbit should be paid during further design stages. Doubtless special mountings, fittings, etc., will be mandatory to permit a successful alignment or realignment effort.  Failure of any component will require its replacement, again a function which a man can accomplish if components are suitably designed.  Access hatches to the replaceable or alignable components will be needed.

If body-mounted (either gimballed or fixed), some or most of the telescope could be directly accessible from inside the spacecraft.  Still, the work would be in the weightless condition and in a vacuum.

## B.  Mode of Operation

To reduce the work effort on the observer-astronaut, the telescope systems should be programmable under the observer's control.  Complete operation from a single console containing at least one TV monitor appears highly desirable.  The length of an "observing session" should be set in large part by studies of astronauts in present programs.  There is no astronomical reason to think of observing sessions lasting longer than an hour or two, except in unusual circumstances (great flares at the limb) when perhaps four or five hours continuing observation would be of great importance.  (We have in mind here a recommendation to be made later; a polar retrograde orbit which permits nearly continuous solar observation, or a high orbit of long period.)  However, for a low orbit of low inclincation, periodic respite for the observer is afforded by entering earth's shadow.

A TV camera is incorporated in our design which views the slit of the large spectrograph.  This camera can be used by the observer in guiding the telescope to place a particular feature on the slit, or to line up the telescope on some event of interest.  Therefore hand controls for him are needed.

However, fine guidance should proceed automatically.

Films must be changed by the man.  If the telescope is body-mounted, this may be accomplished from within the spacecraft in a vacuum.  If the telescope is tethered, extra-vehicular excursions will be required.  Access hatches, film cassettes, releases, etc., must be designed with the gloved condition in mind.  Air supply quantities will be determined by how often films are to be changed.  A special storage location must be provided for both exposed and un-exposed films, to protect them from radiation damage and from loss of moisture. Similar cautions apply to the films while in use in the telescope.

A significant fraction of telescope time will be devoted to study of phenomena which are at present not entirely predictable.  It may be that the phenomena will not yet be predictable when a space coronoagraph is flown. These phenomena may have to be treated as "targets of opportunity."  The man's role in observing them will be of great importance, since by their un-expected nature the telescope could not automatically be set for their observa-tion.  However, his success will be only as good as his ability to detect the beginning of the events.

How a detection system might be designed and employed is open to consid-eration.  Three possibilities are (1) an all-sun $H\alpha$ monitor, with image vis-ible to the astronaut; (2) a UV sensor set, for example, at the He II 304 line and with an alarm threshold; and (3) a direct link from ground-based solar observations to satellite to warn of events.

It is our recommendation, in any event, that a link to the orbiting tele-scope be established to permit ground-based solar observers to talk to the observer-astronaut.  By such means observations could be coordinated and dis-cussed, plans elaborated or changed, new programs initiated.

# VI. SPECIAL PROBLEMS

The subcontractor has discussed, in his report, some of the basic technical problems associated with a manned orbiting coronagraph.

A few problems which may also be mentioned are the following.

## A. Micrometeoritic Hazard

Micrometeoritic particles in the vicinity of the earth have been intensively investigated. These pose a threat to the surface of the objective lens. The rate at which scattered light in the instrument increases with time, due to pitting of the objective, should be assessed before the feasibility of successful flight operation is finally judged.

## B. Cleanliness of Environment

Sources of local contamination such as venting of crew wastes, condensation of exhaust gases, etc., must be minimized for successful observation of the low corona. Local contamination must be virtually eliminated if the K-corona is to be observed, using external occultation.

## C. External Occultation

Provision of an external occulter will extend the range of coronal observation indefinitely outward from the sun. The external occulter shields the objective from direct photospheric radiation, reducing the scattered sunlight and fluorescence in the telescope to very low values, below $10^{-9}$ $B_{\odot}$. External occultation has been discussed at length by Newkirk and Bohlin.[11]

Since each part of the lens is to be shielded by the occulter, there remains a portion above the solar limb which is vignetted. If $\alpha$ is the angular size of the vignetted portion above the limb in radians, $a$ is the objective

---

[11] Newkirk, G., Jr., and David Bohlin; Applied Optics, 2, 131, 1963.

lens diameter and $\underline{d}$ is the distance from lens to occulter, then

$$d = \frac{a}{\alpha} \quad .$$

The diameter D of the occulter should be, approximately,

$$D = 0.00931 \, d + a \quad .$$

Some values for our 10-inch diameter lens are

| $\alpha$ | $\underline{d}$ | $\underline{D}$ |
|---|---|---|
| 3' arc | 291 meters | 3.0 meters |
| 6' | 147 | 1.6 |
| 10' | 87 | 1.0 |
| 30' | 29 | 0.5 |
| 60' | 15 | 0.4 |

For a fixed-diameter occulter—we here choose 3 m—the vignetting at various distances $\underline{d}$ is

| $\underline{D}$ | $\underline{d}$ | $\alpha$ |
|---|---|---|
| 3.0 meters | 291 meters | 3' arc |
| 3.0 | 200 | 10' |
| 3.0 | 150 | 18' |
| 3.0 | 100 | 35' |
| 3.0 | 50 | 87' |
| 3.0 | 25 | 190' |

Thus an occulter of fixed diameter at varying distances from the telescope may also be employed.

It will probably not be feasible dynamically to attach an occulter to the telescope via a boom of the length required, and therefore, if employed, the occulter should be a separately-orbiting, loosely-tethered (or a free) device. Whether it is possible to deploy such an object to the required position relative to the telescope is a question we have not attempted to answer.

However, assuming it to have been deployed, we attempted to determine its usefulness. once in position it must be permitted to drift, since use of gas jets for steering during an exposure will result in objectionable light-scattering to the detriment of the observation. The rate of drift of the occulter, relative to the telescope-sun line, was computed by integrating the equations of motion for both the telescope and occulter.

We assumed that the occulter was on the telescope-sun line at time t = 0, and that at t = 0 both objects were traveling parallel and at identical speeds. $\phi$ is the angle, measured at the telescope, between the lines telescope-sun and telescope-occulter. $\phi$ is initially zero, and increases as the occulter drifts off the telescope-sun line.

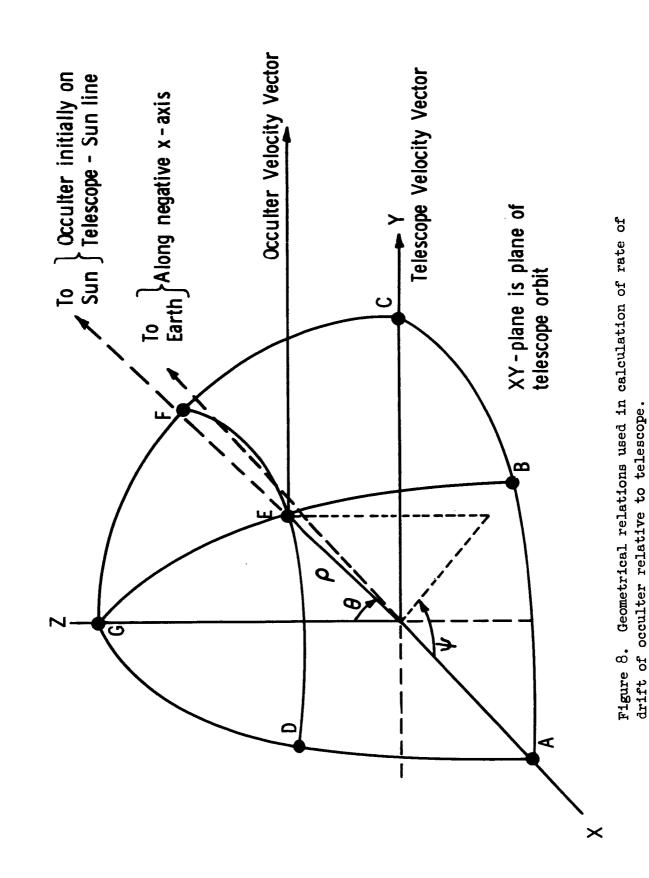Its rate of drift may depend upon its initial distance from the telescope $\rho$, upon the semimajor axis of the telescope orbit and upon the orientation of the initial telescope-occulter vector relative to the telescope's intial velocity vector.

Two circular telescope orbits were investigated: one a 330 km high orbit, the other a synchronous 24-hour orbit. For both of these, two occulter distances $\rho$ were investigated: $\rho$ = 30 m and $\rho$ = 300 m. For each of these four combinations, seven initial configurations of telescope-occulter vector and telescope velocity vector were assessed. The selected initial configurations are displayed in Figure 8. Calculations made for initial configurations in the single octant used by us may be approximately generalized for initial configurations in the other octants, because of the spatial symmetry involved. The integrations span a time interval of 5 minutes, starting from t = 0.

INITIAL CONFIGURATIONS INVESTIGATED

| Semimajor Axis of Telescope Orbit (km) | Occulter Distance $\rho$ (meters) | $\Psi_0$, $\Theta_0$ Degrees |
|---|---|---|
| 6,700 | 30 | 0, 90 (A) |
| 42,240 | 300 | 45, 90 (B) |
| | | 90, 90 (C) |
| | | 0, 45 (D) |
| | | 45, 45 (E) |
| | | 90, 45 (F) |
| | | --, 90 (G) |

Results of the integrations are displayed in Figures 9 through 15. Each figure refers to a particular initial configuration ($\Psi_0$, $\Theta_0$) and contans data referring to both orbits and both inital occulter distances. We deduce that,

Figure 8. Geometrical relations used in calculation of rate of
drift of occulter relative to telescope.

Figure 9. Rate of drift of occulter relative to telescope in two different orbits, for initial configuration A.

Figure 10. Rate of drift of occulter relative to telescope in two different orbits, for initial configuration B.

Figure 11. Rate of drift of occulter relative to telescope in two different orbits, for initial configuration C.

Figure 12. Rate of drift of occulter relative to telescope in two different orbits, for initial configuration D.

Figure 13. Rate of drift of occulter relative to telescope in two different orbits, for initial configuration E.
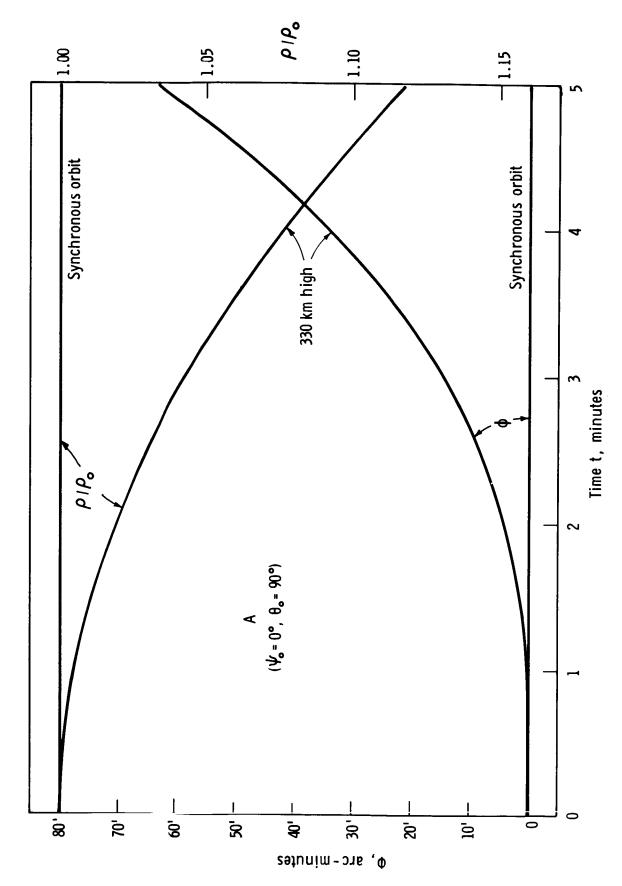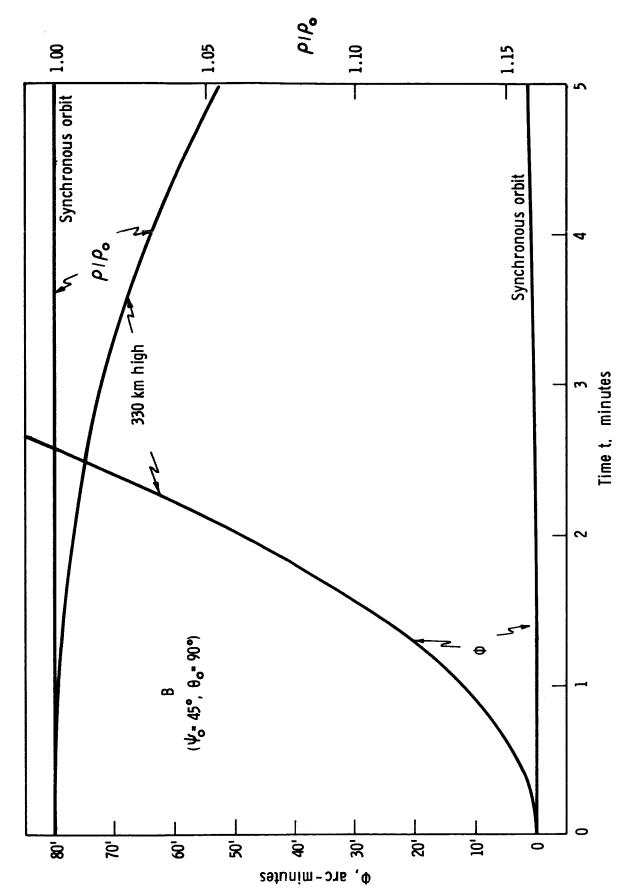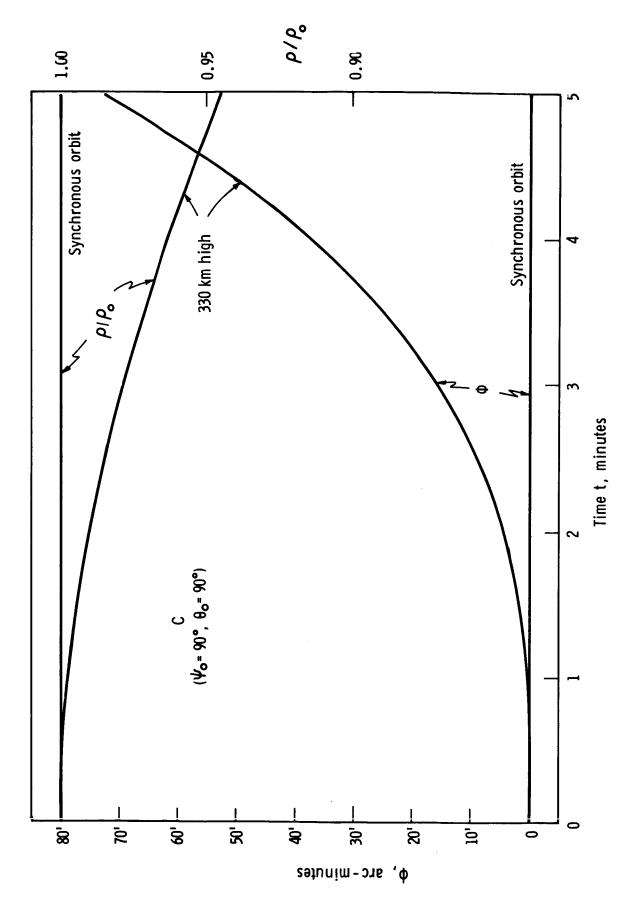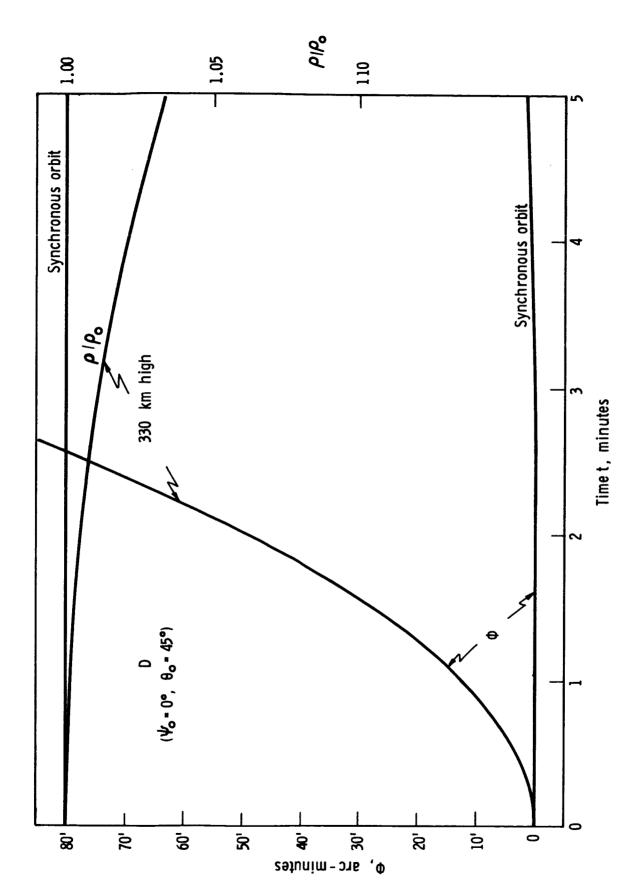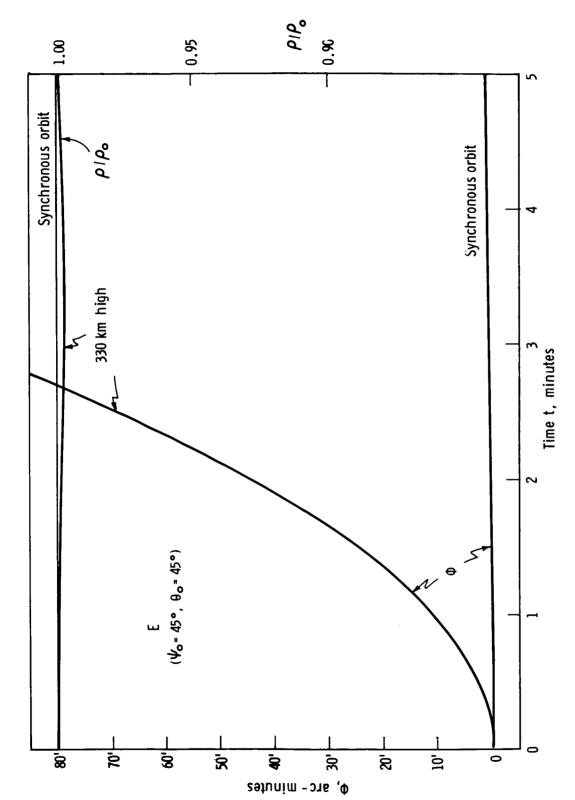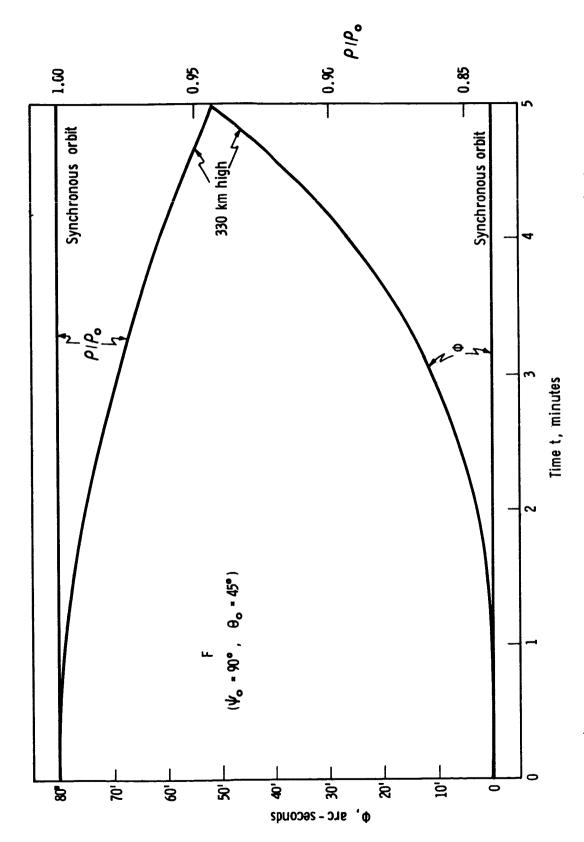
Figure 14. Rate of drift of occulter relative to telescope in two different orbits, for initial configuration F.
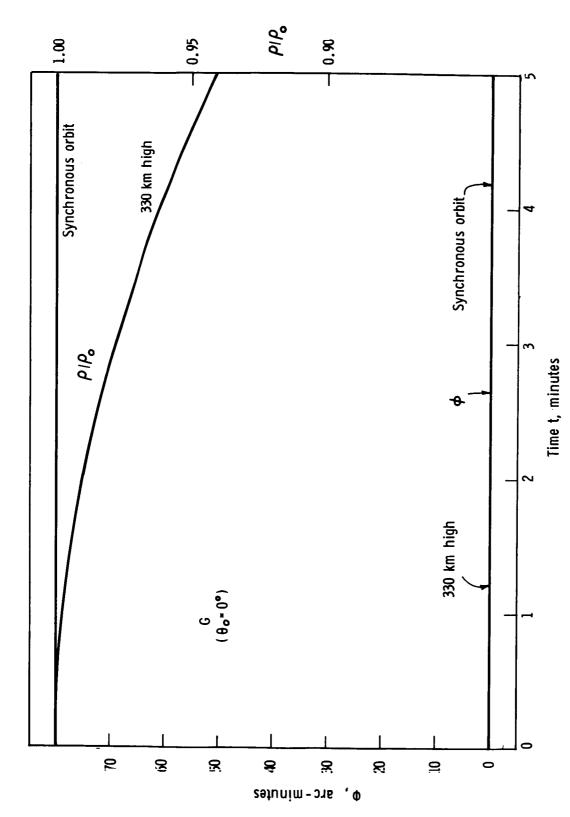
Figure 15. Rate of drift of occulter relative to telescope in two different orbits, for initial configuration G.

for a 5-minute interval:

(i) The radial rate of occulter drift, relative to telescope, is such that the curve $\rho(t)/\rho_0$ is independent of $\rho_0$, for any circular telescope orbit.

(ii) The angular rate of drift, $d\phi/dt$, is such that the curve $\phi(t)$ is independent of $\rho_0$, for any circular telescope orbit.

Hence each figure contains a single curve $\rho(t)/\rho_0$ and $\phi(t)$ for each telescope orbit, each curve referring to both values of $\rho_0$.

(iii) The rate of drift of the occulter is acceptably small for all initial configurations in the synchronous orbit, but is too large in the low orbit for most initial configurations.

(iv) The rate of occulter drift is acceptably small for both orbits when the occulter is placed on a telescope-sun line which is perpendicular to the plane of the telescope orbit (configuration G, Figure 15).

We therefore conclude that, after deployment, an external, freely-drifting occulter can be of some use over a reasonable time period. The required conditions are (a) a telescope orbit of large major axis or (b) a telescope orbit plane perpendicular to the solar direction.

It should be here emphasized that the astronomical importance of the telescopes investigated by us will be considerable, even if external occultation is not provided.

The last two rows of Table III, page 21, list the exposure times which can be expected if occultation can be provided.

# VII. RESUME

## A. Optical Design

There are no developmental requirements on the optical design. Achievement of diffraction-limited resolution is practical. The major difficulty will be in selection of a lens of suitable scattering and fluorescing properties.

A crucial question is the rate of increase of scattered light due to micromeoritic pitting of the objective lens.

## B. Mechanical Design

The subcontractor's report indicates feasibility and suggests areas for further design studies. The important areas are in thermal design and in adoption of a gimballing system.

## C. Control and Guidance

It will be necessary to develop an error sensor for fine-guidance of the telescope. There remain significant technical problems in guiding a telescope fixed to a manned spacecraft. Some of these can be avoided through operating the telescope in a tethered condition.

## D. Platform

A platform with Apollo characteristics of mass, moments of inertia and angular drift rate will serve satisfactorily as a mount for a gimballed telescope. A similar platform, but with finer pointing capability and much slower angular drift rate could serve for a body-fixed telescope. In both cases the presence of man will perturb the pointing control drastically.

## E. Orbit

A lengthened duty cycle can be attained if the telescope can be placed into a high orbit or a polar retrograde orbit without injury to its observers.

APPENDIX A

CALCULATION OF EXPOSURE TIMES

# CALCULATION OF EXPOSURE TIMES

Let the specific intensity of radiation from an observable solar feature be $I = \int I(\lambda)d$ ergs cm$^{-2}$ sec$^{-1}$ ster$^{-1}$. The 10-inch coronagraph lens subtends, at the sun

$$4\pi \frac{\pi(12.7 \text{ cm})^2}{4\pi(1.5 \times 10^{13} \text{ cm})^2} = 7.20 \times 10^{-25} \text{ steradians} \quad .$$

Hence from unit area on the sun, the telescope receives

$$I \times 7.20 \times 10^{-25} \text{ ergs sec}^{-1} \text{ (per square centimeter)} \quad .$$

A unit area on the photographic emulsion corresponds to an area $\underline{A}$ on the sun. At the f/42 focus, 1 cm$^2$ corresponds to

$$A_{42} = \left[ \left( \frac{1 \text{ arc-sec}}{45 \text{ microns}} \times \frac{10^4 \text{ microns}}{1 \text{ cm}} \right) \times \left( 715 \frac{\text{km}}{\text{arc-sec}} \times 10^5 \frac{\text{cm}}{\text{km}} \right) \right]^2$$

$$= 2.53 \times 10^{20} \text{ cm}^2 \quad .$$

At the f/3.6 focus, 1 cm$^2$ corresponds to

$$A_{3.6} = \left[ \left( \frac{1 \text{ arc-sec}}{4 \text{ microns}} \times 10^4 \frac{\text{microns}}{\text{cm}} \right) \times \left( 7.15 \times 10^7 \frac{\text{cm}}{\text{arc-sec}} \right) \right]^2$$

$$= 3.2 \times 10^{22} \text{ cm}^2 \quad .$$

Hence an area of 1 cm on the emulsion at a focus receives energy at a rate

$$A_i \times I \times 7.20 \times 10^{-25} \text{ ergs sec}^{-1} \text{ (per square centimeter)} \quad .$$

The quantity of energy received at 1 cm$^2$ in a focal surface is, in photometric units

$$0.680 \; \frac{\text{meter-candle-seconds}}{\text{ergs cm}^{-2}} \; \times \; A_i \; \times \; I \; \times \; 7.20 \times 10^{-25} \; \text{ergs sec}^{-1} \; \text{cm}^{-2}$$

$$= \; A \; \times \; I \; \times \; 4.9 \times 10^{-25} \; \text{meter-candles} \quad -$$

Losses by absorption in the telescope, in filters and due to dispersion into various grating orders may be estimated. If the total light loss is expressed as a decimal fraction L, then the quantity of energy received at 1 cm$^2$ of a focal surface is

$$(1 - L) \; \times \; A \; \times \; I \; \times \; 4.9 \times 10^{-25} \; \text{meter-candles} \quad .$$

We assume the use of a fast, fine-grain emulsion for which the required exposure is 0.1 meter-candle-second. Hence the exposure time at a focal surface is

$$\tau \; = \; \frac{0.1}{(1-L) \; \times \; A_i \; \times \; I \; \times \; 4.9 \times 10^{-25}} \; \text{seconds} \quad .$$

In the large spectrograph, the third order dispersion at H$\alpha$ is 1.5 A/mm. A 25$\mu$-width slit projects to 24$\mu$ at the spectrum focal plane. Thus

$$\text{Projected slit width} \; = \; 0.035 \, \text{Å} \quad .$$

Spicule energy in H$\alpha$ is $2.4 \times 10^4$ ergs cm$^{-2}$ sec$^{-1}$ ster$^{-1}$ over a band width of 3.4 Å = 97 projected slit widths. Since a 30% transmitting filter is retained to eliminate overlapping orders, and assuming a grating efficiency in the third order of 30%, the exposure time for the spicule H$\alpha$ line in the large spectrograph is

$$\frac{97}{0.30} \; \times \; \text{exposure time at f/42 direct focus} \; = \; 71 \; \text{seconds} \quad .$$

EXPOSURE TIMES AT VARIOUS FOCI

| Focus | $A_i$ (cm$^2$) | $I$ $\frac{\text{ergs}}{\text{cm}^2\ \text{sec ster}}$ | Loss, % | | | (1-L) | $\tau$ (sec) |
|---|---|---|---|---|---|---|---|
| | | | Telescope | Filter | Grating | | |
| f/42 | 2.5 x 10$^{20}$ | 2.4 x 10$^4$ (spicule) | 50 | 70 | -- | 0.15 | 0.22 |
| f/3.6 (Direct focus) | 3.2 x 10$^{22}$ | 62. (Coronal green line at $\rho$=1.2) | 50 | 70 | -- | 0.15 | 0.69 |
| f/2 (Coronal spectrograph) | 1.0 x 10$^{23}$ | 62. (Coronal green line at $\rho$=1.2) | 50 | -- | 70 | 0.15 | 0.21 |
| f/42 | 2.5 x 10$^{20}$ | 5.8 (K corona at $\rho$=4, $\Delta\lambda$=500$\lambda$) | 50 | -- | -- | 0.50 | 280. |
| f/3.6 | 3.2 x 10$^{22}$ | 5.8 (K corona at $\rho$=4, $\Delta\lambda$=500$\lambda$) | 50 | -- | -- | 0.50 | 2.2 |

52

APPENDIX B

SUBCONTRACTOR'S REPORT

(Evaluation by the Bendix Systems Division of the Bendix Corporation)

ORBITING CORONAGRAPH

EVALUATION STUDY

FINAL REPORT

December 1965 to March 1966

BSR 1275

March 31, 1966

Prepared for:

The University of Michigan
Ann Arbor, Michigan
under
Subcontract No. 3 of
Contract No. NASr-54(09)

Authors:

R. Blythe
H. I. McDevitt
E. D. Shoua
T. T. Trexler

BENDIX SYSTEMS DIVISION
of
THE BENDIX CORPORATION
Ann Arbor, Michigan

## CONTENTS

CONTENTS (CONT.)

ILLUSTRATIONS

## ILLUSTRATIONS (CONT.)

## TABLE

# SECTION 1

## INTRODUCTION

The Bendix Systems Division under contract with The University of Michigan and the technical direction of the Department of Astronomy, Chairman Prof. Mohler, and Dr. Teske, performed a preliminary analysis of the feasibility of coronagraph application for solar observations from an orbiting space vehicle.

The analysis and preliminary conceptual design effort consisted of three tasks

1.  Evaluation of proposed optical designs

2.  Telescope structural design and analysis

3.  Evaluation of candidate control techniques.

The general conclusion derived from this preliminary work is that it is entirely feasible and within the current state-of-the art of all technological and physical areas to design, fabricate, launch, deploy, and perform meaningful observations with an orbiting coronagraph.

SECTION 2

OPTICAL EVALUATION

Two designs for a coronagraph have been considered and evaluated. The first design (linear) consists of optical components similar to the Rush-Schnable[1] design except that most angles of incidence are near normal to ease the problem of polarization analysis. The second design uses folded optics for the purpose of conserving space but consequently places a heavy burden on the polarization analysis.

## 2.1 LINEAR DESIGN

### 2.1.1 Objective Lens

Referring to Figure 1, the first element to be considered is the 10 inch objective lens (a). The limiting resolution of the system to this point is given by the Fraunhofer diffraction of the circular aperture (lens A), therefore the diameter (a) of the image spot between the first mimina is

$$a = \frac{1.22f\lambda}{d} \tag{1}$$

where

f = nominal focal length of lens

d = diameter of lens

$\lambda$ = wavelength corresponding to f

For a focal length for (A) of 457 cm (at 5890 A°) (A) is approximately 13 microns. This figure is next compared with a figure obtained using the spherical aberration obtained for the best shape factor for spherical surfaces to see whether or not aspheric figuring is necessary. The shape factor $(g_D)$ for minimum spherical aberration is just slightly different from that for zero coma at the index $(n_D)$ corresponding to 5890 A° for BSC-2 glass. For zero coma[2]

[1] J. Rush and G. Schnable, Applied Optics, Dec. 1964, p. 1347.
[2] Jenkins and White, Fundamentals of Optics

SIDE VIEW

TOP VIEW

Bendix Systems Division
Ann Arbor, Michigan
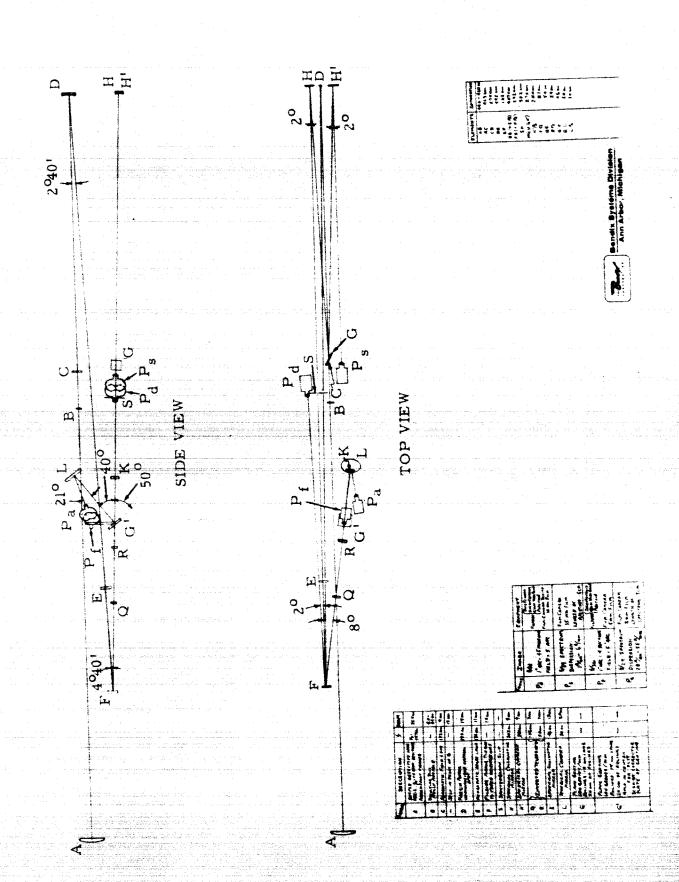
Figure 1 Optical Arrangement—Unfolded Design

2-2

$$q_D = \frac{G}{W} p \qquad (2)$$

where

$$p = \frac{2f}{S} - 1 = -1$$

$S$ = distance to sun

$$G = \frac{3(2n + 1)}{4n}$$

$$W = \frac{3(n + 1)}{4n(n - 1)}$$

For $n_D = 1.517$; $G = 1.99$, $W = 2.41$, and $q_D = .83$.

The radii of curvature for this lens would be 258 cm. and 2780 cm. with the more convex surface toward the sun. The change in image distance for this lens is obtained from[3]

$$\frac{1}{S_h'} - \frac{1}{S'} = \frac{h^2}{8f^3} \cdot \frac{1}{n(n-1)} \left[ \frac{n + 2}{n - 1} q^2 \right.$$

$$\left. + 4(n + 1) pq + (3n + 2)(n - 1) p^2 + \frac{n^3}{n-1} \right] \qquad (3)$$

where

$S_n'$ is the image distance for a ray entering the lens at a distance h from the optical axis

$S'$ is the image distance for paraxial rays

for

$h = 12.7$ cm

$n = 1.517$

---

[3] Ibid.

$$f = S' = 457 \text{ cm}$$

$$q = .83$$

$$p = -1$$

From this calculation $S_h' = 456.64$ which indicates that peripheral rays cross the axis approximately 0.36 cm. in front of the nominal focal plane. At the nominal focal plane, the lateral spherical aberration corresponding to this $S_h'$ would be $202 \times 10^{-2}$ cm which is approximately fifteen times the diffraction limited spot size. Some aspherizing is therefore necessary to obtain diffraction limited resolution in the system.

## 2.1.2 Occulter Movement

The chromatic aberration determines the on-axis movement of the occulter (b). Using the index of refraction at $0.33\mu$ to be 1.540 for BSC-2, the image distance for $0.33\mu$ is $436 \pm 2$ cm. The image distance for $\lambda = 1\mu$ $(n = 1.510)$ is $462 \pm 2$ cm. The occulter therefore should have an axial movement of approximately 30 cm for the wavelength region 3300 $A^0$ - 10,000 $A^0$.

The occulter diameter $(d_o)$ should be somewhat greater than the largest image of the sun which would occur at the lowest index $(n = 1.510)$.

$$d_o = \frac{d_s}{S_s} f_{in}$$

where

$d_s$ = diameter of sun

$S_s$ = distance to sun

$f_{in}$ = 462 cm; image distance at $1\mu$

At $1\mu$, $d_o$ would be 4.31 cm, therefore the occulter should be perhaps 4.4 cm in diameter.

## 2.1.3 Occulter Positioning Mechanism

Inasmuch as the occulter will be completely movable within the area of the field stop (field lens), it would be desirable to have the occulter

considerably larger than $d_o$ (eg. 5 cm) to ease the requirements on the positioning mechanism. For this configuration, the requirements on the positioning and holding servo can be loose at all times except when observing close to the limb. In this case the holding servo should be maintained by a tight loop.

A suggested design for the occulter and its associated mechanism would have the occulter mounted at the vertex of a tetrahedral frame. Spider elements (thin perpendicular to the optical axis and thick along the optical axis) would connect the vertex with the four points of the base. The base would be the moving part of a 3 axis lathe type slide mechanism (similar to the Kulicke and Soffa micrometer positioning unit) with motor drive applied to the lead screws.

For an observation position at a considerable distance from the sun's limb ($> 1/10 \ r_s$ from the limb), the occulter can automatically be placed over the sun's image. The occulter is moved to a given $Z_o$ position outside of the desired wavelength region ($Z_{1\mu} - Z_{.33\mu}$) above which is an insensitive IR detector in a semi-circular arc. The occulter is then indexed in x and scanned in y (or vice versa) where three index steps are necessary to cause a 5 cm occulter to cover the entire transfer lens diameter. The detector output (amplitude as a function of the scanned direction) is fed to processing circuits which determine the mean y position

$$\left( \frac{Y_1 + Y_2}{2} \right)$$

and drive the occulter to that position. The occulter is then scanned in x and the above process repeated to find the proper x position. The occulter is thus set in its x and y positions automatically and driven by the control center (astronaut) to its desired Z position corresponding to a particular wavelength region.

The lateral movement of the occulter should correspond to the diameter of the field stop which in this case is the field lens (C). The occulter should ideally have a lateral movement of approximately 13 cm. This would correspond to a field of two solar diameter on either side of the sun's limb.

### 2.1.4 Mangin Corrector and Relay Lens

The field lens (C) images the primary objective (A) onto the stop in front of the Mangin Mirror (D). The distance from the field lens (C) to the stop in this design will be about 273.5 cm. The purpose of the stop is to eliminate the light diffracted from the edge of (A), therefore the size (diam.) of the stop would be slightly less than the size of the image of (A) at (D). For a focal length of (C) equal to 172 cm, the size of the image of A at D is 15 cm so that a 13 cm diameter stop in front of D is more than enough to eliminate several hundred fringes. The change in diameter corresponding to the first fringe is about $10^{-3}$ cm.

The Mangin Mirror should be slightly larger than the stop (approx. 14 cm) and would have spherical surfaces with the back surface aluminized except for a small spot in the center (back vertex) to allow the image due to the second surface reflection within the primary lens (A) to pass. The second surface reflection is imaged approximately 64.5 cm from lens (A) and is approximately 0.6 cm in diameter. Using this as the object for the field lens gives an image at the Mangin mirror of approximately 0.45 cm in diameter. The spot should therefore be slightly larger than this diameter.

The Mangin Mirror is canted slightly off axis to allow the light to just miss the field lens on the return. If the Mangin has a focal length of 140 cm, it will image the occulter and associated focal plane in the vicinity of the field lens and slightly below it. A 2.5° tilt of the Mangin gives sufficient clearance to form a 9 cm image below (C). The Mangin is figured to correct for the chromatic aberration introduced by (A) and focuses all wavelengths at approximately the same position. The image-plane is used as the object plane for the relay lens (E). Lens (E) will also be figured to correct for the astigmatism produced by the Mangin.

### 2.1.5 Czerny-Turner Spectrograph

For a field of view of 5 arc-minutes the slit height of the Czerny Turner should be about 1.3 cm. The slit jaws are conceived to be totally reflecting (either glass or metal) and at an angle of 45° to the optical axis. The light which doesn't go through the slit is then reflected into a TV camera which serves as an alignment tool as well as a real time data record. There will be a monitor in the control capsule which the astronaut will view to align the coronagraph on a particular solar region. For

times other than alignment, the camera will be switched to a video tape mode which will provide the experiment with a real time data record. When the Bowen spectrograph is in use, light reflected from its jaws is fed into the same TV camera for the same purpose. The collimating mirror (H), which directs the light to the grating (G) is situated at the focal distance (302 cm) from the slit. The pertinent angles, dispersion orders etc, are obtained from the grating equation:

$$d(\sin i + \sin \theta) = m\lambda \tag{5}$$

where

$m$ = order

$\lambda$ = wavelength

$i$ = angle of incidence

$\theta$ = diffraction angle

$d$ = grating line spacing

and its derivative

$$d \cos \theta = m d\lambda / d\theta \tag{6}$$

The linear dispersion is

$$\frac{d\lambda}{dl} = \frac{d \cos \theta}{mf} \tag{7}$$

where

$f = 1/\theta$

Referring to Figure 1, the angle HGH' is about 4.5° which means that $i + 4.5° = \theta$. Putting this value into the grating equation for a 600 1/mm grating and $.5 \times 10^{-4}$ cm wavelength gives a 1st order diffraction angle $\theta$ of 11° and incidence angle of 6.5°. For 2nd order $\theta$ is about 20° and $i$ is about 15.5°. The 1st order dispersion is obtained from Equation (7) and is about 5.65 A°/mm. For 1st order use, the blaze angle $\beta$ should be 9° where

$$\beta = \frac{i + \theta}{2} \tag{8}$$

The camera mirror H (focal length = 280 cm) focuses the spectrum on the exit camera $P_s$ which is discussed in a later section.

## 2.1.6 Bowen Spectrograph

The folding mirror (F) directs the light either into the Czerny-Turner Spectrograph (SHGH'$P_s$), which has just been discussed, or the Bowen spectrograph (G'KG'L$P_a$) through a telephoto lens (QR) or into the camera $P_d$ for direct observation. A 9 cm diameter mirror is used to avoid vignetting in any direction. Lens (Q) is placed at its focal length (-218 cm) from the relay lens (E) and essentially collimates the light from E. R is then placed such that the slit opening of the Bowen is at the focal length of R (30 cm). The diameter of these optics is chosen to be compatible with the speed of the Bowen which is chosen to be F/3.6 (entrance). The Bowen slit is mounted into the back side of the grating G' (600 l/mm) and has totally reflecting jaws. The light reflected from the jaws is directed into the TV camera as previously discussed. Mounted in front of the grating is a corrector plate to correct for residual spherical aberration. The angle of incidence corresponds to the size of the mirror K and is approximately 37° in order to fill the grating. Using Equation (5), the diffraction angle $\theta$ for 2nd order, 5000 A° is about 0° from the grating normal. From Equation (7), the 2nd order dispersion is approximately 30 A°/mm for a focal length for L of 30 cm. The camera mirror (L) moves about the grating such that other wavelength and orders may be sampled. The appropriate blaze angle $\beta$ would be 18.5° for 2nd order use. The camera $P_a$ is attached to the same frame and moves with L in order to photograph the spectrum.

The camera $P_f$ is mounted on the same frame as the grating (G') and can be rotated into the place of the grating for photographic observation of the distant solar regions.

## 2.1.7 Cameras

With the exception of the optical guiding TV camera, there are four recording cameras called for in the design of the solar coronagraph. Both cine cameras and TV recording systems were explored; the latter because of the high astronaut oxygen expenditure used in loading and

unloading the film (cine) cameras. The TV recording system was discarded in favor of the film system because of the lack of availability of a high resolution (250 line pairs/mm) vidicon or orthicon, as well as the weight and environmental problems inherent in a TV system. The features deemed desirable for all of the cine cameras are as follows:

1.  NASA certified spaceworthiness, due to the outgassing problems basic to normal camera lubricating systems, normal rubber gaskets, many plastics, such as teflon, and normal camera film substances

2.  Touch-release film magazine loading and unloading because of lack of astronaut manual dexterity due to necessary use of relatively inflexible vacuum gloves, and because experience in Gemini flights has shown high oxygen expenditure by the astronaut in loading and unloading the film magazines in space

3.  Automatic film threading variable shutter speeds, film advance, etc for the reasons enumerated in (1) and (2) immediately above

4.  Large film capacity with up to 1000 ft of film, using normal thick based film, with greater capacity using thin based films.

The differences between the cameras lies primarily in their uses, which manifests themselves (a) in different film format and orientation and (b) in the amount of film advance per frame.

5.  Some method of sealing the camera, perhaps with a plane glass or plastic window over the format aperture, which will be necessary because there are to be no optics directly mounted on the cameras.

Turning now to the availability of cameras, it is noted that there are presently available, as off the shelf hardware, only 16 mm and 70 mm cameras, fulfilling requirements one through four listed under desirable feature, above. It is apparent that 35 mm and 100 mm cameras may be available in the near future as they are in the design stage now. To the best of our knowledge, no 8 mm spaceworth camera is presently available or is under consideration, however, our inquiry may have generated some interest in future 8 mm space cameras.

Fulfilling condition five, above, appears to be a minor problem, and it is assumed at this point that this problem can be met and solved without undue concern.

The unofficially quoted (by telephone) prices of these NASA certified cameras range from a low, for stripped down cameras, lacking features (2) and/or (3), or parts thereof, of $40,000 for the 16 mm cameras and of $50,000 for the 70 mm cameras to a high of $100,000 for the 16 mm and $125,000 for the 70 mm cameras which completely satisfy conditions one through four, with only minor adjustments to be made to the existing cameras. Graduations in price would of course appear as more features are added or major revisions are called for.

The following discussion analyzes the requirements of the individual cameras designated in Figures 1 and 2.

The most desirable format size for the camera $P_s$ would be about 5 cm x 1.5 cm except when a reference spectra is needed. In this case the format size should be somewhat larger in the shorter dimension. The 5 cm dimension would allow a 100 $A^o$ look at a dispersion of 2 $A^o$/mm. Ideally, this camera should be a 70 mm camera (for the 5 cm dimension) with a variable fractional frame advance and a variable shutter speed from 1 to 1000 milliseconds. Two certified spaceworthy versions of this size camera are presently available with slight modifications.

Camera $P_d$ is used for direct photographic observation and would need a 1.3 x 1.3 cm format for a 5' field of view. This is very close to the format size on presently available certified 16 mm cameras which are capable of meeting the above requirements.

For a 5 min field of view, the slit height of the Bowen spectrograph would be about 1.5 mm. To see the entire visible region at a nominal dispersion (40 $A^o$/mm) would require about 8 cm of film. The film format should therefore be 8 cm x 1.5 mm. A 100 mm camera would be ideal but it appears that none is presently available which meets all requirements although companies are planning to produce such a camera. An alternative would be an 8 mm camera mounted perpendicular to the preferred way with an 8 cm (10 frame) aperture and 10 frames advance. This camera is also not presently available, and not likely to be in the near future. The suggested way is than to use the 70 mm camera with some loss of spectral bandwidth. The other alternative would be to look into the state of 100 mm cameras presently under development.

Camera $P_f$, which swings into position in place of the Bowen grating (G'), should ideally be an 8 mm camera which would give about a 20 min field of view. Inasmuch as a spaceworthy camera is not available in 8 mm size, either a development program should be undertaken to develop such a camera, or the 16 mm camera could be used at the expense of using more film. The 16 mm camera would give about a 40 minute field of view.

### 2.1.8 Faster Objective Lens
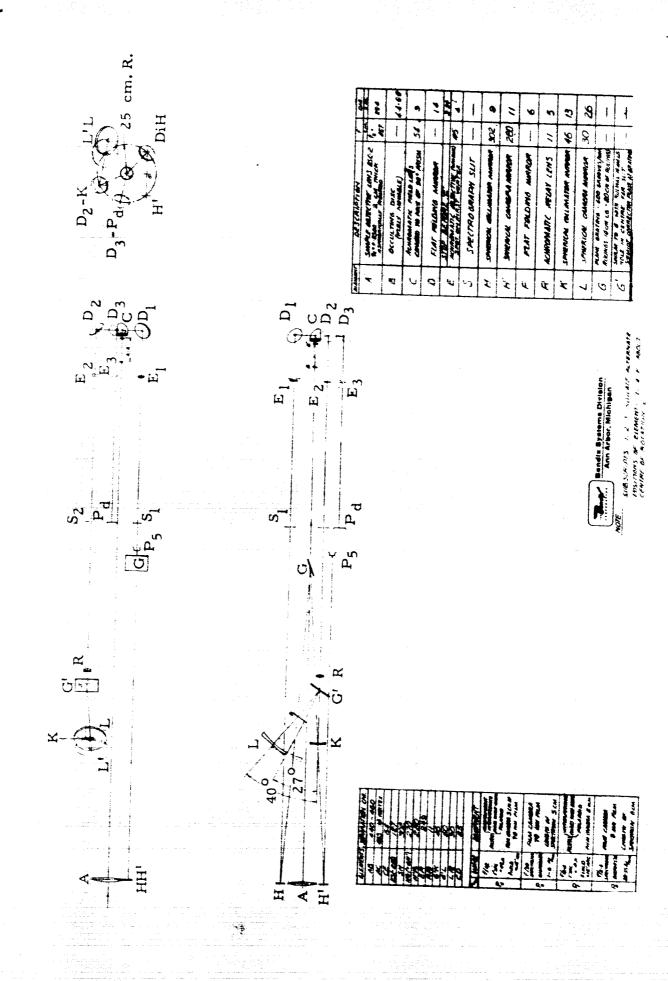
In order to shorten the entire structure, a shorter focal length objective lens (A) would be necessary. A brief analysis on an F/15 381 cm focal length lens was carried out. The diffraction limited spot size between 1st minima for this lens would be about $9\mu$ at $\lambda = 5890$ A$^\circ$. The lateral spherical aberration at the nominal focal length would be about $291\mu$ which means that more aspherizing is needed as compared with the F/18 lens. The chromatic aberration for this lens would be about the same as for the F/18 lens.

It is concluded that it would be feasible to shorten the focal length by about 76 cm and consequently shorten the entire structure (assuming a shorter focal length field lens) by about 10% but the additional figuring required on the objective lens (A) might make it undesirable.

### 2.2 FOLDED DESIGN

The folded design, shown in Figure 2, was conceived to compact and shorten the length dimension of the coronagraph. The major disadvantage of this design is that the two right angle reflections (at C and D) introduce additional polarization into the light incident on E in such a way that it is difficult to correct for the introduced polarization. The optics of the folded design are very similar to those of the linear design consequently the discussion will be minimal.

The objective lens A (focal length = 457 cm.) focuses the solar image on the occulter and its associated focal plane. The spherical and chromatic aberration of lens A, size of the occulter, its movement and positioning mechanism are all the same in the linear design. Lens (C) images A onto the stop in front of (E). For a focal length of C of the 54 cm, the distance between C and the stop should be about 62 cm. The right angle prism and the folding mirror D may be placed almost anywhere within that distance but the preferable positioning would be for C to be attached to the right

Figure 2. Optical Arrangement—Folded Design

angle prism and D to be placed such that AD approximately equals AC. Lens E images B and its focal plane onto the slit S. For a focal length of 45 cm for (E) the distance ES equals 124 cm and D should be about 20 cm from C.

The proposed design has BCDE rotating about ABC into three positions to direct the light into the Czerny Turner, the Modified Bowen and the camera $P_d$ directly. For a 15 minute field of view the slit height on the Czerny Turner should be about 3.3 cm. Camera $P_d$ should therefore be a 70 mm camera. The Czerny Turner spectrograph itself has the same grating and mirrors as in the linear design, consequently the dispersion is the same. Camera $P_s$ would therefore require a 5 cm (for a 100 A$^o$ bandwidth) x 5 cm (slight height) format and should also be a 70 mm camera with the film axis oriented in either direction with respect to the spectrum axis.

The third step around the axis brings the image through (E) and (R) and focuses on the slit mounted in the backside of the Bowen grating G'. Mounted on the same structure as the grating is camera $P_f$ which swings into the place of the grating when direct observation is desired. The components of the Bowen are the same as in the linear design, consequently the minimum format size is 8 cm (for 3200 Å bandwidth) x 3.3 mm (slit height). A 100 mm camera would be best suited for this configuration with a second choice being an 8 mm camera with the film axis parallel to the spectrum.

## 2.3 EXPOSURE CALCULATION

The intensity of a small spicule in the $H_\alpha$ light for a bandwidth of about 3.4 A$^o$ is approximately $2 \times 10^4$ erg cm$^{-2}$ sec$^{-1}$ ster$^{-1}$. [4] In order to obtain the energy density on the film, we shall assume (without loss of exactness) a 1 cm$^2$ film area being exposed. Then the equivalent area of spicule intensity at the sun can be found from the following geometry of

_____

[4] R. B. Dunn, Photometry of the Solar Chromosphere p. 129-130 Table 14 AFCRL 65-398, June 1965, Environmental Research Papers No. 109.

A
sun

Lens

$1 \text{ cm}^2$ film

$9.3 \times 10^7$ mi        457 cm
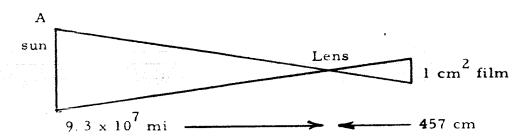
Figure 3  Spicule Observation Geometry

$$A = \left( \frac{9.3 \times 10^7 \times 5.28 \times 10^3 \times 30 \text{ cm}}{4.57 \times 10^2 \text{ cm}} \right)^2 \times 1 \text{ cm}^2 = 10.6 \times 10^{20} \text{ cm}^2$$

The energy density emitted is

$$E^1 = \frac{2.4 \times 10^4 \text{ erg}}{\text{cm}^2 \text{ ster sec}} \times 10.6 \times 10^{20} \text{ cm}^2 = 21.2 \times 10^{24} \frac{\text{erg}}{\text{sec ster}} \quad (9)$$

The energy collected by a 10" diameter lens at the earth is

$$E'' = E' \frac{\omega_{oe}}{\Omega_{oe}} = \frac{21.2 \times 10^{24} \text{ cm}}{\text{sec ster}} \times \frac{\frac{\pi}{4}(25.4 \text{ cm})^2}{216 \times 10^{24} \text{ cm}^2} \simeq \frac{50 \text{ erg}}{\text{sec}} \quad (10)$$

This is incident upon $1 \text{ cm}^2$ of film, so the energy density upon film, if this were at the first focal plane (at the occulter position), is

$$E = \frac{E'}{a} = \frac{50 \text{ erg}}{\text{cm}^2 \text{sec}} \times \frac{\text{watt sec}}{10^7 \text{ erg}} \times \frac{500 \text{ lumens}}{\text{watt}} \times \frac{1 \text{ meter candle}}{\text{lumen}/\text{m}^2} \times \frac{10^4 \text{ cm}^2}{\text{m}^2}$$

$$(11)$$

$$= 25 \text{ meter candles.}$$

If the exposure required is about 1/30 meter candle second[5]

$$t = \frac{1/30 \text{ m.c.s.}}{25 \text{ m.c.}} = 1/750 \text{ second for no filter or other losses.} \quad (12)$$

---

[5] For fast spectroscopic of Tri-X speed film exposed to a density of 1.

Since an $H_\alpha$ filter has about 10% transmission and the system beyond magnifies the images about twice, the exposure time would, for the camera $P_d$ be increased about 40 times additionally, hence

$$t = 40 \times 1/750 \text{ sec} \simeq 1/20 \text{ sec} \qquad (13)$$

For a grating efficiency of 60%, and a slit width of $10\mu$, the exposure at the Czerny-Turner spectrograph becomes about 1/2 second.

During this time, at a drift rate of 3 arc sec/sec, the sun's image will move approximately 0.2 slit widths.

Thus for the spectroscopic work, and especially for faint spicules, it is advisable to have a drift rate certainly not greater than 3 arc seconds per second of time, and preferably less.

## 2.4 CONCLUSIONS

Each of the designs—linear and folded, have advantages and disadvantages. The major disadvantages of the straight through design are the limited field of view and the increased length. The advantages are that it does permit polarization measurements, it has a simpler beamshifting mechanism to select which instrument is to be used, and it can fit into the LEM adapter.

The disadvantages of the folded telescope are that polarization measurements, which are a very important part of the scientific experiments, cannot feasibly be done, the design does not permit a simple chromatic correction such as is done with the Mangin mirror, and it requires more complicated and heavy mechanism to accomplish the task of switching the beam from instrument to instrument. The advantages are that it will fit into the smaller command module, and it may have a somewhat greater undistorted field of view.

It is concluded, since the scientific value of the straight through design is so much greater, that this design be used.

# SECTION 3

## CONCEPTUAL DESIGN AND ANALYSIS OF THE
## CORONAGRAPH SUPER-STRUCTURE

Depending on the relative positions of the optical elements, as dictated by the requirements and nature of the experiments to be performed, two conceptual designs of a super-structure are presented. The aim of such a **super**-structure is to house the optical elements, and to ensure that their relative positions are fixed and constant at all times; taking into account the following two factors:

1. The integrity of the super-structure should be such that it can resist any external load imposed on it here on earth or at launch with negligible resulting deformations. This could be achieved by designing a super-structure such that the maximum applied load be well within the elastic limit of the material used in design. If the elastic limit of the material used varies with temperature, then the design should be for the minimum expected limit

2. The material used in design should be visco-elastic in nature and capable of rapidly damping any free or forced vibrations of small magnitudes (similar to those expected to result from astronaut's movement, motors, servo-mechanisms, voice, etc) that will be imposed on the coronagraph during its operation.

## 3.1 MAIN FEATURES OF THE SUPER-STRUCTURE

Two conceptual designs have been defined to house the optical elements:

1. A reinforced spiral column fixed between two or more end and intermediate plates (see drawing Figure 4). The plates could be a honeycomb or sandwich type which offers a high flexural stiffness to weight ratio; while the spiral could be made of hollow tubing
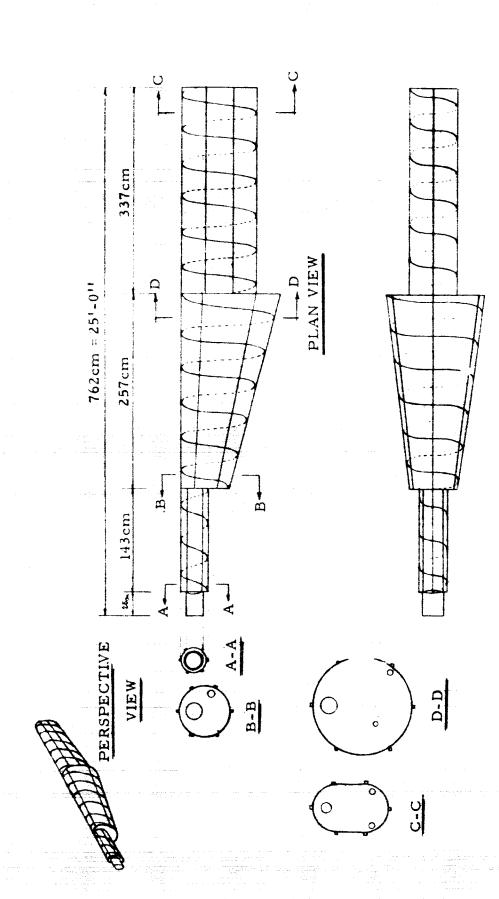
Figure 4 Unfolded Coronagraph Design

PLAN VIEW

END VIEW

PERSPECTIVE VIEW

A-A

B-B

C-C

D-D

762cm = 25'-0"

143cm    257cm    337cm

Bendix Systems Division
Ann Arbor, Michigan

3. A statically determinate truss-column fixed between two or more end or intermediate sandwich plates (see drawing Figure 5 for the unfolded design and Figure 6 for the folded design).

   Because of the accuracy of alignment involved, the dimensions of the different members of the coronagraph should be within ±0.02".

## 3.2 CHARACTERISTICS OF THE CORONAGRAPH

The following characteristic features of the unfolded and folded coronagraph designs are summarized hereunder (see Tables 1 and 2).

### 3.2.1 Unfolded Coronagraph Design

Overall Dimensions - 762 cm long x 80 cm wide x 60 cm breadth.

Weight - Approximate total weight including optical elements and cameras = 440 lb.

Location of Center of Gravity - The center of gravity has been evaluated using the center of the mirror D as a reference point (see Table 1 and Figures 1 and 7).
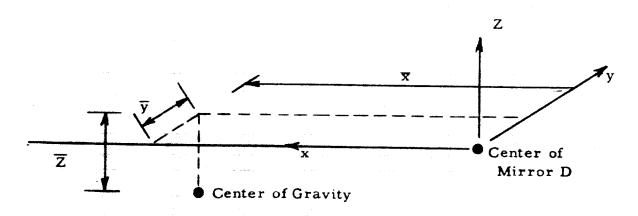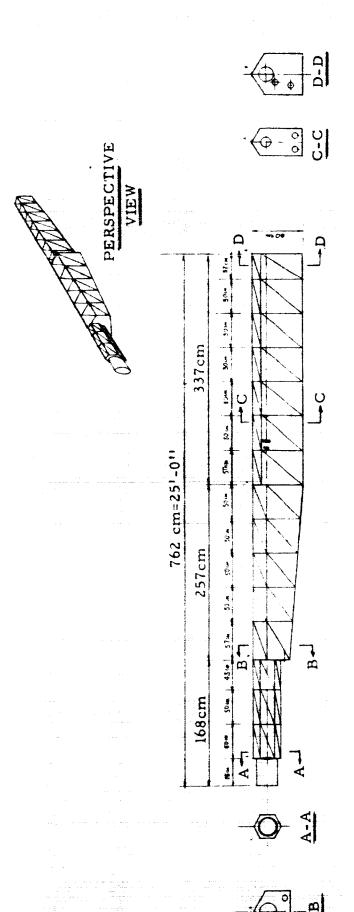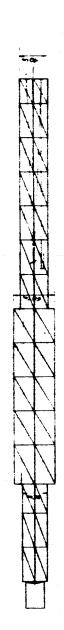


Figure 7   Location of Center of Gravity - Unfolded Design

PERSPECTIVE
VIEW

D-D

C-C

PLAN VIEW

762 cm = 25'-0"

168cm    257cm    337cm

A-A

B-B

END VIEW

Figure 5  Unfolded Coronagraph Design

Figure 5(a) Unfolded (Linear) Coronagraph Model

Figure 5(b) LEM Adapter - Coronagraph Comparison

PERSPECTIVE
VIEW

PLAN VIEW

END VIEW

A–A

498cm=16'-5"

25 cm   52.5cm   52.5cm   52.5cm   52.5cm   52.5cm   52.5cm   52.5cm   52.5cm   53cm
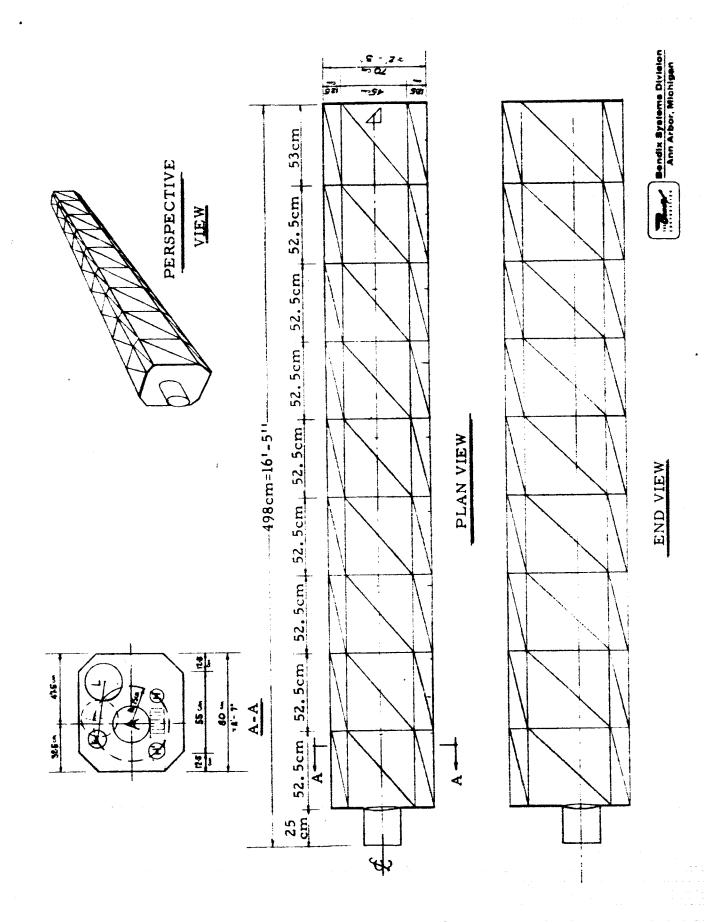
Figure 6 Folded Coronagraph Design

| MEMBER | WEIGHT (LBS) | MASS (Kg) | X (cm) | Y (cm) | Z (cm) | MX (Kg-cm |
|--------|--------------|-----------|--------|--------|--------|-----------|
| LENS A | 5.0 | 2.27 | 737.00 | 00.00 | 00.00 | 1673 |
| OCC. MECH. B | 20.0 | 9.07 | 305.75 | -10.00 | 00.00 | 2773 |
| LENS C | 1.5 | 0.68 | 274.00 | 00.00 | 00.00 | 186 |
| MIRROR D | 1.5 | 0.68 | 00.00 | 00.00 | 00.00 | 0 |
| LENS E | 5.0 | 2.27 | 455.75 | 12.25 | -24.00 | 1035 |
| MIRR. MECH. F | 4.0 | 1.81 | 593.50 | 20.00 | -25.00 | 1074 |
| SLIT S | 0.5 | 0.23 | 299.50 | 15.00 | -25.00 | 69 |
| MIRROR H | 1.5 | 0.68 | 00.00 | 10.20 | -48.00 | 0 |
| MIRROR H' | 2.0 | 0.91 | 00.00 | -10.20 | -48.00 | 0 |
| TELEPHOTO Q | 0.5 | 0.23 | 510.00 | 5.00 | -32.50 | 117 |
| TELEPHOTO R | 0.5 | 0.23 | 477.00 | 00.00 | -32.50 | 110 |
| MIRROR K | 1.5 | 0.68 | 372.00 | -12.40 | -40.00 | 253 |
| MIRROR L | 6.0 | 2.72 | 372.00 | -12.40 | 00.00 | 1012 |
| GRATING G | 3.0 | 1.36 | 277.24 | 00.00 | -40.00 | 377 |
| GRATING G' | 5.0 | 2.27 | 447.00 | -5.00 | -37.50 | 1015 |
| CAMERA P₁ | 30.0 | 13.61 | 448.00 | -5.00 | -17.50 | 6097 |
| CAMERA P₂ | 30.0 | 13.61 | 412.00 | -20.00 | -12.50 | 5607 |
| CAMERA P₃ | 55.0 | 24.95 | 287.00 | 25.00 | -37.50 | 7161 |
| CAMERA P₄ | 55.0 | 24.95 | 279.24 | -15.00 | -37.50 | 6967 |
| PLATE 1 | 1.3 | 0.59 | 737.00 | 00.00 | 00.00 | 435 |
| PLATE 2 | 5.3 | 2.40 | 594.00 | 00.00 | -15.00 | 1426 |
| PLATE 3 | 9.0 | 4.08 | 337.00 | 00.00 | -30.00 | 1375 |
| PLATE 4 | 5.7 | 2.59 | 00.00 | 00.00 | -25.00 | 0 |
| EQ. FOR B & B' | 15.0 | 6.80 | 457.00 | -20.00 | -32.50 | 3108 |
| T.V. CAMERAS | 5.0 | 2.27 | 322.00 | 5.00 | -40.50 | 731 |
| SHIELD # 1 | 25.4 | 11.52 | 168.50 | 25.00 | -22.50 | 1941 |
| 2 | 25.4 | 11.52 | 168.50 | -25.00 | -22.50 | 1941 |
| 3 | 19.6 | 8.89 | 168.50 | 00.00 | -55.00 | 1498 |
| 4 | 12.2 | 5.53 | 168.50 | 12.50 | 12.50 | 932 |
| 5 | 12.2 | 5.53 | 168.50 | -12.50 | 12.50 | 932 |
| 6 | 5.5 | 2.49 | 665.50 | 00.00 | 00.00 | 1657 |
| 7 | 17.9 | 8.12 | 462.00 | 00.00 | -47.50 | 3751 |
| 8 | 14.9 | 6.76 | 462.00 | -30.00 | -23.75 | 3123 |
| 9 | 14.9 | 6.76 | 462.00 | 30.00 | -23.75 | 3123 |
| 10 | 11.2 | 5.08 | 462.00 | -10.00 | 10.00 | 2347 |
| 11 | 11.2 | 5.08 | 462.00 | 10.00 | 10.00 | 2347 |

WEIGHT: MASS:
439.2 Lbs 199.22 Kg

X,Y,Z COORDINATES
MEASURED FROM CENTER
OF MIRROR D

ΣMx = 66,110
Kg cm
C.G. COORDI
FROM CEA
X꜀ᴳ = 331o

MIRROR

X ←

SIDE VIEW

3-6-1
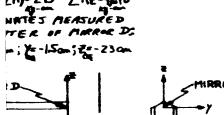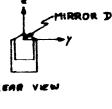
# TABLE 1  PHYSICAL CONSTANTS OF CORONAGRAPH
## UNFOLDED DESIGN

| | | $\bar{x} = x - x_{cg}$ | | $\bar{y} = y - y_{cg}$ | | $\bar{z} = z - z_{cg}$ | | $M\bar{y}^2 + M\bar{z}^2$ | $M\bar{x}^2 + M\bar{z}^2$ | $M\bar{x}^2 + M\bar{y}^2$ |
|---|---|---|---|---|---|---|---|---|---|---|
| My (kg-cm) | Mz (kg-cm) | x DIST. FROM CG (cm) | $M\bar{x}^2$ (kg-cm) | y DIST. FROM CG (cm) | $M\bar{y}^2$ (kg-cm) | z DIST. FROM CG (cm) | $M\bar{z}^2$ (kg-cm) | $Mh^2_{ox}$ (kg-cm) | $Mh^2_{oy}$ (kg-cm) |
| 0 | 0 | 406.00 | 374,178 | 1.50 | 5 | 23.00 | 1,201 | 1,206 | 375x10 |
| -91 | 0 | 25.25 | 5,783 | 8.50 | 655 | 23.00 | 4,798 | 5,453 | 11 |
| 0 | 0 | 57.00 | 2,209 | 1.50 | 2 | 23.00 | 359 | 360 | 3 |
| 0 | 0 | 331.00 | 74,501 | 1.50 | 2 | 23.00 | 359 | 360 | 75 |
| 28 | -54 | 129.75 | 35,927 | 13.75 | 429 | 1.00 | 2 | 431 | 35 |
| 36 | -45 | 262.50 | 124,720 | 21.50 | 837 | 2.00 | 7 | 844 | 125 |
| 5 | -6 | 31.50 | 228 | 16.50 | 63 | 2.00 | 1 | 63 | — |
| 7 | -33 | 331.00 | 74,501 | 11.70 | 93 | 25.00 | 925 | 518 | 75 |
| -9 | -44 | 331.00 | 99,704 | 8.70 | 69 | 25.00 | 569 | 637 | 100 |
| 1 | -7 | 179.00 | 7,369 | 6.50 | 10 | 9.50 | 21 | 30 | 7 |
| 0 | -7 | 146.00 | 4,903 | 1.50 | 1 | 9.50 | 21 | 21 | 5 |
| -8 | -27 | 41.00 | 1,143 | 10.90 | 81 | 17.00 | 197 | 277 | 1 |
| -34 | 0 | 41.00 | 1,572 | 10.90 | 323 | 23.00 | 1,439 | 1,762 | 6 |
| 0 | -54 | 53.76 | 3,931 | 1.50 | 3 | 17.00 | 393 | 396 | 4 |
| -11 | -85 | 116.00 | 30,545 | 3.50 | 28 | 14.50 | 477 | 505 | 31 |
| -60 | -238 | 117.00 | 156,307 | 3.50 | 167 | 5.50 | 412 | 578 | 187 |
| -272 | -170 | 81.00 | 89,295 | 18.50 | 1,658 | 10.50 | 1,501 | 6,159 | 91 |
| 629 | -936 | 99.00 | 48,303 | 26.50 | 17,521 | 14.50 | 5,246 | 22,767 | 54 |
| -344 | -923 | 51.76 | 66,843 | 13.50 | 9,547 | 14.50 | 5,246 | 9,793 | 72 |
| 0 | 0 | 406.00 | 97,253 | 1.50 | 1 | 23.00 | 312 | 313 | 98 |
| 0 | -36 | 263.00 | 166,006 | 1.50 | 5 | 8.00 | 154 | 159 | 166 |
| 0 | -122 | 6.00 | 147 | 1.50 | 9 | 7.00 | 200 | 209 | — |
| 0 | -65 | 331.00 | 283,763 | 1.50 | 6 | 2.00 | 10 | 16 | 284 |
| -136 | -221 | 126.00 | 107,957 | 18.50 | 2,327 | 9.50 | 614 | 2,931 | 109 |
| 11 | -92 | 9.00 | 189 | 6.50 | 96 | 17.50 | 695 | 791 | 1 |
| 208 | -257 | 162.50 | 304,200 | 26.50 | 8,090 | 0.50 | 3 | 8,093 | 309 |
| -208 | -259 | 162.50 | 304,200 | 23.50 | 6,362 | 0.50 | 3 | 6,365 | 304 |
| 0 | -489 | 162.50 | 234,750 | 1.50 | 20 | 32.00 | 9,103 | 9,123 | 244 |
| 69 | 69 | 162.50 | 146,027 | 14.50 | 1,084 | 35.50 | 6,969 | 8,053 | 153 |
| -69 | 69 | 162.50 | 146,027 | 11.00 | 669 | 35.50 | 6,969 | 7,638 | 153 |
| 0 | 0 | 334.50 | 278,607 | 1.50 | 6 | 23.00 | 1,317 | 1,323 | 280 |
| 0 | -386 | 131.00 | 139,347 | 1.50 | 18 | 24.50 | 4,874 | 4,892 | 144 |
| -203 | -161 | 131.00 | 116,008 | 31.50 | 6,708 | 0.75 | 4 | 6,712 | 116 |
| 203 | -161 | 131.00 | 116,008 | 28.50 | 5,491 | 0.75 | 4 | 5,495 | 116 |
| -51 | 51 | 131.00 | 87,178 | 11.50 | 672 | 33.00 | 5,532 | 6,204 | 93 |
| 51 | 51 | 131.00 | 87,178 | 8.50 | 367 | 33.00 | 5,532 | 5,899 | 93 |

$\Sigma My = 293$ kg-cm   $\Sigma Mz = 1140$ kg-cm

...NATES MEASURED
...TER OF MIRROR D:
...; $Y_c = -1.50$ cm; $Z_c = -23$ cm

MIRROR D

REAR VIEW

3-6-2

$$Mb_{ox}^2 + I_{xx} \qquad M\bar{h}_{oy}^2 + I_{yy} \qquad M\bar{h}_{oz}^2 + I_{zz}$$

| $Mh_{oz}^2 (kg\cdot cm^2)$ | $I_{xx} (kg\cdot cm^2)$ | $I_{yy} (kg\cdot cm^2)$ | $I_{zz} (kg\cdot cm^2)$ | $I_{ox} (kg\cdot cm^2)$ | $I_{oy} (kg\cdot cm^2)$ | $I_{oz} (kg\cdot cm^2)$ |
|---|---|---|---|---|---|---|
| 374×10³ | 0.2×10³ | — | — | 1.4×10³ | 375×10³ | 374×10³ |
| 6 | | | | 5.5 | 11 | 6 |
| 2 | | | | 0.4 | 3 | 2 |
| 75 | | | | 0.4 | 75 | 75 |
| 36 | | | | 0.4 | 35 | 36 |
| 126 | | | | 0.8 | 125 | 126 |
| — | | | | — | — | — |
| 75 | | | | 0.5 | 75 | 75 |
| 100 | | | | 0.6 | 100 | 100 |
| 7 | | | | — | 7 | 7 |
| 5 | | | | — | 5 | 5 |
| 1 | | | | 0.3 | 1 | 1 |
| 5 | 0.1 | | | 1.9 | 6 | 5 |
| 4 | | | | 0.4 | 4 | 4 |
| 31 | | | | 0.5 | 31 | 31 |
| 186 | | | | 0.6 | 187 | 186 |
| 94 | | | | 6.2 | 91 | 94 |
| 66 | | | | 22.8 | 54 | 66 |
| 71 | | | | 9.8 | 72 | 71 |
| 97 | 0.1 | | | 0.4 | 98 | 97 |
| 166 | 4.3 | 2.1×10³ | 2.2×10³ | 4.5 | 168 | 168 |
| — | 10.0 | 5.0 | 5.0 | 10.2 | 5 | 5 |
| 284 | 9.7 | 2.3 | 2.3 | 9.7 | 286 | 286 |
| 110 | | | | 2.9 | 109 | 110 |
| — | | | | 0.8 | 1 | — |
| 312 | | | | | | |
| 311 | | | | | | |
| 235 | 181.7 | 497.8 | 497.8 | 221.0 | 1,656 | 1,649 |
| 147 | | | | | | |
| 147 | | | | | | |
| 279 | 2.7 | 5.6 | 5.6 | 4.0 | 286 | 285 |
| 139 | | | | | | |
| 123 | | | | | | |
| 121 | 124.2 | 237.1 | 237.1 | 153.4 | 799 | 796 |
| 88 | | | | | | |
| 88 | | | | | | |

$$\sum I_{ox} = 454.4×10³ \; Kg\cdot cm^2 \qquad \sum I_{oy} = 9,665×10³ \; Kg\cdot cm^2 \qquad \sum I_{oz} = 9,660×10³ \; Kg\cdot cm^2$$

## FIXED ELEMENTS

| MEMBER | WEIGHT(lb) | MASS Kg | X(cm) | Y(cm) | Z(cm) | Mx (Kg-cm) | My (Kg-cm) |
|---|---|---|---|---|---|---|---|
| A | 5.0 | 2.27 | 0.0 | 0.0 | 0.0 | 0.00 | 0.00 |
| B | 20.0 | 9.07 | 450.0 | 0.0 | 0.0 | 4,581.50 | 0.00 |
| C | 1.5 | 0.68 | 463.0 | 0.0 | 0.0 | 514.84 | 0.00 |
| H | 1.5 | 0.68 | 0.0 | 18.5 | -17.0 | 0.00 | 12.53 |
| H' | 2.0 | 0.91 | 5.0 | -18.5 | -17.0 | 0.00 | -16.835 |
| SHIELD | 141.9 | 64.36 | 245.5 | 7.0 | 0.0 | 15,722.185 | 450.75 |
| R | 0.5 | 0.23 | 177.5 | -11.0 | 22.0 | 40.825 | -2.53 |
| K | 1.5 | 0.68 | 120.0 | -11.0 | 22.0 | 81.60 | -7.48 |
| L | 6.0 | 2.72 | 115.0 | 21.25 | 17.5 | 312.80 | 57.80 |
| G | 3.0 | 1.36 | 270.0 | 0.0 | -17.0 | 367.20 | 0.00 |
| G' | 5.0 | 2.27 | 270.0 | -11.0 | 22.0 | 612.90 | -24.97 |
| P₁ | 55.0 | 24.95 | 303.5 | -21.5 | 5.0 | 7,572.325 | -536.425 |
| P₀ | 55.0 | 24.95 | 280.0 | -19.0 | 17.0 | 6,986.00 | -474.05 |
| P₂ | 30.0 | 13.61 | 140.5 | 5.0 | 19.5 | 1,912.205 | 68.05 |
| P₆ | 30.0 | 13.61 | 270.0 | 11.0 | 22.0 | 3,674.70 | 149.71 |
| FRONT PLATE | 12.3 | 5.58 | 0 | 7.0 | 0.0 | 0.00 | 39.06 |
| REAR PLATE | 12.3 | 5.58 | 473.0 | 7.0 | 0.0 | 2,639.34 | 39.06 |
| D₁ | 1.5 | 0.68 | 463.0 | 18.5 | -16.75 | 314.84 | 12.58 |
| E₁ | 5.0 | 2.27 | 424.0 | 18.5 | -16.75 | 962.48 | 41.995 |
| S₁ | 0.5 | 0.23 | 303.5 | 18.5 | -16.75 | 69.805 | 4.225 |

$$\sum W = 388.5 \text{ lb} \qquad \sum M = 180.32 \text{ kg}$$

$$X_{CG} = \frac{\sum r_x}{\sum M} = 250.47 \text{ cm} \qquad Y_{CG} = \frac{\sum My}{\sum M} = -1.04 \text{ cm} \qquad Z_{CG} = \frac{\sum Mz}{\sum M} = 1.55 \text{ cm}$$

$$\sum Mx = 45,165.545 \qquad \sum My = -186,679$$

X, Y, Z, AND C.G. COORDINATES
MEASURED FROM CENTER OF
MIRROR A.

MIR

3-7-1

## FOLDED DESIGN

| MZ (kg cm) | x̄ (cm) | MX̄²(kg cm²) | ȳ (cm) | MȲ²(kg cm²) | z̄ (cm) | MZ̄²(kg cm²) | MȲz̄(kg cm²) | MȲz̄ (kg cm²) |
|---|---|---|---|---|---|---|---|---|
| 5.03 | 250.47 | 142,408.45 | .54 | 2.46 | 1.55 | 5.45 | 7.91 | 142,414.90 |
| 0.00 | 199.53 | 361,176.54 | .14 | 4.8 | .55 | 21.19 | 31.60 | 361,118.63 |
| 0.50 | 212.53 | 361,214.72 | .55 | 5.74 | 1.55 | .63 | 2.37 | 30,716.55 |
| -.56 | 210.47 | 42,059.25 | 19.54 | 259.63 | 18.55 | 253.95 | 4.73.62 | 42,893.74 |
| 5.47 | 250.47 | 59,519.05 | 17.46 | 277.41 | 18.5 | 313.13 | 590.04 | 59,402.18 |
| 0.00 | 3.97 | 12,366.56 | 9.14 | 4,160.53 | .55 | 154.52 | 4,314.95 | 12,715.18 |
| 5.06 | 72.97 | 1,224.06 | 1.96 | 22.82 | 20.45 | 76.14 | 119.01 | 1,320.85 |
| -4.96 | 30.47 | 11,607.25 | 1.96 | 67.46 | 20.45 | 284.58 | 351.84 | 11,859.63 |
| 47.60 | 135.47 | 49,917.75 | 2.29 | 1,351.42 | 15.95 | 691.77 | 2,043.39 | 50,609.74 |
| -23.12 | 1.53 | 8.73 | 1.54 | .47 | 18.55 | 467.98 | 469.45 | 986.71 |
| 49.74 | 1.53 | 726.53 | 9.52 | 225.19 | 20.45 | 149.32 | 1,174.51 | 1,815.15 |
| 124.75 | 53.03 | 70,160.91 | 20.40 | 10,444.36 | 5.45 | 296.97 | 10,741.33 | 70,460.88 |
| -424.15 | 29.53 | 21,256.92 | 17.46 | 8,047.91 | 18.55 | 8,585.36 | 16,633.27 | 30,342.28 |
| 26.395 | 109.97 | 104,091.19 | 2.04 | 496.51 | 17.95 | 4,385.18 | 4,881.69 | 168,976.37 |
| 299.42 | 1.53 | 5,917.14 | 12.04 | 1,972.93 | 20.45 | 5,691.74 | 7,664.67 | 10,882.81 |
| 5.05 | 250.47 | 350,062.53 | 8.04 | 560.70 | 1.55 | 13.41 | 374.11 | 350,075.94 |
| 0.00 | 222.53 | 276,319.37 | 8.04 | 360.70 | 1.55 | 13.41 | 374.11 | 276,332.78 |
| -11.39 | 212.53 | 30,714.92 | 4.54 | 259.63 | 18.30 | 227.73 | 487.36 | 30,942.65 |
| -38.0225 | 173.53 | 68,555.24 | 9.54 | 8,6671 | 18.30 | 760.20 | 1,626.91 | 69,115.94 |
| -38.5225 | 53.03 | 646.80 | 19.54 | 8782 | 18.30 | 77.02 | 164.84 | 723.82 |

ΣMz =

279.560



FRONT VIEW            SIDE VIEW

3-7-2

| $I_{b_{zz}}$ (kg·m²) | $I_{xx}$ (kg·m²) | $I_{yy}$ (kg·m²) | $I_{zz}$ (kg·m²) | $I_{ox}$ (kg·m²) | $I_{oy}$ (kg·m²) | $I_{oz}$ (kg·m²) |
|---|---|---|---|---|---|---|
| 2,411.47 | 183.06 | 91.53 | 91.53 | 190.97 | 142,505.93 | 142,?·?44 |
| 1,?? ·5 | 100.18 | 50.09 | 50.09 | 131.78 | 361,161.72 | 361,156.74 |
| 0,715.66 | 6.88 | 3.44 | 3.44 | 9.25 | 30,719.99 | 30,719.10 |
| 2,919.58 | 6.89 | 3.45 | 3.45 | 500.51 | 47,897.43 | 47,925.?? |
| 7,366.76 | 13.76 | 6.88 | 6.88 | 604.30 | 57,415.94 | 57,375.3? |
| 1,720.89 | 4,187.16 | 1,254,027.79 | 1,254,027.79 | 112,504.?? | 1,760,742.96 | 1,270,?92.0? |
| 1,247.48 | 0.72 | 0.36 | 0.36 | 119.73 | 1,321.21 | 247.84 |
| 1,642.71 | 14.37 | 7.18 | 7.18 | 346.21 | 11,866.81 | 11,849.89 |
| 1,269,19 | 22.184 | 14.92 | 14.92 | 2,275.23 | 50,724.66 | 51,389.11 |
| 520.20 | — | — | — | 9.9.45 | 786.71 | 520.20 |
| 091.02 | — | — | — | 1,174.51 | 1,815.15 | 1,091.02 |
| 1,608.27 | — | — | — | 10,741.33 | 70,460.88 | 10,608.27 |
| 9,804.83 | — | — | — | 16,633.27 | 30,342.38 | 29,834.83 |
| 5,087.70 | — | — | — | 4,881.69 | 168,976.37 | 165,087.70 |
| 1,164.07 | — | — | — | 7,664.67 | 10,882.88 | 7,164.0? |
| 1,423.23 | — | — | — | 314.11 | 350,075.94 | 350,423.23 |
| 1,680.07 | — | — | — | 374.11 | 176,332.78 | ?,680.0? |
| 1,974.55 | 16.66 | 8.33 | 8.33 | 504.02 | 10,950.99 | 10,982.5? |
| 1,222.45 | 4.54 | 2.27 | 2.27 | 1,057.45 | 69,118.2? | 44,327.72 |
| 734.62 | — | — | — | 165.94 | 721.22 | 734.62 |

|  |  |  | $\sum I_{ox}$ | $\sum I_{oy}$ | $\sum I_{oz}$ |
|---|---|---|---|---|---|
|  |  |  | 161,309.54 kg·m² | 2,976,029.6? kg·m² | 2,792,029.27 kg·m² |

$$\bar{x} = 331 \text{ cm}$$

$$\bar{y} = 1.5 \text{ cm}$$

$$\bar{z} = -23 \text{ cm}$$

Moments of Inertia - Principal Moments of Inertia about the C.G. of the coronagraph were evaluated as follows:

Roll: $I_{ox} = 455 \times 10^3 \text{ Kg cm}^2$

Pitch: $I_{oy} = 4665 \times 10^3 \text{ Kg cm}^2$

Yaw: $I_{oz} = 4660 \times 10^3 \text{ Kg cm}^2$

The scale model of the linear coronagraph design is shown in Figure 5(a) and 5(b).

### 3.2.2 Folded Coronagraph Design

Overall Dimensions - 498 cm long x 80 cm wide x 70 cm breadth.

Weight - Approximate total weight including optical elements and cameras = 390 lb.

Location of Center of Gravity - The center of gravity has been evaluated using the center of the objective lens A as a reference point (see Table 2 and Figures 2 and 8).
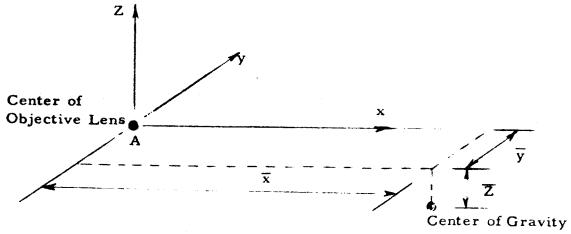


Figure 8   Location of Center of Gravity - Folded Design

$\bar{x}$ = 250 cm

$\bar{y}$ = -1. 00 cm

$\bar{z}$ = 1. 6 cm

Moments of Inertia - Principal Moments of Inertia about the C. G. of the coronagraph were evaluated as follows:

Roll:     $I_{ox}$ = 161 x $10^3$ Kg $cm^2$

Pitch:    $I_{oy}$ = 2976 x $10^3$ Kg $cm^2$

Yaw:      $I_{oz}$ = 2882 x $10^3$ Kg $cm^2$

## 3.3  OBJECTIVE LENS HOOD AND COVER

A lens hood 25 cm long will be attached to the objective lens A, to avoid any optical contamination of the objective lens.

A hood cover will be provided which will be kept closed by the Apollo crew except when exposing film. The crew should always en-sure that the hood cover is closed before dumping liquid - waste over-board from the spacecraft.

## 3.4  TEMPERATURE CONTROL

Thermal control of the coronagraph will be accomplished by means of:

1.  Allowing for an opening in the side of the super-structure through which most of the sun's central rays will be reflected by means of the inclined mirror in the occulting disc.

    Since the solar incidient power          = 0. 135 watts/$cm^2$
    and the frontal area of the objective lens = $\pi/4$ $(25)^2$ = 491 $cm^2$
    then the input power = 0. 135 x 491         = 66. 4 watts
    assuming that the efficiency of the reflecting mirror in the
    occulting disc is = 90%

Therefore, the net input power into the coronagraph

$$= 0.1 \times 66.4 \qquad = 6.64 \text{ watts}$$

This input power of 6.64 watts or 2.26 BTU/hr will be quite small during the duration of each experiment, and will be stabilized by use of thermal control coatings

2. A two layer heat shield will surround the super-structure. The inner surface and the outer surface will be covered with a high emissivity coating as required for proper temperature stabilization for the specific mission orbit characteristics. Thermal Control Coatings encompasses two heat balance parameters:

a. Solar absorptance '$\alpha$' which is defined as the ratio (or percentage) of solar radiation falling on a surface which is absorbed. The value of $\alpha$ is obtained by integration of the energy absorbed related to the Johnson Curve (intensity vs wavelength) of the sun. The wavelength region of 0.25 to 3.8$\mu$ is used, encompassing 98% of the solar energy. The value is obtained experimentally by means of reflectance techniques using the Gier-Dunkle integration sphere

b. Infrared emittance '$\epsilon$' which is obtained by integration of energy between 1.0 and 27$\mu$ compared to a 300°K black body. Reflectance techniques are used for the experimental determination of $\epsilon$. The Gier-Dunkel heated hohlraum is used in this determination

The ratio ($\alpha/\epsilon$) is used in the heat balance equations for radiant energy transfer. Three types of surfaces may be used described by their $\alpha/\epsilon$ ratio as:

$\alpha/\epsilon$ <1 White Paints - body tends to be cold

$\alpha/\epsilon$ =1 Grey Paints - body holds near earth temperature

$\alpha/\epsilon$ >1 Polished Metals - body tends to be hot

At approximately the earth's radius from the sun, surfaces with $\alpha/\epsilon = 0.2$ tend to equilibrate (adiabatic plate) near $230^\circ$K; surfaces with $\alpha/\epsilon = 1$ equilibrate near $313^\circ$K; surfaces with $\alpha/\epsilon = 3.5$ tend to equilibrate near $500^\circ$K. Uniformity of temperature distribution depends on the substrate

Materials which may be useful for thermal control of the coronagraph's super-structure may be broadly grouped as to exterior use or interior use

The exterior materials can probably be limited to:

a.    Inorganic white paint, $\alpha/\epsilon = 0.2$

b.    Second surface Vycor - Silver mirrors, $\dfrac{\alpha}{\epsilon} = \dfrac{0.06}{0.81} = 0.075$

c.    Inorganic Black paint, $\alpha/\epsilon = 1$

d.    Aluminum flake pigmented paint, $\alpha/\epsilon = 1$

e.    Evaporated gold surfaces, $\alpha/\epsilon = 10$

The interior surfaces can be limited almost entirely to:

a.    Inorganic Black paint

b.    Evaporated gold surfaces

If the inner shield operates under cold conditions during part of the mission, electrical heating elements will be mounted to the inner shield to raise its temperature to the equilibrium level of approximately room temperature ($75^\circ$F). Thermostat controlled heaters could maintain this temperature to within $\pm5^\circ$F.

The objective lens cover will be kept closed except during specific exposure periods to avoid major changes in the thermal balance within the structure in order to ensure that no warping of the super-structure takes place due to an uneven thermal stress distribution.

## 3.5 LOCATION OF GIMBALLING SUPPORT ON SUPER-STRUCTURE

The best theoretical position to place the gimballing mechanism and support the coronagraph to a platform is at its Center of Gravity, or as close to it as possible. However, since the coronagraph will have three axes of stabilization (roll, pitch and yaw), plus constant pointing towards the sun; then two possibilities exist.

1.  If the roll of the spacecraft is controlled to within $\pm 3^{\circ}$/hr (which is required to attain the accuracy of the line image on the photographic film) then only two axes of stabilization (pitch and yaw) will be required for the coronagraph. This will be attained by gimballed supports from the platform to the super-structure placed in a plane containing the center of gravity of the coronagraph as shown below. See Figure 9.
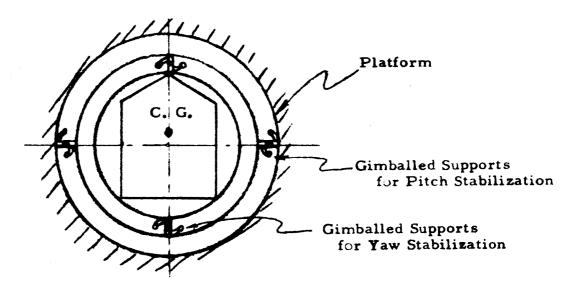


Figure 9   Pitch and Yaw Gimballing

2.  If the roll of the spacecraft cannot be controlled to within $\pm 3^{\circ}$/hr. then stabilization for the three axes of the coronagraph will be required. Since the roll stabilization desired is a pure rotation of the coronagraph about the optic axes AD, then two alternatives exist

a. The gimballing system could be attached to the back plate at the center of Mirror D (as shown in Figure 10). This has the disadvantage of cantilevering the super-structure which makes it very susceptible to vibrations
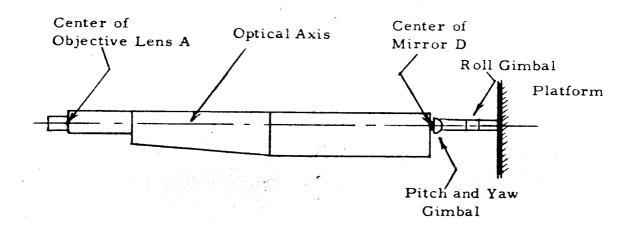


Figure 10 Roll, Pitch and Yaw Gimballing

b. The gimballing systems and supports for pitch and yaw could be placed on a plane containing the Center of Gravity of the system, however it has to be supported on an eccentric roller support which will permit a roll stabilization about the optic axis AD, (see Figure 11). This arrangement has the disadvantage of requiring more space and equipment
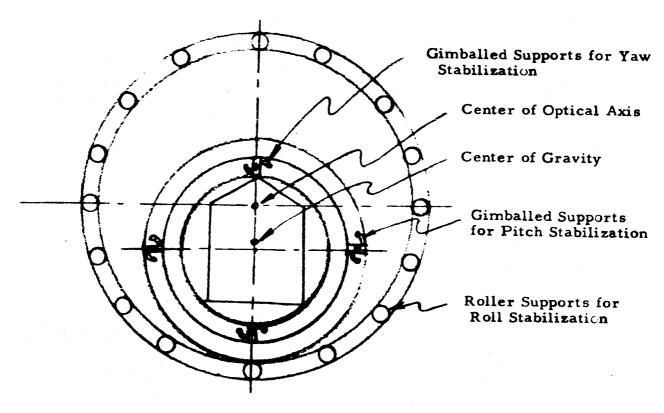
Figure 11   Roll, Pitch and Yaw Gimballing

## 3.6  CAMERA LOCATIONS ON SUPER-STRUCTURE

It is highly desirable to have all the film - cameras located at or near the super-structure so that they can be easily accessible to the astronauts. However, if such an arrangement cannot be fulfilled, then openings shall be provided on the super-structure through which the Apollo crew can change or recover experiment films.

## 3.7  LOCATION OF CORONAGRAPH ON THE APOLLO SPACECRAFT

From the overall dimensions of the super-structures of both the folded (Figure 5) and the unfolded (Figure 3) designs, the only feasible position which will allow enough space to accommodate the coronagraph will be the LEM adapter (see Figure 12).
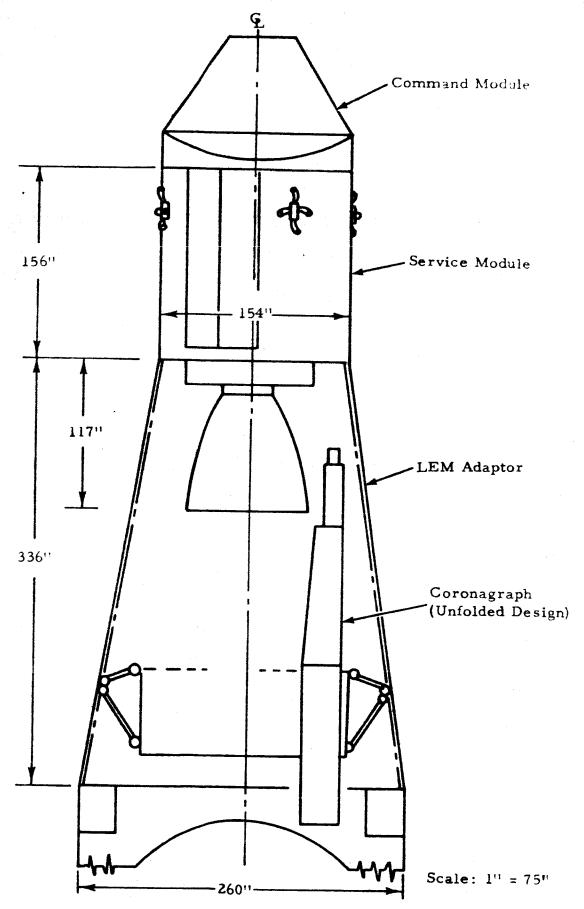
Figure 12  Possible Location of Coronagraph

Command Module

Service Module

LEM Adaptor

Coronagraph
(Unfolded Design)

156"

154"

117"

336"

260"

Scale: 1" = 75"

## 3.8 ASTRONAUT SUPPORT

A.   Restrict their movements to an absolute minimum during the experiments since such movements will be the biggest source of vibrations.

B.   Restrict any liquid waste disposal during each experiment.

C.   Change or recover experiment films.

# SECTION 4

## CORONAGRAPH CONTROL ANALYSIS

Based upon astronomical objectives of coronagraph application, various coronagraph control techniques have been evaluated. The objectives have been to specify the prime space vehicle constraints, and to recommend candidate control concepts which satisfy the coronagraph operational requirements. The results are, by necessity, conceptual in nature and reflect design parameters which candidate control concepts must meet

### 4.1 PROBLEM DEFINITION

In order that the control analysis may achieve the overall objectives of assessing the feasibility of an orbiting coronagraph, the general problem is constrained. The guide lines and necessary assumptions are outlined below.

The control requirements are defined and outlined and are based upon operational modes of the orbiting coronagraph. The operational modes, or the manner in which the coronagraph is used, are considered on the basis of achieving desirable astronomical objectives.

4.1.1 Mission Definition

4.1.1.1 Orbit

1. Circular e = 0.0

2. Altitude 200 n. mi. to synchronous 19,368 n. mi
   500 n. mi. (OSO, OAO)

3. Occultations - minimum

4. Inclination 33° (OSO), 32° (OAO)

5. Flight Duration 1 to 1 1/2 years

4.1.1.2 Vehicle

    1. Prime: Manned, Apollo, CSM/LEM Lab.

    2. Secondary: deployed satellite tethered to prime vehicle.

4.1.1.3 Astronomical Operational Modes

    1. Inner Corona Observation

       a. Direct solar line pointing

       b. Duration of data taking: 5 min to 2 hrs.

       c. Duty Cycle: 1/Orbital Revolution to Continuous

       d. Accuracy: 0.3 arc sec

$$\text{Minimum Resolving Power} = \frac{1.22\lambda}{D} = 0.35 \text{ arc sec}$$

$$D = 10 \text{ in.}$$

$$\lambda = 0.35\,\mu$$

       e. Drift Accuracy: Exposure Time 0.1 sec, 3 deg/hr.

    2. Outer Corona Observation

       a. Off Axis Solar Pointing: Continual (0.3 sec) to 5 Solar Radii (1.3 deg), roll axis control to 5 deg/hr.

       b. Duration of Data Taking: Same

       c. Duty Cycle: Same

       d. Accuracy: 2%, Camera FOV (5 arc min) = 6 arc sec

       e. Drift Accuracy: 3 deg/hr

4.1.1.4 Operational Control Modes

    1.    Fine Solar Axis Tracking

    2.    Fine Off Axis Solar Pointing

    3.    Fine Off Axis Solar Pointing: Roll Control

4.1.2 Attitude Control and Stabilization Operational Modes

The specific nature and components of an attitude control and stabilization system for an orbiting vehicle with an on-board pointing requirement are greatly affected by the technique of mounting the pointing instrument to the spacecraft. Gimballed mountings as opposed to body fixed methods alter the final form of the system. However, irrespective of the mounting technique, there are a class of several operational maneuvers of the spacecraft/pointing instrument which are required of the vehicle control system.

The general operational maneuvers are:

1.    Initial Orientation and Stabilization

Prior to a mission mode operation such as solar observation, the spacecraft must acquire a gross reference and eliminate tumbling. Whether the orientation and stabilization is initiated following launch or simply after free flight, such as might occur during solar occultation, the control and instrumentation mechanization is the same.

2.    Observable Acquisition

Once the gross initial reference has been acquired, the pointing instrument must be slewed to acquire the desired reference observable. The similarities between the observable acquisition and initial orientation mode are great but dependent upon the basic technique of attitude reference. The observable acquisition mode requires pointing command of the pointing instrument relative to the gross reference. The pointing commands are dictated by the technique of search pattern and dependent upon the field of view of the acquisition sensor and errors in the initial reference.

3. Coarse Tracking

Acquisition of the selected observable enables coarse tracking to be initiated. If the pointing instrument is gimballed, tracking is maintained by torquing the instrument in response to the coarse tracker error signal, relative to the gimbal/vehicle mounts or effectively the basic attitude reference of the vehicle. In the other instance when the pointing instrument is body fixed or when gimbal angular freedom is restricted, coarse track is maintained by torquing the spacecraft to eliminate the sensed error signal.

However, the problem is one of tracking and not pointing.

4. Fine Tracking

When the steady-state limit cycle of the coarse track mode is achieved, the fine tracking mode is initiated. Fine tracking operational modes are identical to coarse tracking technique, but depending upon overall system requirements, fine actuating techniques and sophisticated error sensing is needed. Roll stabilization about the observable LOS is necessary.

5. Fine Pointing - Off Axis Tracking

Off axis tracking with the accuracy of the fine tracking mode requires torquing the pointing axis relative to a highly accurate previously established reference attitude. Roll stabilization is provided by orthogonal celestial lines of reference.

4.1.3 Coronagraph Mounting Modes

There are basically two alternate techniques for mounting the coronagraph to the vehicle structure:

1. Body Fixed

2. Gimballed

The feasibility of the body fixed technique depends upon structural rigidity and the ability of the spacecraft control system to null out disturbance torques due to man motion and the physical environment with the major constraint of high inertia and required fine tracking.

Elimination of large disturbance torques due to man motion is possible in a tethered body fixed deployed open loop configuration, but disturbance torques are transmitted through the flexible tether. Also translational thrusting capabilities are necessary to periodically eliminate relative vehicle drifting due to orbital separation.

Gimballing the telescope to the spacecraft, which has relatively high inertia as compared to the telescope, depends upon the maintenance of fine track with sufficient servo response of the massive gimballed telescope inertia. Since the problem is one of fine tracking, gimbal alignment errors are not important. However, off-axis satellite pointing accuracies greater than 13 arc sec represent a significant technical problem.

The coronagraph operation requires that high tracking accuracies be maintained. Since the experiment requires on-board manned support, and since the basic class of vehicle is of the Apollo class, various modes of control defined above do not require evaluation. For instance, the assumption can be made that the initial orientation and stabilization control mode is performed by the existing on-board attitude control system. Also since acquisition can be manually aided, regardless of structural implementation, the study concentrates on the requirements of the coarse track, fine track, and point while fine track modes.

The options on mounting the coronagraph to the vehicle are summarized in Table 3, together with required operational modes.

TABLE 3

MOUNTING MODES

| Operational Control Modes | Solar Axis Tracking |
| | Off Solar Axis Pointing (Command Roll Mode) |
| Vehicle Type | Manned Apollo |
| | Tethered Satellite |
| Mounting Techniques | Body Fixed |
| | Gimballed |

The body fixed system, when in the tracking mode, requires the vehicle actuation system to cancel disturbance torques. The signal for corrective torquing is received from the tracking error sensor which indicates an off null correction is required. The principal difficulty in this configuration is slewing the mass of the entire vehicle and telescope with the required speed of response so that the null detector error signal remains within the allowable pointing angle limit cycle amplitude region.

The off-axis pointing mode complicates the body fixed control mode. To point at a prescribed angular orientation from the sun line is an effective open loop maneuver. Therefore an attitude reference is required to provide angular orientation about the sun line of sight.

The angular orientation reference can be accomplished through inertial techniques, celestial orientation sightings of one star to fix the locus of the pointing, and two stars to fix the line of the commanded LOS, or a single star tracking instrument providing off axis pointing capabilities. The pointing and tracking commands are implemented by the vehicle actuation system and in the presence of large disturbing torques, high inertia.

The gimbal mounted technique has an advantage for solar tracking when the moments of inertia of the vehicle are high with respect to the coronagraph inertia. The gimbal degree of freedom requirements depend upon the accuracy of the vehicle attitude control system. During tracking, the vehicle attitude control system should remain in a fixed inertial system so the gimbal motion required would be small perturbation compensation. Again, ratios of coronagraph to spacecraft inertia are important due to reaction torque coupling.

The gimbal technique is advantageous during off axis pointing since a point command may be given through gimbal angular orientation. But machining, gimbal alignment, and pointing angle transducers represent a problem due to relatively large errors which induce unsatisfactory pointing errors on this open loop maneuver. Therefore the requirement again is for an off axis solar tracker.

The problems which arise for the prime manned vehicle are identical to those of the tethered satellite. However, disturbance torques are minimized.

### 4.1.4  Mission Analysis

#### 4.1.4.1  Circular Orbit Characteristics

Figure 13 shows typical circular orbit characteristics. Plotted against altitude $h_c$ are the variables spacecraft tangential velocity $V_c$, angular velocity $\omega$, and orbital period T. It is important to note that low altitude orbits have orbital periods from 1.5 to 2.1 hours which implies a relatively high frequency of solar occultation.

#### 4.1.4.2  Commanded Pointing Angle Inputs

Regardless of telescope mounting techniques, the fine track mode requires alignment of the coronagraph boresight axis to the solar line of sight LOS in the presence of spacecraft S/C orbital motion and solar motion on the celestial sphere. Figure 14, shows azimuth and elevation tracking angle commands as a function of time for parametric values of S/C orbit (inclination $i_c$, solar LOS, orbit line of nodes angle $\Omega_c$, altitude $h_c$). The tracking commands are measured relative to inertial alignment upon fine track acquisition.

The major tracking component is seen to be due to solar drift with sinusoidal variations imposed upon the solar drift component. Note also, although the tracking angles are extremely small, the magnitude is twice the order of magnitude of the pointing accuracies. Figure 15 shows typical orbital component pointing angle amplitudes.

#### 4.1.4.3  Occulation Conditions

The total available time for data gathering is a direct function of ratio of orbital time spent in occultation to orbital period. Figure 16 shows the proportion of time spent in the earth eclipse in the form of a normalization factor,

$$\sigma / \Delta \gamma \quad \text{max.}$$

where

$\sigma$ = S/C angular subtense from earth/sun LOS
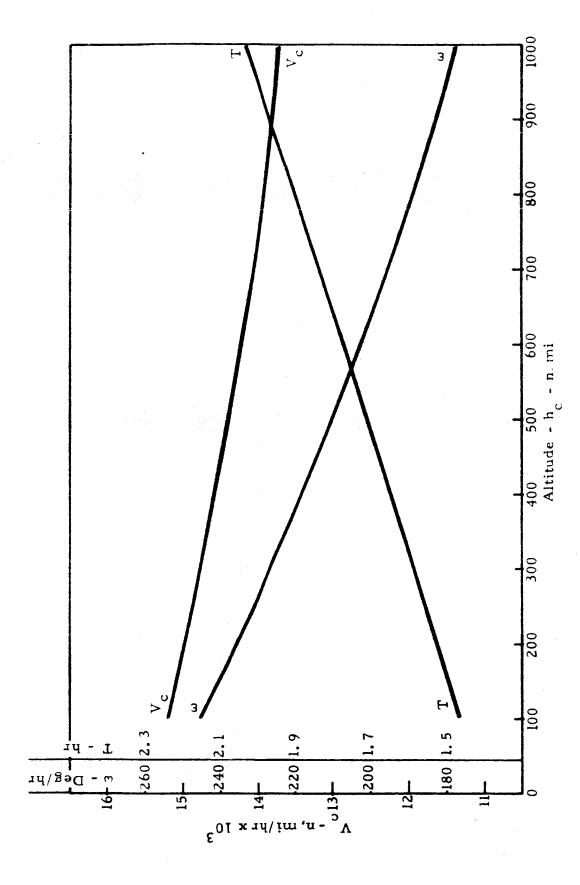
$\Delta \gamma$ = maximum $\sigma$

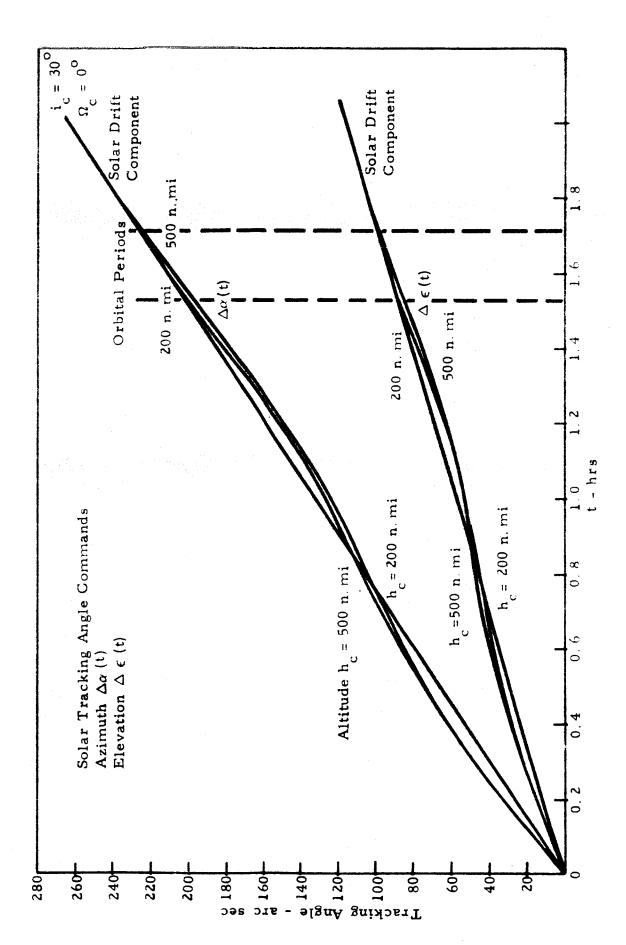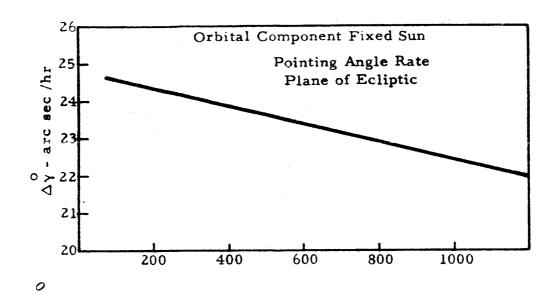Figure 13 Circular Orbit Characteristics
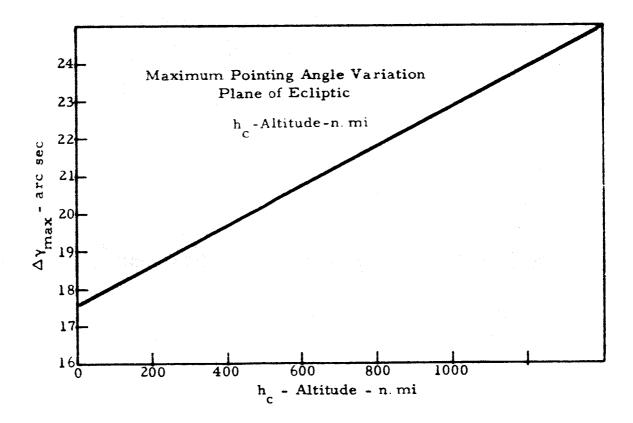
Figure 14 Tracking Angle Commands

4-9

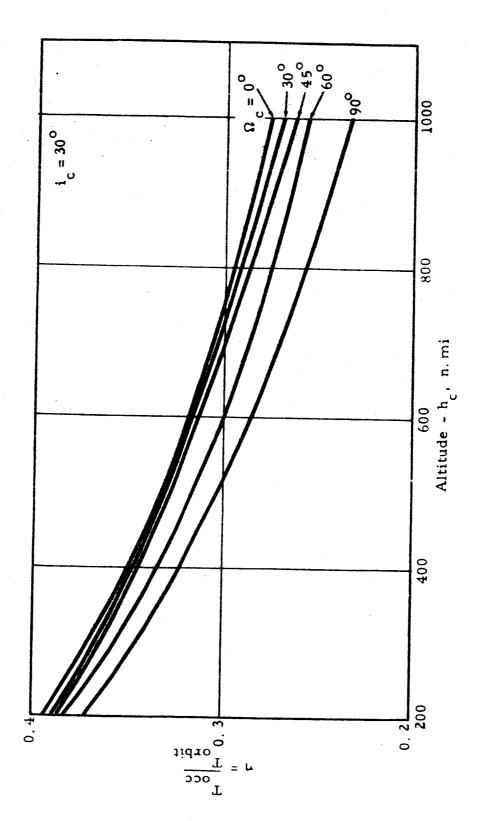Figure 15  Maximum Pointing Angle Amplitude

Figure 16  Solar Occultation Ratio

Whenever $\sigma < 8.8$ arc sec and the spacecraft is on the earth's far side, relative to the sun, occultation occurs.

Figure 16 shows the proportion of orbital time with respect to orbital period spent in the eclipsed condition. Nominal values are 30 to 40%. Certainly for low altitude orbits, the efficiency of the data gathering duty cycle and continuous tracking are severely limited.

### 4.1.4.4 Drifting Between Two Bodies in Rendezvous

The technique of utilizing a deployed satellite as an external occulter for the purpose of shading the objective lens in the off axis pointing mode requires alignment accuracies typical of the 0.3 arc sec requirement. Two major problem areas in the use of the external occulter are station keeping and propulsion requirements to eliminate orbital drift. Figure 17 shows the orbital drift conditions between two bodies in rendezvous. The normalized drift ratio $\delta/\Delta$ is effectively the perturbation in the occulter satellite relative to the spacecraft celestial observable LOS, or in the event a tethered satellite is considered, the relative drift between the prime vehicle and the deployed vehicle.

The drift rate at proposed low altitudes are intolerably large. At synchronous altitudes, conditions of drift rates appear favorable.

### 4.1.5 Disturbance Torques

The principal disturbance torques considered are earth gravity gradient, earth magnetic field, solar pressure, rotational and translatory man motion, and coronagraph reaction torques. The magnitude of these disturbance torques must be cancelled by the vehicle reaction control system within the dynamical response time required to maintain fine solar tracking. The following data indicates maximum or average magnitude levels and does not reflect transient responses.

### 4.1.5.1 Gravity Gradient

The average gravity gradient disturbance torque magnitude is given by

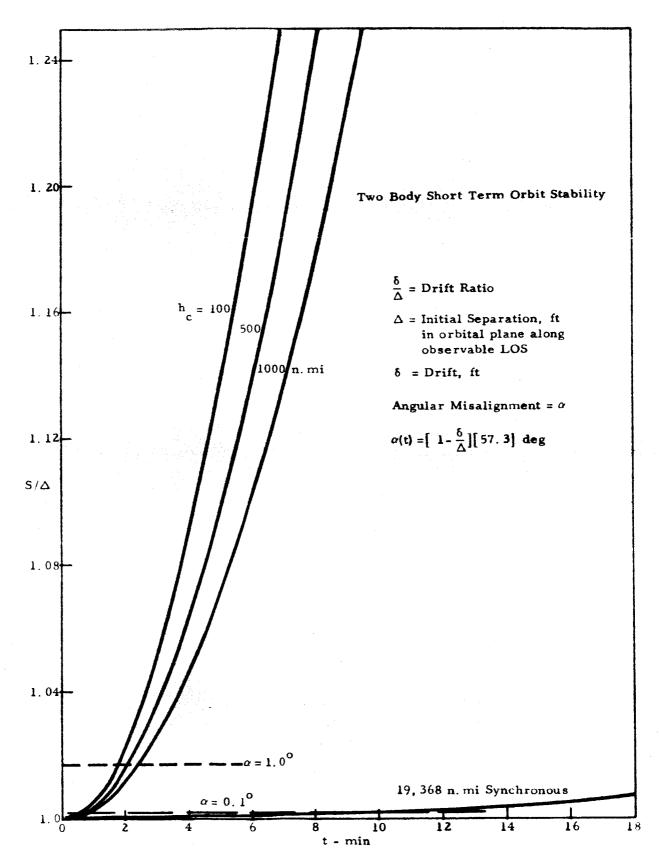$$T_{ave} = 3/4\,\omega^2\,(I_x - I_y)\,\sin 2\theta \qquad (14)$$

Figure 17  Relative Drift

where

$\omega$ = S/C inertial angular velocity

$I_x$ = S/C longitudinal (roll) moment of inertia

$I_y$ = S/C lateral (pitch) moment of inertial

$\theta$ = inclination of S/C longitudinal axis to the orbital plane

Figure 18 shows the maximum magnitude gravity gradient torque.

## 4.1.5.2 Earth Magnetic Field

The maximum value of the magnetic field induced torque as a function of altitude is shown in Figure 19. The parametric conditions are normalized coil data on-board the S/C.

## 4.1.5.3 Solar Pressure Disturbance Torques

Figure 20 shows maximum average solar pressure disturbance torques as a function of cg-cp moment arm and effective resultant area.

## 4.1.5.4 Internal Disturbance

Principal internal disturbance torques arise from man motion and coronagraph motion inertial reaction torques. Generally internal disturbance torques not only act as forcing function to the vehicle attitude equations of motion, but also effect the coefficients of the differential equations desscribing the vehicle attitude motion. However, this analysis is constrained to simplification and considers only the forcing function aspect. The linear time variable parameter approach is not taken.

For translatory motion relative to the vehicle c.g.,

$$\vec{T} = -m(1 - \frac{m}{M}) (\vec{r}_o + r \vec{(t)}) \times \vec{a}(t) \qquad (15)$$

where

m = element mass

M = system mass
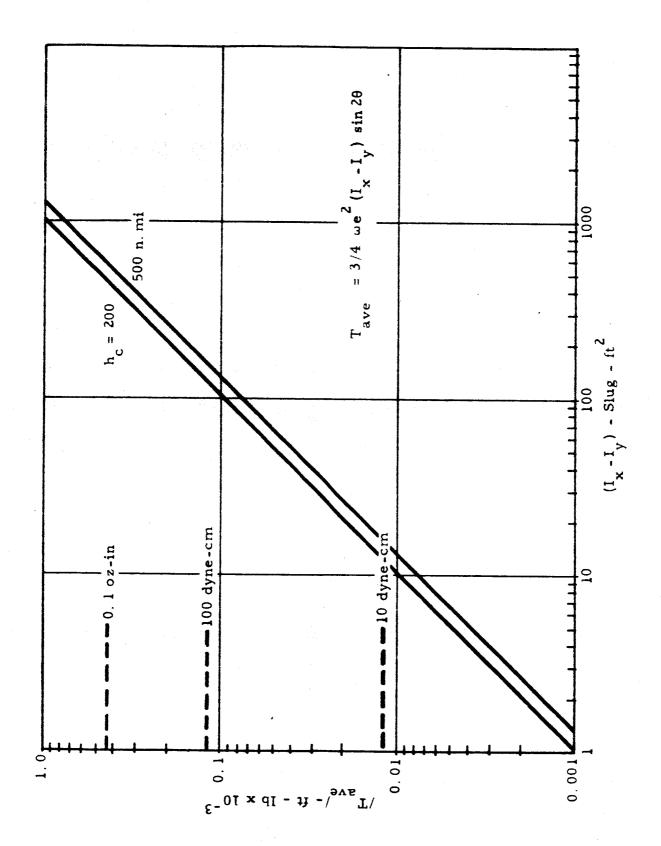
Figure 18 Average Gravitational Disturbance Torques
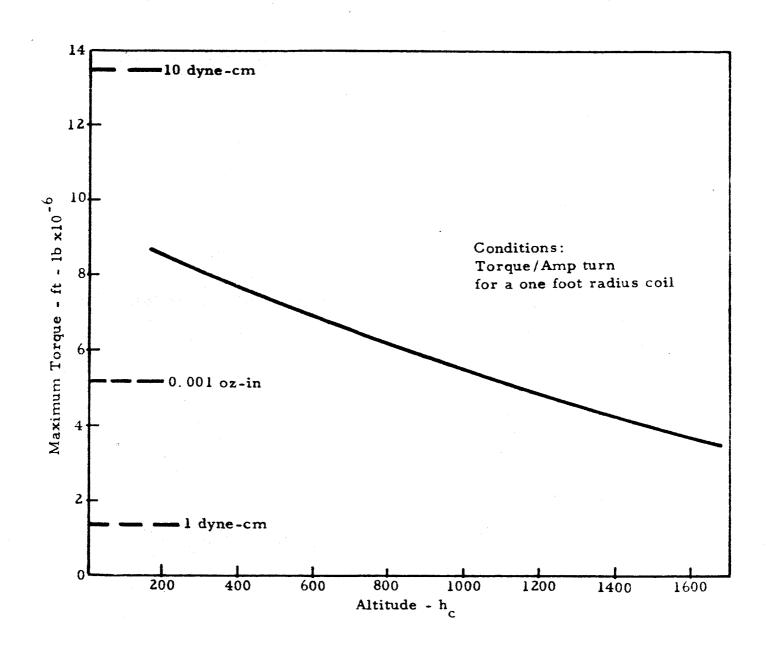
Figure 19   Typical Magnetic Field Disturbance Torques
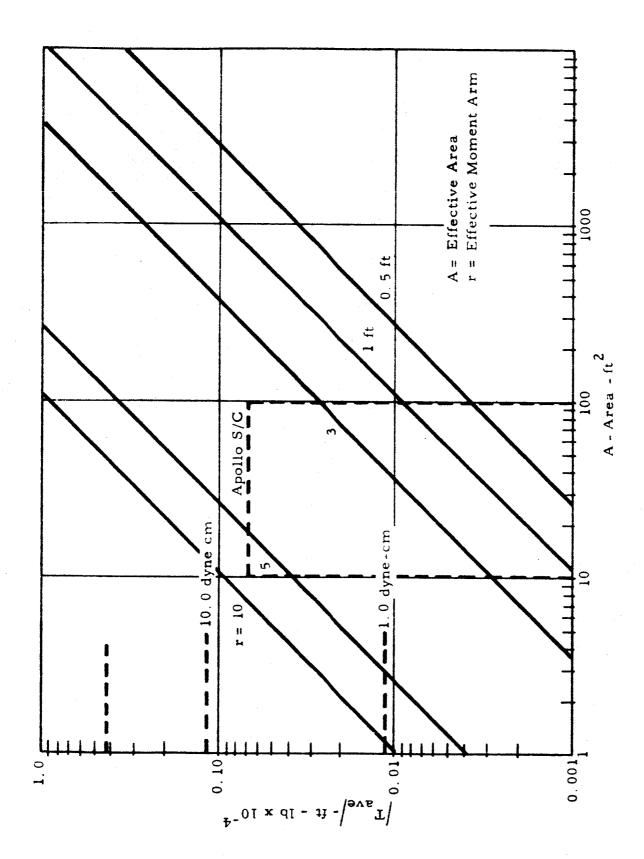
Figure 20 Solar Pressure Disturbance Torques

$\vec{r}_o$ = initial position vector

$\vec{r}(t)$ = position vector perturbation

$\vec{a}(t)$ = element acceleration

For rotational motion relative to the vehicle c.g.,

$$T = I_x \omega_D \vec{I}_x + I_y \omega_D (\vec{\omega} \times \vec{I}_x) \qquad (16)$$

where

$I_x$ = element longitudinal moment of inertia

$I_y$ = element diametral moment of inertia

$\omega_D$ = element angular velocity

$\vec{\omega}$ = S/C inertial angular velocity

The man model is based upon the 90 percentile man. Figure 21 shows the geometric composition. Table 4 shows the physical character-istics. Figures 22 and 23 show typical maximum disturbance torques due to translational and rotational motion respectively.
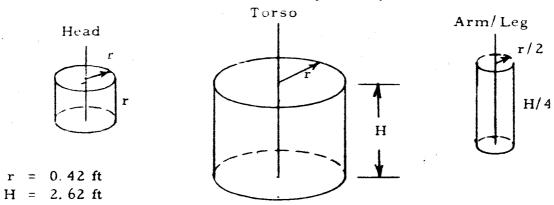


Figure 21  90 Percentile Man
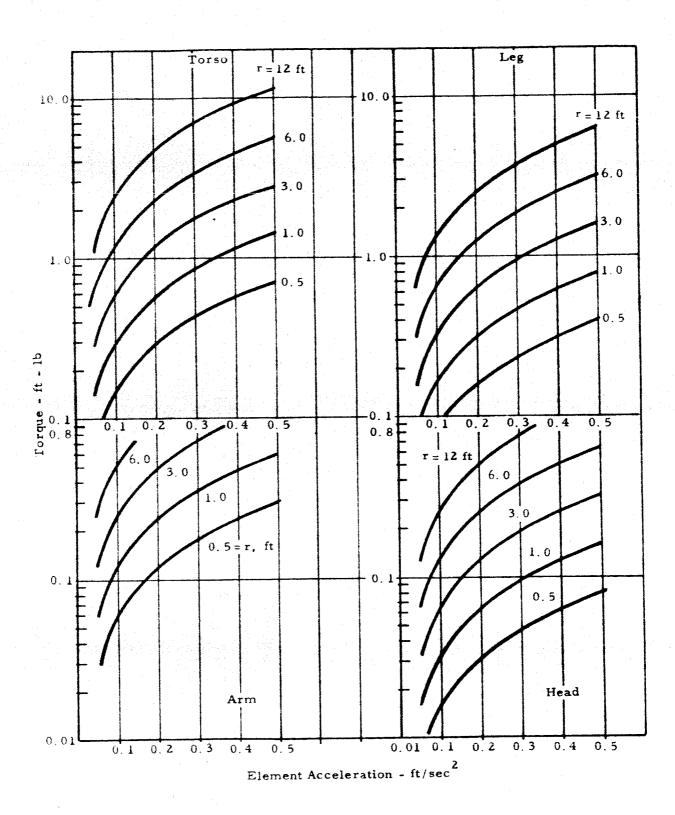
Figure 22  Disturbance Torques, Translatory Man Motion
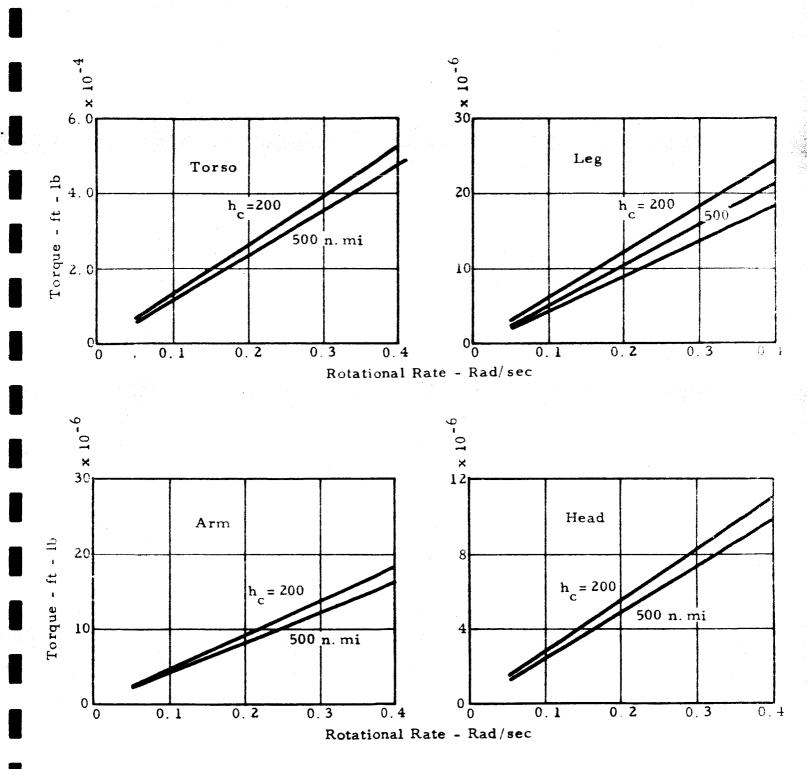
Figure 23  Disturbance Torques, Rotational Man Motion

## TABLE 4

## MAN MODEL

| Element | Volume | $I_x$ slug-ft$^2$ | $I_y$ slug-ft$^2$ | Mass Slugs | Total Mass |
|---------|--------|---------|---------|------------|------------|
| Head | 0.227 | 0.026 | 0.024 | 0.3 | 0.3 |
| Torso | 5.72 | 1.04 | 1.15 | 2.9 | 2.9 |
| Leg | 0.0881 | 0.018 | 0.053 | 0.8 | 1.6 |
| Arm | 0.0881 | 0.013 | 0.040 | 0.6 | 1.2 |
| Total Mass 6.0 slugs = 192 | | | | | |

The inertial reaction disturbance torques arising from coronagraph angular velocity in the fine track mode are shown in Figure 24.

4.1.5.5 Disturbance Torque Summary

A summary of the disturbance torques acting on the coronagraph space platform is shown in Table 5.

## TABLE 5

## DISTURBANCE TORQUE SUMMARY

| Disturbance Torque | Magnitude - Slug-ft | |
|--------------------|---------------------|---|
| | Vehicle | |
| | Manned Apollo | Tethered Satellite |
| Gravity | 0.002 | 0.0002 |
| Magnetic Field | $10^{-5}$ | $10^{-6}$ |
| Solar Pressure | $10^{-5}$ | $10^{-7}$ |
| Man Motion | 0.1 | |
| Coronagraph Reaction | $5 \times 10^{-7}$ | $5 \times 10^{-8}$ |
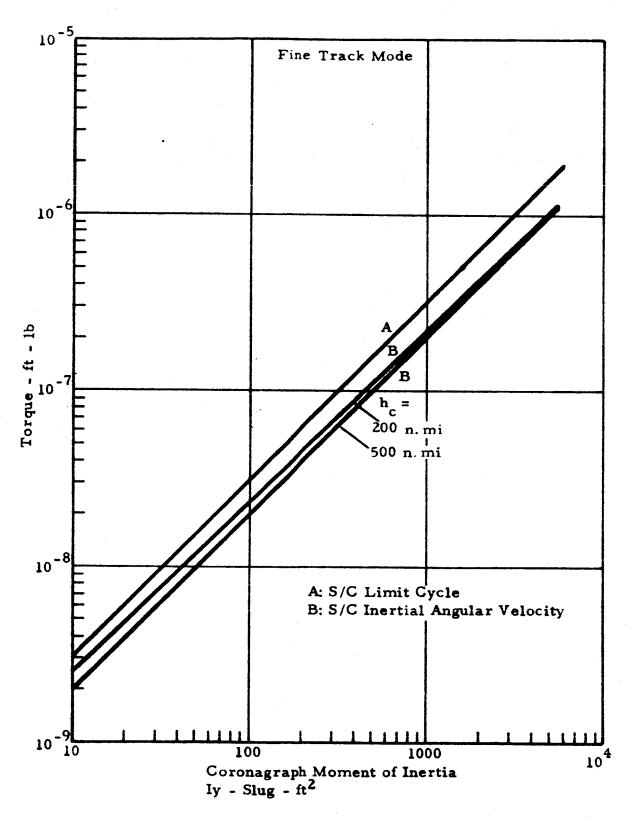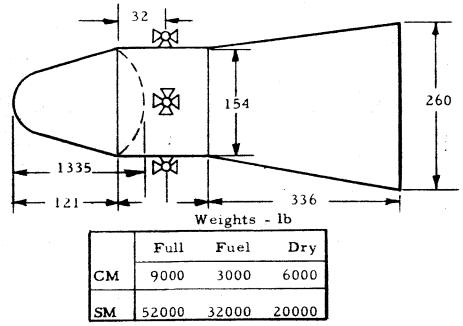
Figure 24 Disturbance Torques, Coronagraph Reaction Torque

From an analysis of the disturbance torque curves and the summary table, the conclusion is made that man motion exceeds the perturbation induced by other disturbances. Hence man-motion should be restricted to a high degree.

### 4.1.6 Prime Vehicle Characteristics; Physical and Control

The following data may be considered only as nominal operating point data for the Apollo CSM and LEM Adapter vehicle. The dimensions (inches) and weights of the S/C are shown in Figure 25, and are estimated to provide data inputs to the control analysis.



Weights - lb

|      | Full  | Fuel  | Dry   |
|------|-------|-------|-------|
| CM   | 9000  | 3000  | 6000  |
| SM   | 52000 | 32000 | 20000 |

CG Location: Within 5 in. diameter of longitudinal axis.

Figure 25 CSM/LEM Adapter

Calculated (through geometrical approximations) moment of inertias of the CSM are approximately

$$I_x = 15.2 \times 10^3 \text{ slug ft}^2$$
$$I_y = 20.1 \times 10^3 \text{ slug ft}^2$$
$$I_z = 21.2 \times 10^3 \text{ slug ft}^2$$

Attitude control sensor dead bands p, y $= \pm 0.1^{\circ}$

$$r = \pm 0.5^{\circ}$$

## 4.1.7 Instrumentation State of the Art (SOA)

As a prelude to defining coronagraph control concepts, a SOA assessment is made examining current instrumentation technologies. Table 6 is a matrix of attitude sensor capabilities, and Table 7 is a presentation of SOA actuation techniques.

### TABLE 6

### FINE TRACK ATTITUDE SENSORS

| Component | $3\sigma$ SOA Accuracy |
|---|---|
| Sun Tracker | 1 arc sec |
| IR Earth Tracker | 360 arc sec |
| OAO Star Tracker | 0.1 arc sec |
| Star Tracker | 2 arc sec |
| AOT Telescope | 10 arc sec |
| Displacement Gyros | $0.001^{\circ}/hr$ |
| Rate Gyros | $0.005^{\circ}/sec$ |

## 4.2 CONTROL CONCEPTS

The matrix of concepts for coronagraph control is shown in Table 8. The deployment modes considered are the Apollo body fixed and gimballed modes, and body fixed tethered satellite. The high accuracy null detector in each concept is a 0.1 arc sec accuracy sun tracker with off-axis pointing capabilities to $2^{\circ}$. The sensor pickoffs determine azimuth and elevation relative to a defined plane. The plane definition is provided by an orthogonally mounted star tracker (or trackers, dependent upon stellar density of celestial sphere locus). Single axis flow diagrams for each of the preliminary concepts are shown in Figures 26 to 28.

As an aid to occulter control, the off axis adapter of the sun tracker could provide reference data for occulter positioning.

TABLE 7

ACTUATION TECHNIQUES

| Technique | Thrust Level Lb | | | Torque Level Lb - Ft Min Max Nom | Min Δt Millisec | Specific Impulse Sec | (Momentum) Total Impulse Lb-Sec | Reaction Time (Time Constant) | Other |
|---|---|---|---|---|---|---|---|---|---|
| | Min | Max | Nom | | | | | | |
| Plasma Rocket | $10^{-6}$ | 10 | $10^{-4}$ | Moment Arm | 0.05 | 5,000 | 10,000 | Up to 1000 pulse per sec | Requires excess elec power |
| Micro Rockets | 0.001 | 1.0 | | Moment Arm | | 300 | 5,000 | 1.9 ms | See exponential force expressions |
| Micro Rockets | 0.0001 | 1.0 | 8 | Moment Arm | 2 | 100 | 5,000 | 0.6 ms | Least reliable |
| Bipropellant (Apollo, Gemini, Surveyor) | 1.0 | 90 | 8 | Moment Arm | 8 | 300 | $8 \times 10^3$ to $800 \times 10^3$ | 15 ms | |
| Monopropellant (Mercury, Centaur) | 1.0 | 80 | 10 | Moment Arm | | 150 | 100 to 50,000 | 22 ms | Intermediate reliable |
| Cold Gas | 0.001 | 1.0 | 0.5 | Moment Arm | 5 | 80 | 500 to 5,000 | 5 to 7 ms | Most reliable |
| Typical Experimental Satellite Req | 0.01 | 10 | 0.2 | Moment Arm | | | 100 to 5,000 | | |
| Reaction Wheels OAO Fine | | | | 0 (20%) 2 oz in. Linearity | | | Ft-lb-sec 2.06(1200) | Inertia 0.022 | Due to larger disturbance, torques dumping may be required. |
| OAO Coarse OGO | | | | 0 (20%) 32.7 oz in. 6.5 | | | 3.56 (1200) 1.66 (1850) rpm | 0.034 0.011 sl/ft$^2$ | |

## TABLE 8

### CORONAGRAPH CONTROL CONCEPTS

| Deployment Mode | Apollo CSM/LEM Lab | | Tethered Satellite |
|---|---|---|---|
| Mounting Mode | Body Fixed | Gimballed | Body Fixed |
| Stabilized Reference<br>r-roll<br>p-pitch (elev)<br>y-yaw (az) | Inertial-r<br>Solar LOS-p, y | Celestial-r<br>Solar LOS-p, y | Celestial-r<br>Solar LOS-p, y |
| Acquisition (and Coarse Track) | Wide Angle Sun Sensor (Manually Aided) | Wide Angle Sun Sensor (Manually Aided) | Wide Angle Sun Sensor (Manually Aided) |
| Principal Actuation Techniques | Reaction Jets (Bipropellant) | Reaction Jets (Bipropellant) | Microrockets (Monopropellant) (Momentum Dumping) |
| Coarse Actuator | Reaction Jets | Reaction Jets | Coarse Inertia Wheels |
| Fine Actuator | Microrockets | Servo Motor (Hydraulic, DC) | Fine Inertia Wheels |
| Fine Null Sensor<br>Position<br>Rate | Sun Tracker (Az, Elev)<br>Rate Gyro | Sun Tracker (Az, Elev)<br>Signal Processing | Sun Tracker (Az, Elev)<br>Signal Processing |
| Roll Reference | Displacement Gyro | Star Tracker | Star Tracker |
| Off Axis Reference | Sun Tracker | Sun Tracker | Sun Tracker |
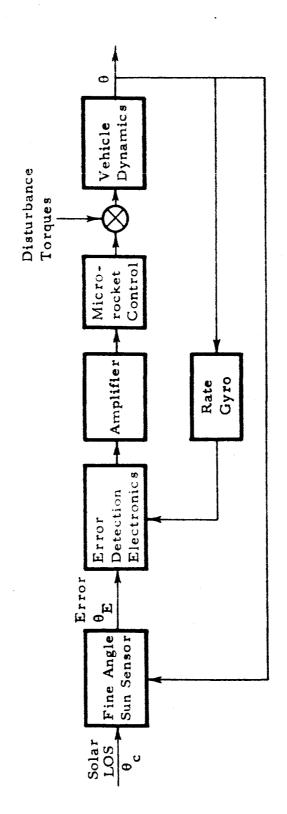
Figure 26 Fine Track Mode—Body Fixed Apollo S/C
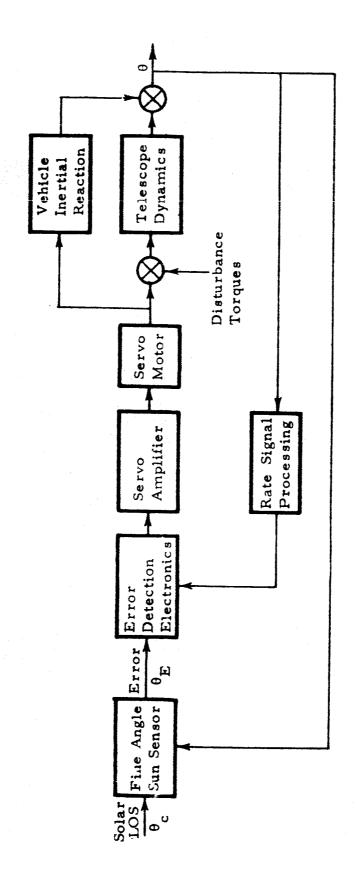
Figure 27  Fine Track Mode—Gimballed Apollo S/C
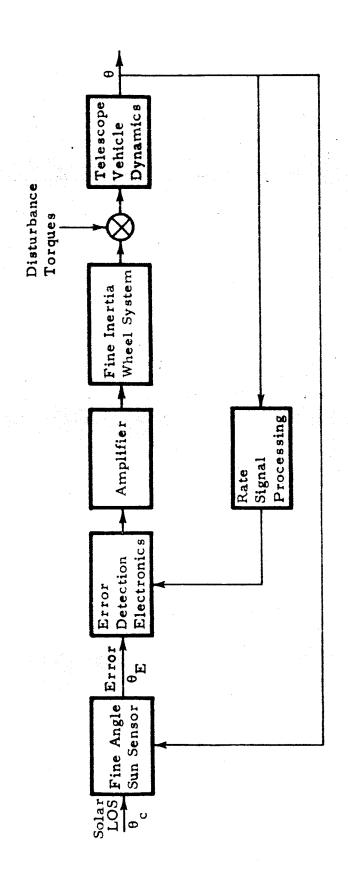
Figure 28 Fine Track Mode—Body Fixed Tethered Satellite

## 4.3 FINE ANGLE ERROR SENSOR

The fine angle error sensor listed in Table 8 is the source of the error signal which is used to actuate the coronagraph control system in the fine track mode. The error sensor (also depicted in Figures 26, 27, and 28, ) performs three functions in the conceptual design. The tracker:

1.    Indicates solar LOS to a 3 $\sigma$ null accuracy of $\sigma_\alpha$ = 0.1 arc sec

2.    Generates elevation and azimuth (pitch, yaw) error signals

3.    Provides off axis tracking capabilities out to 5 solar radii (1.5°).

The error sensor, during the Fine Solar Track Mode must be parallel to the telescope optical boresight. In the Fine Track Off Axis Pointing Mode the relative angle between the error sensor and the coronagraph boresight axis must be maintained at a prescribed azimuth and elevation. The two techniques for off axis pointing are:

1.    Orientation of solar LOS by precisely driving two prisms mounted internally to the fine angle error sensor. The sensor is body fixed to the coronagraph structure

2.    Driving the error sensor boresight axis, which is mounted in a pitch and yaw gimbal configuration, relative to the coronagraph structure.

Both techniques are open loop pointing procedures. The 3 $\sigma$ null errors between the error sensor boresight axis and the coronagraph optical axis are:

In the former case (1.),

$$\sigma_e = \left[ \sigma_\alpha^2 + \sigma_p^2 + \sigma_a^2 \right]^{1/2} \tag{17}$$

where

$\sigma_e$ = 3σ pointing error

$\sigma_\alpha$ = 3σ instrument null error

$\sigma_p$ = 3σ prism orientation error

$\sigma_a$ = 3σ structural alignment error

Typical state-of-the-art values are:

$\sigma_\alpha$ = 1 arc sec

$\sigma_p$ = 1 arc sec

$\sigma_a$ = 0.1 arc sec

∴ $\sigma_e$ = 1.4 arc sec

In the latter case,

$$\sigma_e = \left[ \sigma_\alpha^2 + \sigma_g^2 + \sigma_a^2 + \sigma_t^2 \right] \tag{18}$$

where

$\sigma_g$ = gimbal alignment error $\cong$ 10 arc sec

$\sigma_t$ = pointing angle transducer error $\cong$ 2 arc sec

then

$\sigma_e$ = 10.2 arc sec.

Thus the conceptual error sensor design will be boresighted to the telescope optical axis with internal off axis pointing capabilities.

The fine track position error sensor which is utilized in each of the three modes of coronagraph deployment is a high accuracy wide angle sun sensor. The sensor has the two axis capability for generating off null signals from the solar LOS in both azimuth and elevation (yaw and pitch). Additionally, the wide angle field of view (FOV), in conjunction with the two

precisely driven psisms allow off axis tracking to any commanded azimuth and elevation within the initial LOS/FOV. The sun tracker in all instances of operational modes is mounted body fixed, parallel to the telescope boresight axis. The FOV required to point off axis to 5 solar radii from the sun LOS is approximately 1.5°, which is the FOV required of the instrument.

The Eclipse-Pioneer Division of the Bendix Corporation designed and developed a fine sun sensor with an off axis adapter which provides the operational off axis performance capability desired. The sun sensor was designed for space applications and has a quoted null accuracy of 1 arc sec 3σ.

However, the 3σ null accuracy required for coronagraph operation is 0.3 arc sec. Generally, the state-of-the-art null accuracy for field operational sun sensors is 5 arc sec 3σ. In a tightly controlled laboratory environment, the representative null accuracies which can be achieved in off-the-shelf hardware is about 1 arc sec 3σ. Thus, the requirement for the null sensor is not met by state-of-the-art hardware and the equipment must be developed for the coronagraph experiment utilization.

Application of other sensors also fail. TV systems for the null sensor are restricted also since the accuracy requirement is not met. For example: a 1.5° FOV, 2000 line system has a 3σ null accuracy of 2.7 arc sec.

To provide the specified accuracy and FOV constraints, the following parameters are typical of the optical system of the prescribed error sensor:

$$\sigma_\alpha = \tan^{-1} \frac{2\,r_i}{f} \tag{19}$$

$$\alpha = 2\,\tan^{-1} \frac{r_f}{f} \tag{20}$$

$$\alpha \leq \frac{1.22\,\lambda}{2\,r_f} \tag{21}$$

where

$$\sigma_\alpha \quad = \quad 3\sigma \text{ instrument accuracy}$$

$$r_f \quad = \quad \text{collector radius}$$

$$r_i \quad = \quad \text{image radius}$$

$$\alpha \quad = \quad \text{FOV}$$

$$\lambda \quad = \quad \text{wavelength}$$

$$f \quad = \quad \text{focal length}$$

Now

$$\sigma_\alpha \quad = \quad 0.1 \text{ arc sec}$$

$$\alpha \quad = \quad 1.5 \text{ deg}$$

then

$$f \quad = \quad 7.65 \, r_f$$

$$r_i \quad = \quad 0.186 \times 10^{-4} \, r_f$$

$$r_f \quad \geq \quad 0.43 \times 10^{-3}$$

so if

$$r_f \quad = \quad 1 \text{ in.}$$

$$f \quad = \quad 7.65 \text{ in.}$$

## 4.4 ROLL STABILIZATION

Roll stabilization requirements arise due to excessive spacecraft limit cycle drift rates, or the scientific experiment astronomical objectives. In the former case, vehicle or coronagraph drift rates greater than 3 deg/hr exceed the control requirement specified by film exposure time while in the near corona fine track mode. To satisfy the experiment requirement, the coronagraph optical axis is rolled so that the grating spectrograph slits are properly oriented to the solar or coronal feature under observation. Thus the two specifications arise, maintenance of roll rates $\leq$ 3 deg/hr, (5 deg/hr off axis) and roll orientation.

### 4.4.1 Body Fixed, Apollo S/C

The minimum limit cycle conditions to be expected of the Apollo class of vehicles is nominally a 3.6 deg/hr drift rate, in three axes, and null accuracies of $\pm 0.1^{\circ}$ in pitch and roll and $\pm 0.3^{\circ}$ in yaw. However, if the reaction control system RCS thrusters are supplemented with fine actuation monopropellant microrockets (a typical dynamic response example is shown in Section 4.5.1) the roll stabilization requirement can be met with state-of-the-art inertial technology.

### 4.4.2 Gimballed, Apollo S/C; Body Fixed, Tethered Satellite

Roll stabilization of the coronagraph optical axis, and the celestial reference to define a specified roll orientation can be provided by star tracker references. Two degree of freedom, pitch and yaw (azimuth and elevation) gimballed star trackers mounted orthogonally to the telescope structures will supply the third inertial reference.

Typical state-of-the-art star tracker accuracies are listed in Table 6 and represent performance in ideal environments. However, star trackers such as OAO back up trackers are highly suited for the coronagraph application. Representative tracker accuracies are:

$$\sigma_{\alpha} = 20 \text{ arc sec}$$

$$\sigma_{g} = 13 \text{ arc sec}$$

$$\sigma_{t} = 2 \text{ arc sec}$$

$$\sigma_{a} = 1 \text{ arc sec}$$

$$\therefore \sigma_{e} = 24 \text{ arc sec.}$$

The OAO trackers FOV is $1^O$.[*] Since the earth subtends approximately $120^O$ to $140^O$ at the low earth orbits, three star trackers required to ensure the orthogonal reference.

Upon initial acquisition and commencing of celestial tracking, roll commands must be generated. The roll loop is typical of the loop in Figure 27 with the star tracker and computer coordinate transformations replacing the fine error detector. The coordinate transformation required are star tracker space (p, y) to star tracker mounting space, to coronagraph body fixed space to the vehicle space.

Typical dynamic limit cycles are shown in Figure 30 and 31 of Section 4.5.

## 4.5 CANDIDATE CONTROL CONCEPT PERFORMANCE ANALYSIS

The analytical control block diagrams for each of the candidate control modes are shown in Figures 29 (a), (b) and (c). Figure 29 (a) is the single axis bang bang control loop of the body mounted Apollo S/C configuration. Figure 29 (b) is the gimballed mounting mode of the S/C configuration, and Figure 29 (c) is the fine reaction wheel control loop of the tethered satellite. The control loops in Figure 29 are the simplified analytical representation of the conceptual flow diagrams in Figures 26, 27 and 28, respectively.

### 4.5.1 Body Mounted, Apollo S/C

### 4.5.1.1 Analysis

The following parameters are assumed to be representative of the Apollo S/C configurations as shown in Figure 29 (a).

$$\frac{\sigma}{I} = 3 \text{ deg/sec}^2 \text{ (100 lb thrust)} \tag{22}$$

$$\frac{\sigma}{I} = 0.15 \text{ deg/sec}^2 \text{ (5 lb thrust)} \tag{23}$$

$$\frac{\sigma}{I} = 0.03 \text{ deg/sec}^2 \text{ (1 lb thrust)} \tag{24}$$

---

[*]Gimbal capability is $\pm 60^O$.

Figure 29(a)  Single Axis, Body Mounted Apollo S/C

Figure 29(b)  Single Axis Gimballed Apollo S/C

Figure 29(c)  Single Axis, Body Fixed Tethered Satellite
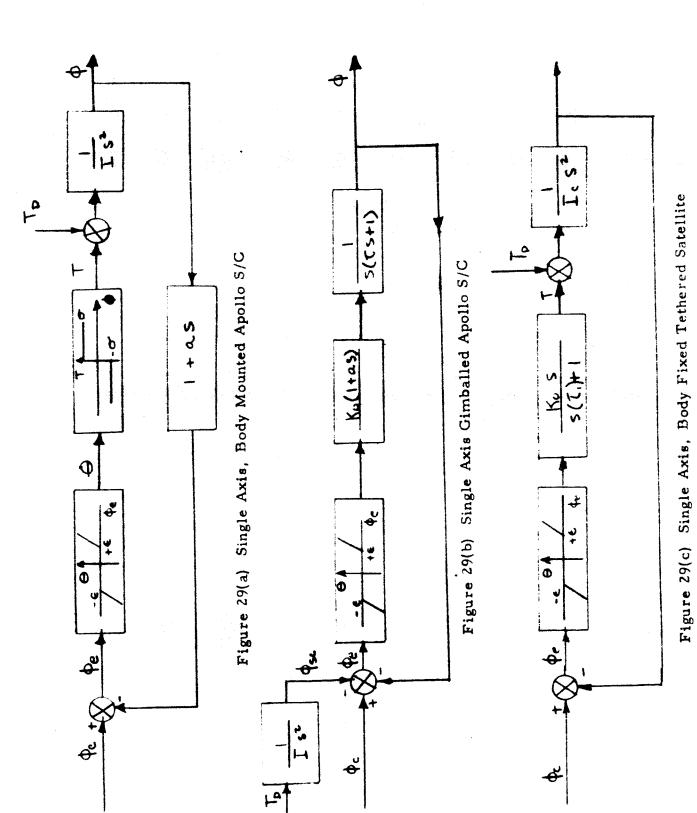
Figure 29  Analytical Control Loops
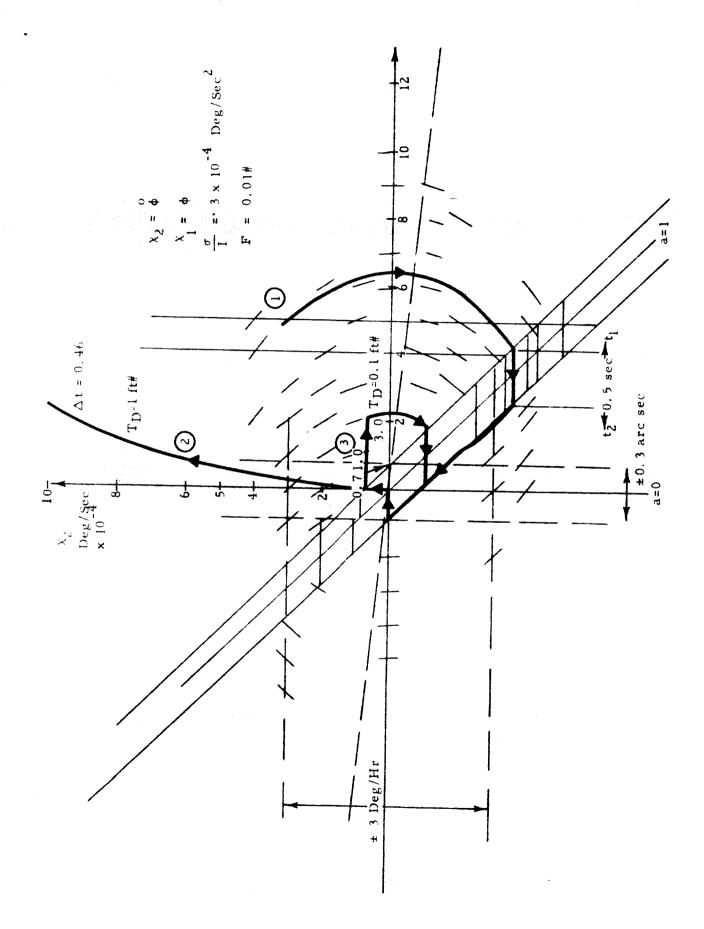
Figure 30 Body Fixed Apollo Limit Cycle
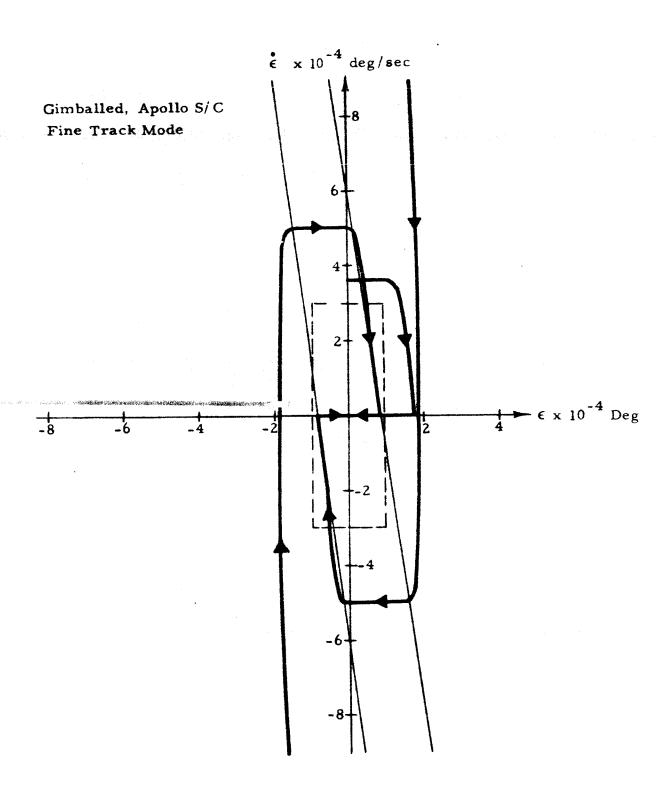
Figure 31  Rate Feedback Control

Then from the control loop, the system state variables are defined:

$$x_2 = \dot{\phi} \text{ pointing rate, deg/sec} \tag{25}$$

$$x_1 = \phi \text{ pointing angle, deg} \tag{26}$$

and the equations of motion are:

$$x_1^o = x_2 \tag{27}$$

$$x_2^o = \frac{T_D}{I} + \text{sgn}\left[-x_1 - a\,x_2\right]\frac{\sigma}{I} \tag{28}$$

where

$T_D$ = S/C disturbance torque, ft-lb

$a$ = rate feedback gain, sec

$I$ = S/C principal moment of inertia, slug/ft$^2$

$\sigma$ = S/C torque level, ft-lb

$\epsilon$ = $3\sigma$ deadband, deg.

The phase plane plot of the system state variables is shown in Figure 30 for:

$$\frac{\sigma}{I} = 3 \times 10^{-4} \text{ (0.01 lb thrust)}$$

$$a = 1 \tag{29}$$

$$I = 20 \times 10^3$$

$$T_D = 1, \ 0.1 \text{ for } t = 0.46 \text{ sec, } 0.7, \ 1.0, \ 3.0$$

For satisfactory system operation during the data taking or fine mode, the locus of the phase plane trajectory must be bounded by:

$$\dot{\phi} = x_2 \leq 3.0 \text{ deg/hr} \qquad (30)$$

$$\phi = x_1 \leq 0.3 \text{ arc sec} \qquad (31)$$

This region is indicated in Figure 30 by the dashed lines near the origin.

Three trajectories are shown in Figure 30

1.  Acquisition Phase: An example is given of switching from the wide angle sun sensor to the fine sun sensor and the coarse reaction control system to the fine jet system. This is the transition from the Coarse Track Mode to the Fine Track Mode. For the given set of initial conditions, the pointing axis is driven to the specified limit cycle region at the origin; total time is 4 sec

2.  Fine Track Mode: The system is initially at the origin and a pulse disturbance torque of 1 ft-lb acts upon the spacecraft. Fine Track is broken if the duration of the pulse exceeds 60 millisec

3.  Fine Track Mode: The system, initially at the origin, is acted upon by a disturbance torque of 0.1 ft-lb. Fine Track is maintained up to a pulse duration limit of 700 millisec.

The conditions and response trajectories for off axis pointing modes are identical to the given trajectories with the exception that the origin of the phase plane is translated to a given $x_1 = \phi_c$.

The propellant system fuel requirements can be calculated for the fine track limit cycle,

The total impulse is

$$I_T = \frac{1}{2r} \frac{x_2^2}{x_1} t, \text{ lb-sec} \tag{32}$$

where

r  = moment arm = 6 ft

t  = duration of Fine Track Mode sec

t  = [mission duration] [1 - proportion of occultation—proportion of acquisition]

   = 1 year [1 - 0.40 - 0.10] = 15 x $10^6$ sec

then

$$I_T = 52.5 \times 10^3 \text{ lb-sec.}$$

For a monopropellant, $I_s \cong 100$, the total fuel weight required is $W_f = 525$ lb.

For a bipropellant system, $I_s \cong 270$, the total fuel weight required is $W_f = 195$ lb.

4.5.1.2 Conclusions

The body fixed Apollo S/C mode is a satisfactory technique of coronagraph mounting if the reaction control system is supplemented with fine reaction control jets (0.01 lb thrust) and disturbance torques due to man motion are restrained to 0.1 ft-lb for a duration of 0.7 sec. For weight minimization a bipropellant system appears practical although the time constant is 1.9 millisec as compared to a 0.6 millisec monopropellant system.

4.5.2 Gimballed, Apollo S/C

4.5.2.1 Analysis

The control loop in Figure 29 (b) represents the single axis point-
ing angle control loop of the gimballed, Apollo S/C deployment with the
telescope in the fine track operational mode.  The control technique may
be accomplished either through dc motor or hydraulic actuation techniques.
Since both the dc motor and hydraulic actuation techniques have the same
simplified models, the loop parameters may be interpreted as characteris-
tics required of each technique.

The control loop in Figure 29 (b) utilizes error rate control as
opposed to the rate feedback control depicted in the associated conceptual
block diagram in Figure 27.  The nomenclature of Figure 29 (b) are de-
fined as:

$T_D$ = disturbance torque acting on spacecraft ft-lb

$I$ = spacecraft S/C moment of inertia, slug-ft$^2$

$\phi_{SC}$ = inertial angular perturbation of S/C, deg

$\phi_c$ = coronagraph commanded pointing angle deg

$\phi_e$ = pointing error, deg

$K_o$ = loop velocity constant, rad/sec

$\tau$ = actuator time constant, sec

$\phi$ = pointing angle

$\tau$ includes the reflected load inertias if torque magnification (gears) tech-
niques are utilized.

The design requirements which must be satisfied to achieve the
desired control response which permits scientific experimentation are the
following:

Null error:

$$\phi_e \leq 0.35 \text{ arc sec}$$

$$\epsilon = [\sigma_\alpha^2 + \sigma_a^2 + \sigma_b^2]^{1/2} \leq 0.3 \tag{34}$$

where

$\sigma_b$ = backlash, null resolution of torque magnification device.

Maximum spacecraft acceleration:

$$\ddot{\phi}_{SC} = 5.2 \times 10^{-2} \text{ rad/sec}^2 \qquad [100 \text{ lb thrust}]$$

$$= 2.6 \times 10^{-3} \text{ rad/sec}^2 \qquad [5 \text{ lb thrust}]$$

$$= 0.5 \times 10^{-4} \text{ rad/sec}^2 \qquad [\text{man motion, 1 ft-lb}]$$

Maximum spacecraft velocity:

$$\dot{\phi}_{SC} = 1.74 \times 10^{-5} \text{ rad/sec} \qquad [3.6 \text{ deg/hr limit cycle}]$$

$$= 1.74 \times 10^{-4} \text{ rad/sec} \qquad [36 \text{ deg/hr limit cycle}]$$

$$= 0.5 \times 10^{-4} \text{ rad/sec} \qquad [\text{man motion 1 ft-lb, 1 sec}]$$

Coronagraph moments of inertia:

(slug-ft$^2$)

| | Unfolded | | Folded |
|---|---|---|---|
| About cg | At End | | About cg |
| $I_x$ = 33.7 | 41.6 | | 11.9 |
| $I_y$ = 346.1 | 1972 | | 221 |
| $I_z$ = 345.8 | 1971 | | 214 |

Linear system analysis:

$\epsilon = 0$.

The system natural frequency is given as:

$$\omega_n = \frac{K_o}{\tau} \tag{35}$$

The dimensionless damping ratio:

$$\zeta = \frac{1}{2} \frac{1 + a K_o}{\sqrt{K_o}} \tag{36}$$

The closed loop transfer function:

$$\frac{\phi}{\phi_c} = \frac{K_o (1 + as)}{\tau s^2 + s (1 + K_o a) + K_o} \tag{37}$$

The error transfer function:

$$\frac{\phi_e}{\phi} = \frac{s (\tau_s + 1)}{\tau s^2 + (1 + a K_o)s + K_o} \tag{38}$$

The selection of error rate control (Figure 29 (b)) over rate feedback (Figure 27) was based on a comparison of linear system responses. The two techniques of control result in identical values of damping and system natural frequency, however, error rate control has a faster response and smaller steady state error due to a ramp input. The main control function input will be a ramp input as is evidenced in Figure 14.

With error rate control, the steady state pointing error due to a ramp input of magnitude $\Delta$ is

$$\phi_e = \frac{\Delta}{K_o}, \tag{39}$$

for rate feedback, the pointing error is

$$\phi_e = \left( \frac{1 + a K_o}{K_o} \right).$$

Since a, $K_o$ are always greater than zero, the former error is smaller. Lead circuit techniques at low frequency levels will eliminate expected large amplitude noise due to signal differentiation.

The design parameters are:

$$\zeta = 0.7$$

$$\omega_n = \alpha \left[ \frac{\text{maximum drift}}{\text{maximum allowable error}} \right]$$

$$= 3/2 \left[ \frac{\dot{\phi}_{SC}}{\epsilon} \right] \tag{41}$$

$$= 18.0 \text{ rad/sec}$$

$$\tau_{system} = 0.055 \text{ sec.}$$

The minimum actuator time constant can be shown to be

$$\tau = \frac{\tau_{system} 2\zeta \Delta}{\epsilon} \tag{42}$$

Where $\Delta$ is the ramp input due to solar sidereal motion.

Then

$$\tau = 0.542 \text{ sec}$$

$$K_o = \omega_n^2 \tau = 175 \text{ rad/sec} \tag{43}$$

$$a = 2 \frac{2\zeta \omega_n^{-1}}{K_o} = 0.138 \frac{\text{sec}}{\text{rad}} \tag{44}$$

As an example, these control loop parameters are reflected into component design values where the actuation technique is considered to be a dc Ward Leonard position control system. Again, the actuation technique could be hydraulic.

Let total armature resistance $R_a$ be approximately 20 ohms

$$R_a = 20 \text{ ohms}$$

$$R_a = r_{ag} + r_{am} \tag{45}$$

$$= 8 + 12$$

Let the motor velocity constant be

$$K_m \cong 2 \text{ volt sec/rad} \tag{46}$$

then

$$I_c = 400 \text{ slug-ft}^2$$

for maximum acceleration transfer through a gear train

$$I_m = \frac{I_c}{n^2} = \text{motor armature inertia}$$

$$n = 100 \tag{47}$$

$$I = 0.04 \text{ slug-ft}^2.$$

The state variables of the system are pointing error and pointing error rate.

$$x_2 = \dot{\phi}_e \tag{48}$$

$$x_1 = \phi_e \tag{49}$$

The equations of motion are:

$$\dot{x}_1 = x_2 \tag{50}$$

$$\dot{x}_2 = -x_2 \left[ \frac{1}{\tau} + \frac{K_o a}{\tau} \right] - \frac{K_o}{\tau} x_1 + \frac{K_o \epsilon}{\tau} \text{sgn}(x_1) - \ddot{\phi}_{SC} - \frac{\dot{\phi}_{SC}}{\tau} \tag{51}$$

where

$$\tau \rightarrow \infty \text{ for } x_1 \leq \epsilon.$$

Figure 31 is a plot of the coronagraph pointing angle limit cycle where the control loop contains rate feedback. Figure 32 shows the limit cycle with the control loop employing error rate control. Curve 1 is the acquisition response and curve 2 the system response to spacecraft rate.

## 4. 5. 2. 2 Conclusions

The analytical results indicate the conceptual design of the gimballed mounting mode can meet the required pointing limit cycle requirements in the presence of expected disturbance torques upon the space vehicle. The constraint limit cycle of 3. 6 deg/hr must be imposed upon the spacecraft.

Significant technical difficulties such as linear actuation at low signals must be solved for both hydraulic and dc motor actuation techniques. Additionally if conventional gearing is applied for torque magnification the backlash or null resolution must be limited to less than 0. 1 arc sec. Thus direct drive offers significant advantages, and hydraulic acquation appears favorable.

## 4. 5. 3 Tethered Satellite

The response of the tethered satellite configuration is given by the analysis of the control loop block diagram in Figures 27 and 29 (c). The loop degenerates into the response characteristics of the gimballed Apollo S/C configuration. Thus, the loop analysis is not derived, but rather the physical characteristics of the control components are defined.
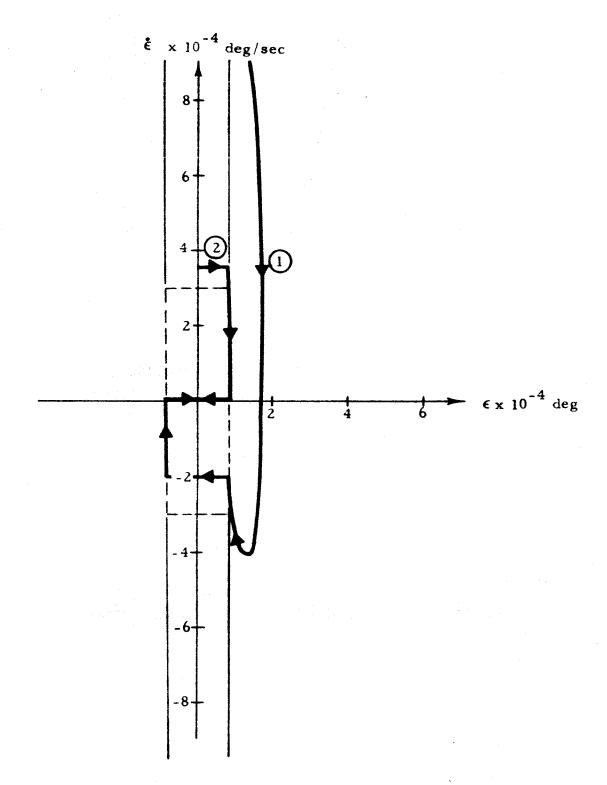
Figure 32  Error Rate Control

## 4. 5. 3. 1 Analysis

For control of the coronagraph spacecraft, assume a maximum principal moment of inertia of the spacecraft $I_c$ to be

$$I_c \text{ max } = 500 \text{ slug } \text{ft}^2.$$

This figure is calculated about the vehicle cg and represents about a 20% increase in the moment of inertia of the coronagraph.

Momentum Storage = (Disturbance Torque) (Duration)

+ (Spacecraft Angular Momentum)

$$= 1. 3 \text{ ft-lb-sec} \qquad (52)$$

Required Maximum Torque = 0. 2 ft-lb = 34. 8 in. oz

a/c Drive Motor Synchronous Speed $\omega_s$ = 1200 rpm.

The speed torque curve is required to be linear throughout the design torque limit range. Since the specified torque limits are:

$$= 38. 4 \le T \le 38. 4 \text{ in. oz}$$

and since the output torque is zero at synchronous speeds, the torque speed curve is defined for operational limits on the reaction wheel speed. Define the required linear range to extend ± 1000 rpm, then the torque speed curve is given as:

$$T = - \frac{38. 4}{1000} \omega + T_{max} \qquad (53)$$

where

$$T_{max} = 46. 0 \text{ in. oz; the stall torque.}$$

The power required at stall is

$$P_s = \frac{\omega_s T_{max}}{663} = 83. 2 \text{ watts} \qquad (54)$$

The inertia required is

$$I_m = .0124 \text{ slug-ft}^2.$$

The weight of this unit would be approximately 8.25 pounds plus 4 pounds motor weight for a total of 12.25 pounds. The wheel diameter would be approximately 20 inches.

### 4.5.3.2 Conclusions

Based on empirical data derived from existing reaction wheel systems the feasibility of fabricating a reaction wheel control system for a tethered coronagraph satellite is wholly within the state-of-the-art. The fine reaction wheel control system, damped by magnetometers, would be momentum dumped by microrocket rotational thrusters. The dumping would be performed during occulation and at which time translational thrusters would properly position the tethered satellite with respect to the prime space vehicle.

# ·SECTION 5

## COST AND DEVELOPMENT SCHEDULES

### 5.1 OPTICAL DESIGN

Figure 33 shows the optical design schedule to fabricate the selected (coronagraph design). The total effort for detail design, fabrication, and check out is scheduled as 26 mm.

The costing of the optical and mechanical elements is shown as follows.

### CORONAGRAPH COSTING

#### LINEAR DESIGN

| | |
|---|---:|
| Objective (a) | $ 3,000 |
| Achromat (c) | 800 |
| Margin (d) | 800 |
| Relay (e) | |
|     Figured | 1,400 |
| Folding Mirror (f) | 100 |
| Spherical Mirror (h) | 200 |
| Spherical Mirror (h') | 200 |
| Grating (g) (1960) | 2,500 |
|     Slit | 500 |
|     Lens (q) | 100 |
|     Lens (r) | 100 |
|     Grating (g') | 2,500 |
|     Slit | 1,000 |
| Mirror (k) | 200 |
| Mirror (l) | 500 |
| Corrector Plate | 500 |
| | ————— |
| | $14,400 |

FIGURE 33(a)

Optical Design Schedule (Folded)

| Task | 1 | 2 | 3 | 4 | 5 | 6 | 7 | 8 | 9 | 10 | Total Manmonths |
|---|---|---|---|---|---|---|---|---|---|---|---|
| Optical Component Design and Fabrication | | | | | | | | | | | 5.0 |
| Optical Component Procurement | | | | | | | | | | | 3.0 |
| Design and Construction of Component Mounts, etc. | | | | | | | | | | | 3.0 |
| Optical Assembly | | | | | | | | | | | 2.0 |
| Mechanical Design Fabrication and Test | | | | | | | | | | | |
| a. xyz occulter mech. | | | | | | | | | | | 3.0 |
| b. Grating (G) mech. | | | | | | | | | | | .5 |
| c. G' & $P_f$ interchange mechanism | | | | | | | | | | | 3.0 |
| d. BCDE rotation mechanism | | | | | | | | | | | 4.0 |
| d. L&$P_a$ mechanism | | | | | | | | | | | 3.0 |
| Integration into Structural Shell | | | | | | | | | | | 2.0 |
| Final Assembly (Optical and Mechanical) | | | | | | | | | | | 1.0 |
| | | | | | | | | | | | 29.5 mm |

5-3

## FIGURE 33

## Optical Design Schedule (Linear)

(months)

| Task | 1 | 2 | 3 | 4 | 5 | 6 | 7 | 8 | 9 | 10 | Total Man/months |
|------|---|---|---|---|---|---|---|---|---|----|------------------|
| Optical Component Design and Fabrication | | | | | | | | | | | 5.0 |
| Optical Component Procurement | | | | | | | | | | | 3.0 |
| Design and Construction of Component Mounts, etc. | | | | | | | | | | | 3.0 |
| Optical Assembly | | | | | | | | | | | 2.0 |
| Mechanism Design Fabrication and Test | | | | | | | | | | | |
| a.  xyz occulter mech. | | | | | | | | | | | 3.0 |
| b.  Grating mech. | | | | | | | | | | | .5 |
| c.  G' and $P_f$ camera mech. | | | | | | | | | | | 2.0 |
| d.  Folding mirror | | | | | | | | | | | 1.5 |
| e.  L&$P_a$ mech. | | | | | | | | | | | 3.0 |
| Integration into Structural Shell | | | | | | | | | | | 2.0 |
| Final Assembly Optical and Mechanical | | | | | | | | | | | 1.0 |
| | | | | | | | | | | | 26.0 mm |

## OCCULTER MECHANISM

| | |
|---|---:|
| Occulter | $ 1,000 |
| Occulter Holder | 500 |
| Occulter XYZ mechanism | 5,000 |
|    including motors electronics | 2,000 |
| Occulter Position (Auto) | 2,000 |
|    IR detector | 500 |
| 3 Position Folding Mirror (F) | |
|    and Mechanism | 700 |
| Grating Mechanism (G) | 500 |
| Mechanism to Move $L$ & $P_a$ | 1,500 |
| Mechanism to interchange | |
|    $G'$ & $P_f$ | 2,000 |
| | $ 15,700 |
| | |
| Cameras | $300,000 |
| | |
| **TOTAL** | **$330,000** |

In reality, since these prices are estimates, a 20% factor at least should be applied, so that the cost of the optics would be of the order of $400,000 to $500,000.

## 5.2 STRUCTURAL FABRICATION

The task schedule to develop and fabricate the coronagraph structure is shown in Figure 34. The material and component costs are:

### FIGURE 34

**Coronagraph Super Structure Prototype
Schedule (Linear)**

| Task | | Total |
|------|------|-------|
| Detail Design | | 6 |
| Fabrication | | 16 |
| Preliminary Alignment | | 3 |

1   2   3   4   5   6   7
(months)

25 mm

Materials: $4,000

### FIGURE 34(a)

**Coronagraph Super Structure Prototype
Schedule (Folded)**

| Task | | Total |
|------|------|-------|
| Detail Design | | 6 |
| Fabrication | | 16 |
| Preliminary Alignment | | 3 |

1   2   3   4   5   6   7
(months)

25 mm

Materials: $3,000

## 5.3 CONTROL DESIGN ANALYSIS SCHEDULE

Since the specific nature of the coronagraph control system is contingent upon the coronagraph mounting mode and operational mode which depends directly upon the U.S. space program evolution and objectives, specific and detailed cost schedules cannot be forecasted..

However, independent of the will not eventual experimental orbiting mission is the requirement for a detailed analysis study, component design study, and total control concept design study. The schedule for the control system development task is shown in Figure 35, and includes development tasks associated with both telescope designs.

### FIGURE 35

### Coronagraph Control System Detail Design Schedule

<u>Task</u>

Analog Computer Analysis

Sensor Design

Actuator Design

Final Concept Formulation
(including electronics)

0   1   2   3   4   5   6        manmonths

     Total Period of Effort:   6 months

     Total Engineering mm:   11

     Total Support mm:     3

        Total mm       14

## 5.4 COST SUMMARY

### Total Optical Design Costs

|  | Folded | Linear |
|---|---|---|
| Labor (29.5 m/m) | 36,875 | (26 m/m) 32,500 |
| Burden | 44,250 | 39,000 |
| Materials | 400,000 | 400,000 |
| G&A | 73,275 | 71,809 |
| TOTAL | $554,400 | $543,309 |

### Total Structural Fabrication Costs

|  | Folded | Linear |
|---|---|---|
| Labor (25 m/m) | 31,250 | (25 m/m) 31,250 |
| Burden | 37,500 | 37,500 |
| Materials | 3,000 | 4,000 |
| G&A | 10,927 | 11,080 |
| TOTAL | $82,677 | $83,830 |

### Total Control Analysis Cost

|  | Folded | Linear |
|---|---|---|
| Labor (14 m/m) | 17,500 | (14 m/m) 17,500 |
| Burden | 21,000 | 21,000 |
| G&A | 5,864 | 5,864 |
| TOTAL | $44,364 | $44,364 |

| | Folded | Linear |
|---|---|---|
| TOTAL COST | $681,441 | $671,503 |